Unlocking the Antiviral Arsenal: Multiparametric Optimization of Small-Molecule Inhibitors against RSV and hCoV-229E

Christina Karhan[a,b]†, Svenja M. Sake[c], Antonia P. Gunesch[c], Christina Grethe[c], Benedikt Hellwinkel[c], Alexander F. Kiefer[a]††, Uladzislau Hapko[a,b], Andreas M. Kany[a], Thomas Pietschmann[c,d,e,f], Anna K. H. Hirsch[a,b,e]*

[a]Helmholtz Institute for Pharmaceutical Research Saarland (HIPS) - Helmholtz Centre for Infection Research (HZI), Campus Building E8.1, 66123 Saarbrücken, Germany.

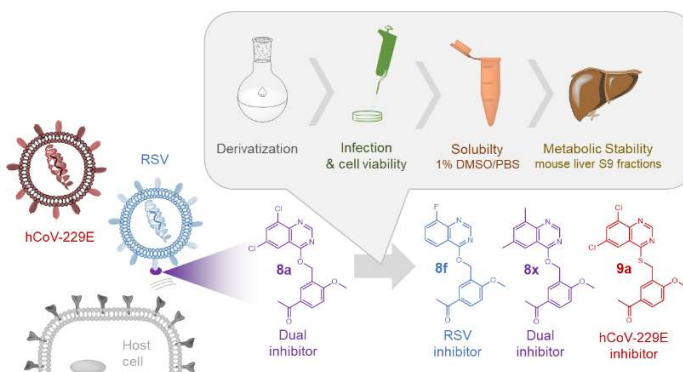[b]Saarland University, Department of Pharmacy, Campus Building E8.1, 66123 Saarbrücken, Germany.

[c]Institute for Experimental Virology, Twincore-Centre for Experimental and Clinical Infection Research, Feodor-Lynen-Str. 7, 30625 Hannover, Germany

[d]German Centre for Infection Research, Hanover-Braunschweig Site, Hanover, Germany

[e]Helmholtz International Lab for Anti-infectives

[f]Cluster of Excellence RESIST (EXC 2155), Hanover Medical School, Hanover, Germany

ABSTRACT: Acute respiratory diseases in humans can be caused by various viral pathogens such as respiratory syncytial virus (RSV), human coronavirus 229E (hCoV-229E), and severe acute respiratory syndrome coronavirus 2 (SARS-CoV-2). To prevent severe cases by an early treatment, one effective strategy is to inhibit viral infection at the entry stage of the replication cycle. However, there is a lack of efficient, FDA-approved small molecule drugs targeting these pathogens. Previously, we identified two dual RSV/hCoV-229E small molecule inhibitors with activity in the single-digit micromolar range. In this study, we focused on optimizing the more promising starting point using a multiparametric hit–optimization approach. Here, we present the results, including valuable insights into the structure–activity relationship (SAR), and report the discovery of a submicromolar RSV entry inhibitor and a highly potent compound against hCoV-229E.

INTRODUCTION

The COVID-19 pandemic has provided meaningful insights into the severity of viral infections and the consequences of rapid outbreaks and serious cases. In addition to coronaviruses, other viruses such as the respiratory syncytial virus (RSV) can also contribute significantly to severe infections. To mitigate such cases and facilitate early treatment, it is essential to inhibit viral replication. RSV infections pose a significant risk, particularly to young children, immune-suppressed individuals, and older people, often resulting in fatal and life-threatening cases.[1] One strategy for preventing RSV replication and mitigating severe cases involves drug development targeting specific steps in its replication cycle, such as the entry mechanism. RSV entry relies on the interaction between its fusion protein (F protein) and the attachment protein (G protein) with host cellular factors.[2–5] Specifically, the RSV-G protein attaches to the host cell surface, triggering a conformational change in the RSV-F protein from a pre-fusional to a post-fusional state, facilitating fusion with the host cell and subsequent entry. This conformational change can be obstructed by an inhibitor that binds to the central cavity of the trimeric preconformational F protein.[2] The characteristics of RSV F, including its pivotal role in viral infection initiation, high conservation of both subgroups, RSV-A and RSV-B,[6] and location in the virus particle's membrane[3] that enhances drug accessibility, have led to the development of numerous inhibitors, some of which have already advanced to clinical trials. Several promising examples of RSV entry inhibitors have emerged, including the optimized version of BMS-433771 (**1**), Rilematovir (**2**),[7]

1

Presatovir (**3**),[8] and Sisunatovir (**4**) (Figure 1).[9] These inhibitors have demonstrated *in vitro* activities ranging from nanomolar to picomolar concentrations. However, as of now, none of them has successfully completed all clinical trials. Some are still under investigation, such as compounds **2**[10,11] and **4**[12], while compound **3** did not meet the clinical trial requirements, specifically showing no efficacy in lower respiratory tract infections[13] and in patients with experimental RSV infection[14]. Currently, the only efficient FDA-approved drugs for RSV are the monoclonal antibodies Palivizumab (Synagis) and Nirsevimab (Beyfortus),[15–17] which target the F protein.
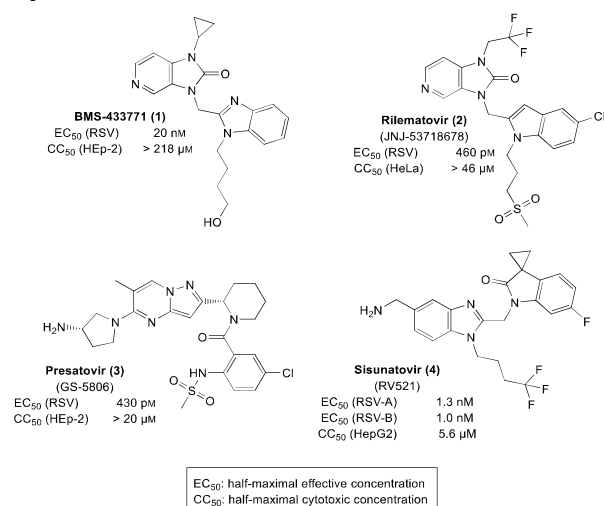

Figure 1: Examples of RSV entry inhibitors that reached clinical trials. EC_{50} and CC_{50} values derived from literature.[8,10–12]
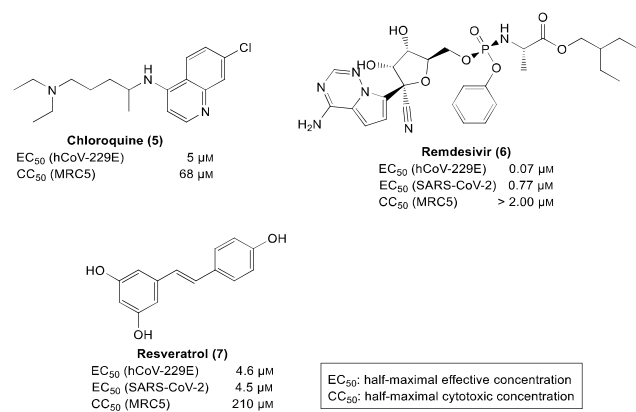

Figure 2: Examples of hCoV-229E and SARS-CoV-2 inhibitors. EC_{50} and CC_{50} values derived from literature.[25–27]

Human coronavirus 229E (hCoV-229E) and severe acute respiratory syndrome coronavirus 2 (SARS-CoV-2) are enveloped, single-stranded RNA viruses, similar to RSV. Nevertheless, they differ in the nature and structure of their surface proteins and the sense of their RNA.[18] While hCoV-229E typically causes mild cold-like symptoms and occasionally severe illness in the same susceptible groups as RSV,[19,20] SARS-CoV-2 is more acute in adults with risk factors such as advanced age or obesity,[21,22] compared to young children.[23] The spike protein (S protein) serves as the entry target for coronaviruses, analogous to the RSV-F protein.[2–5,18,24] It is a type I membrane glycoprotein consisting of two domains:

the receptor binding domain S1, responsible for attachment, and domain S2, which acts as the fusion protein facilitating viral entry.[4,5,24]

Various inhibitors have been discovered against coronaviruses through repurposing screenings (see Figure 2). For instance, the antimalarial drug chloroquine (**5**) inhibits hCoV-229E *in vitro* but only demonstrates activity against SARS-CoV-2 depending on the cell type.[28–30] Remdesivir (**6**), a broad-spectrum antiviral, shows inhibitory effects against both hCoV-229E and SARS-CoV-2,[29] although its efficacy against the latter is still uncertain.[31,32] Resveratrol (**7**) exhibits inhibitory activity against both 229E and SARS-CoV-2, as well as RSV, and shows the most favorable cell viability among these three inhibitors.[25,33] However, further investigation and optimization processes are necessary for resveratrol.[34]

The lack of cost-effective FDA-approved alternatives for RSV infection, along with the urgent need for inhibitors targeting human coronaviruses due to the severe consequences of the COVID-19 pandemic and as alternatives to vaccines, underscores the importance of developing small molecule antivirals.

Furthermore, the potential for combination therapies necessitates the exploration of surrogate compounds. In a recent screening campaign, we identified four promising hit compounds. Notably, two small molecules exhibited micromolar activity against RSV and hCoV-229E without significant cytotoxicity.[35] In this present study, we focused on one of these two compounds (compound 3)[35], which we had qualified as a RSV cell entry inhibitor. We chose this compound because of its dual inhibitory effect on RSV and hCoV-229E and its non-cytotoxic nature. Here, we report on a comprehensive study of this previous hit, designated compound **8a** (Figure 3). To shed light on its structure–activity relationships (SARs) gaining a deeper understanding of its function against RSV and hCoV-229E, we focused on its synthetic derivatization following a multiparametric optimization approach in terms of activity, cell viability, selectivity, solubility, and metabolic stability. Additionally, we evaluated the initial hit compound **8a**, as well as the most active hCoV-229E inhibitors, for their activity against SARS-CoV-2.

RESULTS AND DISCUSSION

To conduct virus-specific SAR studies on screening hit **8a** and its multiparametric optimization, we implemented a systematic and iterative workflow. This workflow involved the derivatization of hit **8a** using both commercially available and synthesized compounds, followed by the biological evaluation of these derivatives against two viruses, namely RSV and hCoV-229E.

In case of RSV, the biological evaluation involved a two-step infection experiment using a luciferase-expressing reporter virus and a host cell, expressing an alternative luciferase enzyme. Virus and compounds were added to these cells, and the first reading was conducted 24 h after application. This step 1 reading therefore determines effects on viral cell entry and RNA replication as well as potential cytotoxicity. The round 2 reading is taken after collecting the culture fluid from these infected cells (24 h post inoculation) and passing these together with residual compound on to naïve

2

cells. Therefore, the round 2 reading cumulates antiviral effects across this extended time duration. As passaging of culture fluids to naïve cells is involved, this round 2 reading can also reveal antiviral effects on late replication cycle steps such as for instance virus assembly and release. The primary objective was to analyze and improve the activity-cytotoxicity profile of starting point **8a**, with particular emphasis on its quinazoline moiety, as well as its linker and benzyl substituent (Figure 3).

8a

IC_{50} (RSV)	3.7 ± 1.1 µM
IC_{50} (hCoV-229E)	1.3 ± 0.6 µM
CC_{50} (HEp-2)	$> 62 \pm 19$ µM
CC_{50} (Huh-7.5)	> 10 µM

IC_{50}: half-maximal inhibitory concentration
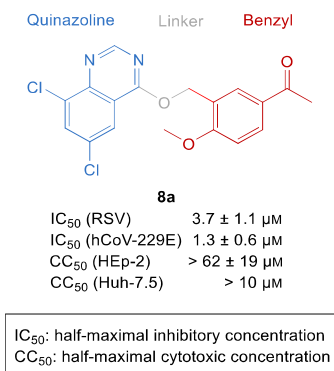CC_{50}: half-maximal cytotoxic concentration

Figure 3: Defined modification parts of starting point **8a** with corresponding activity and cell viability data.

To determine the most effective growth vector targeting RSV and investigate the preferred chlorine directions for addressing hCoV-229E, we first conducted chlorine scrambling experiments (**8b–e**, Table 1). Through this process, we identified position eight (**8b**) as a potential growth vector for the RSV inhibitor, demonstrating increased activity compared to parent compound **8a**, without any cytotoxic effects at compound concentrations up to 10 µM. The remaining positions exhibited either reduced activity, but still higher than the initial compound **8a** (**8e**), or were unfavorable during the initial infection round (**8c**, **8d**). In the second infection round, only position **8c** failed to meet the activity threshold of 25% infectivity, indicating that position seven is the least conducive for chlorine substituents. Determination of dose-dependent response confirmed this trend. Moreover, a differentiated profile against hCoV-229E could be verified here – all *mono*-substitution patterns (**8b-e**) led to decreased activities compared to **8a** on this pathogen. Hence, we started our further optimizations of the initial dual RSV/hCoV-229E inhibitor to develop more selective, promising inhibitors of RSV and hCoV-229E. In order to target RSV, while simultaneously controlling the impact on hCoV-229E, we initially focused on modifying the molecule in the chlorine direction that exhibited the most favorable results, specifically position eight (Table 1). Replacing the chlorine atom by other halogens, such as fluorine (**8f**) or bromine (**8g**), resulted in enhanced activity against RSV in both cases. Nevertheless, the introduction of fluorine demonstrated a greater improvement in activity compared to bromine, showing an activity in the submicromolar concentration range. Regarding hCoV-229E, the fluorine (**8f**) yielded in the same activity range similar to the 8-chloro substitution, while the bromine substituent (**8g**) diminished the activity against hCoV-229E when compared to **8a**. Interestingly, the bioisosteric replacement of the chlorine atom at position eight with a methyl group (**8h**) led to a
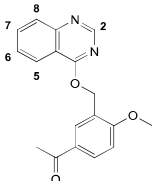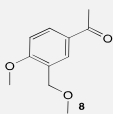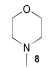
similar activity on both viruses as for the 8-chloro derivative, while the trifluoromethyl group (**8i**), decreased the activity against RSV tenfold in the first and twofold in the second infection round. An activity-decreasing effect of this substituent could also be observed for hCoV-229E.

Additionally, we investigated the effect of more electron-withdrawing groups such as ester **8j,** nitrile **8k** and sulfonylmethyl–functionalized derivative **8l**. The ester was only accepted in the second infection round showing an activity jump between the two RSV infection rounds. But, interestingly, the less bulky nitrile group was more favored than the bulky sulfonyl one having a comparable, strong, electron-withdrawing impact on the aromatic system. This derivative even enhanced the activity of initial hit **8a** reaching a similar activity range as the current frontrunner **8f**, but, unfortunately, showed cytotoxicity. Based on this result, we assumed that only small functionalities with a weak to strong electron-deficient effect are beneficial in position eight of the quinazoline to address RSV. To confirm this hypothesis, we also introduced electron-donating groups of different strength and size. Small, strong electron-donating groups such as hydroxyl (**8m**) and methoxy groups (**8n**) led to similar or no activity compared to initial hit **8a**. Here, it can be also concluded that proton-donating functions are much less tolerated than proton-accepting ones. Moreover, the bulky electron-donating functionalization implementing an aromatic benzyloxy group at position eight (**8o**) was less beneficial but still tolerated against RSV showing that there seems to be space for further growing from direction eight. The introduction of a flexible electron-donating, but also bulky morpholino group (**8p**) showed a slightly improved activity compared to **8a**. Unfortunately, this derivative was cytotoxic. Furthermore, we analyzed weak electron-donating groups such as cyclopropyl (**8q**), phenyl (**8r**) and 4-pyridyl (**8s**). Compared to starting point **8a**, all of these modifications were activity-wise tolerated but were not superior to the current frontrunner **8f**. In general, we can conclude that small electron-deficient groups are more favored than electron-donating ones in position eight to inhibit RSV. Nevertheless, also bulky motifs can be accepted at this position depending on their nature. Among the tested 8-modifications targeting RSV the best one was still fluoro derivative **8f**.

We found interesting antiviral-activity shifts between the two RSV infection rounds for some of the tested derivatives (most prominently for **8j** and **8r**). In both cases we observed a low activity of the compounds in the first-round infection assay, and more potency in the second round. The reason for this is currently unknown. It is possible that it results from preferential inhibition of late replication cycle steps such as for instance virus assembly and/or release. Alternatively, it is conceivable that this may result from accumulation of active compound or metabolites over longer periods of time. Upon examining the hCoV-229E results, none of the 8-modified derivatives exhibited improvements in comparison to the initial hit. This observation leads to the assumption that *mono*-substituted quinazolines are unsuitable motifs for addressing hCoV-229E.

In order to investigate the potential synergistic effect of the chlorine in positions five and eight against RSV, we focused also on *di*-substituted quinazolines (Table 2). Relocation of

3

Table 1. Activity and cell viability profiles of derivatives with *mono*-substituted quinazoline modifications compared to initial hit compound 8a.[a]
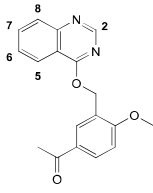

		RSV				HEp-2		hCoV-229E		Huh-7.5	
		% Inf		IC$_{50}$ [µM]		% CV	CC$_{50}$ [µM]	% Inf	IC$_{50}$ [µM]	% CV	CC$_{50}$ [µM]
		I	II	I	II						
8a[+]	6,8-di-Cl	22 ± 5[E]	10 ± 2[E]	3.7 ± 1.1[A]	1.0 ± 0.3[A]	104 ± 9[D]	> S[SI]	20 ± 10[I]	1.3 ± 0.6[A]	146 ± 88[H]	> 10
8b	8-Cl	16 ± 4	9 ± 1[A]	0.7	0.6	104 ± 2	> S[SI]	57 ± 20	n. d.	90 ± 6	n. d.
8c	7-Cl	62 ± 14	35 ± 6[A]	n. d.	n. d.	100 ± 5	n. d.	65 ± 25	n. d.	87 ± 6	n. d.
8d	6-Cl	50 ± 9	24 ± 5[A]	n. d.	n. d.	105 ± 7	n. d.	87 ± 25	n. d.	93 ± 3	n. d.
8e	5-Cl	31 ± 5	15 ± 6[A]	1.2	1.2	106 ± 3	> S[SI]	40 ± 17	n. d.	93 ± 3	n. d.
8f	8-F	15 ± 3	34 ± 40	0.3	0.9	97 ± 4	> 100	61 ± 14	n. d.	195 ± 11	n. d.
8g	8-Br	15 ± 7	8 ± 1	1.0	0.9	102 ± 5	> 20	42 ± 14	6.4	238 ± 68	> 10
8h	8-Me	18 ± 8	7 ± 0	0.6	1.0	104 ± 5	> 20	64 ± 12	n. d.	153 ± 31	n. d
8i	8-CF$_3$	22 ± 14	11 ± 2	3.0	1.9	102 ± 5	> 20	82 ± 16	n. d.	113 ± 17	n. d.
8j	8-COOMe	71 ± 9	25 ± 10	> 10	2.4	93 ± 4	> 100	72 ± 4	n. d.	88 ± 6	n. d.
8k	8-CN	12 ± 3	34 ± 36	0.4	0.4	108 ± 17	73.7	83 ± 8	n. d.	162 ± 15	n. d.
8l	8-SO$_2$Me	67 ± 7	83 ± 17	n. d.	n. d.	100 ± 1	n. d.	99 ± 7	n. d.	114 ± 9	n. d.
8m	8-OH	27 ± 8	27 ± 23	2.4	3.7	102 ± 5	> 20	66 ± 10	n. d.	188 ± 22	n. d.
8n	8-OMe	70 ± 13	61 ± 13	n. d.	n. d.	101 ± 3	n. d.	95 ± 3	n. d.	104 ± 4	n. d.
8o		63 ± 17	12 ± 9	4.0	4.0	92 ± 3	> 20	74 ± 8	n. d.	114 ± 6	n. d.
8p		14 ± 4	21 ± 30	1.2	0.6	97 ± 0	88.5	56 ± 8	12.4	160 ± 9	> 10
8q	8-cycloPr	24 ± 4	1 ± 0	4.6	0.9	96 ± 7	> 20	41 ± 14	9.0	149 ± 29	> 10
8r	8-Ph	75 ± 5	7 ± 2	> 10 (~ 16.3)	0.4	83 ± 8	> 20	78 ± 11	n. d.	97 ± 11	n. d.
8s[+]	8-(4-Pyr)	8 ± 5	0 ± 0	1.7	0.7	84 ± 5	> 20	42 ± 13	8.0	77 ± 12	> 10

[a]Infectivitiy (Inf), cell viability (CV) as well as half-maximal inhibitory (IC$_{50}$) and cytotoxic concentrations (CC$_{50}$) of the tested compounds are listed. For the RSV assay, the cells were infected in two rounds, round 1 (I) and round 2 (II). If not stated otherwise, impact on cell viability of Huh-7.5 cells was determined using FLuc activity measurement. Single-point measurements (counts (n) = 3) were performed at 10 µM compound concentration, otherwise the counts of experiments are marked according to the following legend: A: n = 2, B: n = 4, C: n = 5, D: n = 6, E: n = 7, F: n = 8, G: n = 9, H: n = 10, J: n = 11. Mean values and corresponding standard deviations (SD) of these single-point measurements are given. Dose-response analyses were done once if not described differently; for their counts the same legend as for the single-point measurements was applied. Furthermore, the following abbreviations were used: *: commercial compound; +: impact on viability was determined using MTT assay instead of FLuc activity; S: kinetic solubility in µM; SI: see supporting information (Table S45), n. d.: not determined; Ph: phenyl, Pyr: pyridyl, cycloPr: cyclopropyl.

6-chloro substitution to position five while keeping the second chlorine at its original position eight (**8t**) showed indeed a synergistic effect of 5- and 8-chloro-quinazoline substitutions against RSV. To explore additional impacts of chlorine positions on the inhibitor's activity against RSV, it was found that the original position eight (**8z**) was still the preferred chlorine direction compared to position seven (**8u**). Additional tendencies could be observed by the 8-chlorine-methyl-replacement retaining the original 6-chlorine substitution (**8v**), since this inhibitor was less active. Replacing both initial chlorine atoms bioisosterically in a separate (**8v–w**) or simultaneous manner (**8x**) with methyl
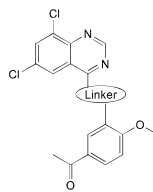
4

Table 2. Activity and cell viability profiles of quinazoline modifications with *di*-substitution patterns compared to initial hit 8a.[b]
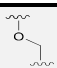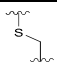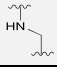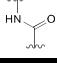

		RSV				HEp-2		hCoV-229E		Huh-7.5	
		% Inf		IC$_{50}$ [µM]		% CV	CC$_{50}$ [µM]	% Inf	IC$_{50}$ [µM]	% CV	CC$_{50}$ [µM]
		I	II	I	II						
8a	6,8-di-Cl	22 ± 5[E]	10 ± 2[E]	3.7 ± 1.1[A]	1.0 ± 0.3[A]	104 ± 9[D]	> S[SI]	20 ± 10[I]	1.3 ± 0.6[A]	146 ± 88[H]	> 10
8t	5,8-di-Cl	12 ± 5	3 ± 0	0.3	0.3	102 ± 6	> 20	72 ± 15	n. d.	177 ± 33	n. d.
8u	5,7-di-Cl	40 ± 12	13 ± 9	4.3	1.3	103 ± 3	> 20	65 ± 11	n. d.	199 ± 40	n. d.
8v	6-Cl-8-Me	36 ± 22	38 ± 8	n. d.	n. d.	105 ± 8	n. d.	40 ± 17	3.0	207 ± 28	> 10
8w	6-Me, 8-Cl	28 ± 4	14 ± 3	1.3	0.7	107 ± 5	> 20	17 ± 6	1.6	285 ± 79	> 10
8x	6,8-di-Me	31 ± 9	14 ± 1	2.7	0.9	105 ± 5	> 20	22 ± 10	2.1	247 ± 76	> 10

[b]Infectivity (Inf), cell viability (CV) as well as half-maximal inhibitory (IC$_{50}$) and cytotoxic concentrations (CC$_{50}$) of the tested compounds are listed. For the RSV assay the cells were infected in two rounds, round 1 (I) and round 2 (II). If not stated otherwise, impact on cell viability of Huh-7.5 cells was determined using FLuc activity measurement. Single-point measurements (counts (n) = 3) were performed at 10 µM compound concentration, otherwise the counts of experiments are marked according to the following legend: A: n = 2, B: n = 4, C: n = 5, D: n = 6, E: n = 7, F: n = 8, G: n = 9, H: n = 10, J: n = 11. Mean values and corresponding standard deviations (SD) of these single-point measurements are given. Dose-response analyses were done once if not described differently; for their counts the same legend as for the single-point measurements was used. Furthermore, the following abbreviations were used: *: commercial compound; +: impact on viability was determined using MTT assay instead of FLuc activity; S: kinetic solubility in µM; SI: see supporting information (Table S45), n. d.: not determined.

Table 3. Activity and cell viability profiles of linker modifications compared to initial hit 8a.[c]

		RSV				HEp-2		hCoV-229E		Huh-7.5	
		% Inf		IC$_{50}$ [µM]		% CV	CC$_{50}$ [µM]	% Inf	IC$_{50}$ [µM]	% CV	CC$_{50}$ [µM]
		I	II	I	II						
8a[+]		22 ± 5[E]	10 ± 2[E]	3.7 ± 1.1[A]	1.0 ± 0.3[A]	104 ± 9[D]	> S[SI]	20 ± 10[I]	1.3 ± 0.6[A]	146 ± 88[H]	> 10
9a[+]		93 ± 14	41 ± 16[A]	n. d.	n. d.	96 ± 2	n. d.	3 ± 1	0.08	84 ± 6	> 10
9b[+]		29 ± 24	0 ± 0[A]	8.00	1.54	71 ± 6	58.4	7 ± 2	1.73	69 ± 4	> 10
9c		78 ± 9	72 ± 47	n. d.	n. d.	94 ± 2	n. d.	103 ± 4	n. d.	121 ± 16	n. d.

[c]Infectivity (Inf) and cell viability (CV) as well as half-maximal inhibitory (IC$_{50}$) and cytotoxic concentrations (CC$_{50}$) of the tested compounds are listed. For the RSV assay the cells were infected in two rounds, round 1 (I) and round 2 (II). If not stated otherwise, impact on cell viability of Huh-7.5 cells was determined using FLuc activity measurement. Single-point measurements (counts (n) = 3) were performed at 10 µM compound concentration, otherwise the counts of experiments are marked according to the following legend: A: n = 2, B: n = 4, C: n = 5, D: n = 6, E: n = 7, F: n = 8, G: n = 9, H: n = 10, J: n = 11. Mean values and corresponding standard deviations (SD) of these single-point measurements are given. Dose-response analyses were done once if not described differently; for their counts the same legend as for the single-point measurements was used. Furthermore, the following abbreviations were used: *: commercial compound; +: impact on viability was determined using MTT assay instead of FLuc activity; S: kinetic solubility in µM; SI: see supporting information (Table S45); n. d.: not determined.

groups, decreased (**8v**), improved (**8w**) or kept the original activity (**8x**) of hit **8a**. Additionally, the bio-isosteric replacements (**8v–x**) retained the original dual inhibitory effect**.** That derivative **8v** was not as active as **8w** and **8x** on RSV underlines the afore discussed importance of an electron-deficient group at position eight**.**

Since positions five and seven were – besides position eight – the most favorable *mono*-chloro substitution patterns against hCoV-229E, we tested both combinations, 5,8- and 5,7-dichloro derivatives (**8t–u**, Table 2). Unexpectedly, the relocation of the initial 6-chlorine atom to position five (**8t**) abrogated the antiviral activity and also the 5,7-dichloro derivative (**8u**) showed no viral inhibitory effect indicating that the 6-chloro substitution is essential for the activity against the coronavirus. Bioisosteric replacements of the original chlorine atoms (**8v–x**) were – in comparison to **8a** – in general tolerated, but position eight (**8v**) seems to be more sensitive to this modification resulting in a slightly decreased activity against hCoV-229E compared to derivatives **8w** and **8x**. Based on these results, it can be inferred that both chlorine substituents are replaceable with methyl groups and retained the initial dual inhibitory character, for compound **8x** even with similar activity compared to starting point **8a**.

Following the comprehensive analysis of the quinazoline moiety, we proceeded to modify the linker part as well. Introducing a sulfide linker (**9a**, Table 3) resulted in a significant decrease in activity against RSV, with no observed cytotoxicity at a compound concentration of 10 μM. However, this modification greatly improved the inhibition of hCoV-229E, yielding a highly active inhibitor of 80 nM activity. The introduction of an amine linker (**9b**) resulted in a notable shift in activity between the two rounds of RSV infection, and was found to be effective against hCoV-229E but it also showed increased cytotoxicity. To potentially reduce this cytotoxicity, enhance solubility and assess the significance of linker flexibility, we replaced the amine linker with an amide function (**9c**). Unfortunately, this modification led to a loss of activity against both viruses, RSV and hCoV-22E.

Lastly, we modified the benzyl moiety of our initial hit **8a**. In order to assess the acceptance and functionality of specific moieties in this part, we initially tested readily accessible compounds with *mono*-substituted benzyl groups (Table 4) while keeping the remaining part of the molecule constant. As a reference point, we selected the simplified derivative **10a**, lacking both functionalities, the 2-methoxy and the 5-acetyl group. This simplification resulted in a decrease of activity against both RSV and hCoV-229E viruses. Following the aforementioned simplification, we analyzed the impact of different substitution patterns on the benzylic moiety, specifically examining *ortho*-, *meta*-, and *para*-substitution patterns. For the *ortho*-substitution patterns (**10b–k**, Table 4), we observed, that a removal of the 5-acetyl group while only retaining the 2-methoxy group (**10b**) led to a loss of RSV inhibition, whereas it was tolerated in terms of hCoV-229E inhibition.
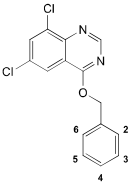
Generally, *ortho*-decorated benzyl derivatives were less accepted for RSV inhibition than the initial *di*-substitution pattern of **8a**. However, certain tendencies regarding RSV inhibition were noted: The elongation of the methoxy group (**10c**) as well as its replacement by an electron-deficient

acetyl (**10d**) or electron-donating ethyl group (**10e**) in *ortho*-position showed similar results compared to the initial methoxy group (**10b**). But, electron-deficient functionalities such as fluorine (**10f**) and bromine (**10g**) as well as more bulky motifs such as phenyl (**10j**) and 3-pyridyl (**10k**) led to improvements in activity. Notably, the most significant increase in activity compared to the *mono*-substituted methoxy derivative **10b** was observed for the introduction of the 3-pyridyl group (**10k**), although this compound was less active than our starting point **8a**. Furthermore, we decorated the benzyl moiety with methyl ester (**10h**) and carboxy group (**10i**). Unfortunately, these moieties did not show any enhancement in RSV activity.

For hCoV-229E, we observed that simplification of the methoxy group (**10b**) to a weaker electron-donating ethyl moiety (**10e**) led to an activity loss. Keeping the electron-deficient acetyl group (**10d**) impaired the activity as well. The introduction of halogens such as fluorine (**10f**) and bromine (**10g**) exhibited lower acceptance compared to the methoxy group. However, it is worth noting that bromine was more tolerated than fluorine, displaying a decrease in activity within a similar range as the acetyl group (**10d**). A similar trend could be observed with methyl ester (**10h**) and carboxy group (**10i**). Furthermore, aromatic systems such as phenyl (**10j**) and 3-pyridyl (**10k**) were introduced in 2-position, but were also not tolerated. Based on these results, we concluded that probably only very small electron-donating groups are favored in *ortho*-position to address hCoV-229E. A clear differentiation between the profile of RSV- and 22E-targeting compounds became clear also here. Taking the *meta*-mono-substitutions of the benzyl moieties (**10l–n**, Table 4) into account, we observed that the highest RSV inhibition was obtained for the electron-donating methoxy group (**10m**) compared to unsubstituted benzyl derivative **10a**. Notably, excluding the *ortho*-methoxy group while retaining the electron-withdrawing *meta*-acetyl group (**10l**) resulted in a complete loss of activity against RSV. For CoV-229E, the methoxy group showed the most promising results of the *meta*-substituents and was even more favored than the unsubstituted compound **10a**, although the *ortho*-direction (**10b**) was slightly more beneficial. Conversely, the introduction of an electron-deficient carboxy group in *meta*-position (**10n**) was unfavorable for both viruses. Furthermore, a couple of *para*-substituted benzylic modifications were tested (**10o–w**, Table 4). Among them, the derivative featuring a nitrile group (**10u**) emerged as the most beneficial in terms of addressing RSV. Regarding the hCoV-229E results, it is noteworthy that the methyl group (**10s**) in this position was well tolerated even in the absence of an *ortho*-methoxy group. Moreover, the methyl group was significantly more beneficial than its bioisostere chlorine (**10p**) which can be attributed to its electron-donating character since all other substituents with electron-withdrawing (**10u–q**, **10t–w**) or strong electron-donating (**10r**) properties were less favored.

In parallel to the *mono*-substitution studies, we also analyzed *di*-substituted benzyl derivatives aiming at a deeper SAR study and gaining ideas for further benzylic optimizations. Thereby, we simplified each original functionality separately and investigated position-dependent synergistic effects of the original di-substitution pattern present in
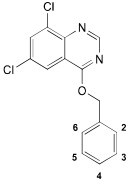
6

Table 4. Activity and cell viability profiles of *mono*-substituted and simplified benzyl changes compared to initial hit 8a.[d]

| | | RSV | | | | HEp-2 | | hCoV-229E | | Huh-7.5 | |
| | | % Inf | | IC$_{50}$ [μM] | | % CV | CC$_{50}$ [μM] | % Inf | IC$_{50}$ [μM] | % CV | CC$_{50}$ [μM] |
		I	II	I	II						
8a[+]	2-OMe, 5-Ac	22 ± 5[E]	10 ± 2[E]	3.7 ± 1.1[A]	1.0 ± 0.3[A]	104 ± 9[D]	> S[SI]	20 ± 10[I]	1.3 ± 0.6[A]	146 ± 88[H]	> 10
10a*	-	58 ± 23	37 ± 24	n. d.	n. d.	94 ± 4	n. d.	41 ± 8[C]	n. d.	92 ± 7[B]	n. d.
10b[+]	2-OMe	96 ± 21	68 ± 33[A]	n. d.	n. d.	100 ± 2	n. d.	2 ± 1	2.1	95 ± 4	> 10
10c	2-(O(CH$_2$)$_2$OCH$_3$)	64 ± 11[P]	54 ± 29[P]	n. d.	n. d.	91 ± 11[P]	n. d.	35 ± 10[P]	3.2	230 ± 32[P]	> 5[P]
10d	2-Ac	76 ± 36	55 ± 8	n. d.	n. d.	100 ± 5	n. d.	42 ± 15	9.8	220 ± 47	> 10
10e	2-Et	73 ± 29	63 ± 5	> 5[P]	> 5[P]	98 ± 2	> 5[P]	66 ± 11	n. d.	199 ± 35	n. d.
10f*	2-F	59 ± 4	31 ± 10	n. d.	n. d.	91 ± 4	n. d.	35 ± 8	5.6	109 ± 27	> 10
10g	2-Br	72 ± 8	45 ± 27	n. d.	n. d.	98 ± 4	n. d.	81 ± 11	n. d.	244 ± 20	n. d.
10h	2-COOMe	53 ± 37[P]	51 ± 40[P]	n. d.	n. d.	89 ± 12[P]	n. d.	83 ± 14[P]	n. d.	154 ± 17[P]	n. d.
10i	2-COOH	87 ± 28	125 ± 16	n. d.	n. d.	100 ± 3	n. d.	101 ± 3	n. d.	114 ± 6	n. d.
10j	2-Ph	50 ± 13	44 ± 10	> 5[P]	> 5[P]	95 ± 6[P]	> 5[P]	79 ± 9[P]	n. d.	128 ± 13[P]	n. d.
10k	2-(3-Pyr)	39 ± 4	8 ± 2	~6.1	1.8	101 ± 3	> 20	70 ± 9	n. d.	159 ± 30	n. d.
10l	3-Ac	129 ± 10	62 ± 25	n. d.	n. d.	105 ± 10	n. d.	74 ± 19	n. d.	92 ± 12	n. d.
10m*[+]	3-OMe	57 ± 19	38 ± 23	n. d.	n. d.	97 ± 7	n. d.	18 ± 5[C]	3.1	94 ± 7[b]	> 10
10n	3-COOH	126 ± 2	108 ± 39[A]	n. d.	n. d.	100 ± 11	n. d.	117 ± 22	n. d.	100 ± 3	n. d.
10o	4-F	87 ± 2[P]	88 ± 15[P]	n. d.	n. d.	96 ± 10[P]	n. d.	49 ± 13[P]	7.8	256 ± 44[P]	> 5[P]
10p	4-Cl	94 ± 2[P]	120 ± 22[P]	n. d.	n. d.	85 ± 5[P]	n. d.	85 ± 5[P]	> 5[P]	96 ± 10[P]	> 5[P]
10q*	4-Br	72 ± 15	73 ± 18	n. d.	n. d.	67 ± 2	n. d.	45 ± 12[C]	n. d.	85 ± 11[B]	n. d.
10r	4-OMe	90 ± 9	113 ± 28	n. d.	n. d.	101 ± 3	n. d.	83 ± 6	n. d.	162 ± 15	n. d.
10s	4-Me	86 ± 59[P]	83 ± 7[P]	> 5[P]	> 5[P]	83 ± 9[P]	> 5[P]	23 ± 9[P]	1.7	272 ± 49[P]	> 5[P]
10t	4-CF$_3$	79 ± 5[P]	107 ± 26[P]	n. d.	n. d.	94 ± 10[P]	n. d.	58 ± 33[P]	n. d.	171 ± 59[P]	n. d.
10u*	4-CN	59 ± 14	38 ± 26	n. d.	n. d.	101 ± 5	n. d.	67 ± 17[C]	n. d.	103 ± 5[B]	n. d.
10v*	4-COOH	77 ± 26	66 ± 38	n. d.	n. d.	96 ± 4	n. d.	97 ± 9[C]	n. d.	98 ± 8[B]	n. d.
10w*	4-COOMe	120 ± 9	110 ± 24	n. d.	n. d.	98 ± 2	n. d.	93 ± 7	n. d.	111 ± 20	n. d.

[d]Infectivity (Inf) and cell viability (CV) as well as half-maximal inhibitory (IC$_{50}$) and cytotoxic concentrations (CC$_{50}$) of the tested compounds are listed. For the RSV assay the cells were infected in two rounds, round 1 (I) and round 2 (II). If not stated otherwise, impact on cell viability of Huh-7.5 cells was determined using FLuc activity measurement. Single-point measurements (counts (n) = 3) were performed at 10 μM compound concentration, otherwise the counts of experiments are marked according to the following legend: A: n = 2, B: n = 4, C: n = 5, D: n = 6, E: n = 7, F: n = 8, G: n = 9, H: n = 10, J: n = 11. Mean values and corresponding standard deviations (SD) of these single-point measurements are given. Dose-response analyses were done once if not described differently; for their counts the same legend as for the single-point measurements was used. Furthermore, the following abbreviations were used: *: commercial compound; +: impact on viability was determined using MTT assay instead of FLuc activity; S: kinetic solubility in μM; SI: see supporting information (Table S45); n. d.: not determined; P: Precipitation at 10 μM, measurement at 5 μM compound concentration in this and further analyses.

7

Table 5. Activity and cell viability profiles of *di*-substituted benzyl modifications compared to initial hit 8a.[e]

		RSV				HEp-2		hCoV-229E		Huh-7.5	
		% Inf		IC$_{50}$ [µM]		% CV	CC$_{50}$ [µM]	% Inf	IC$_{50}$ [µM]	% CV	CC$_{50}$ [µM]
		I	II	I	II						
8a[+]	2-OMe, 3-Ac	22 ± 5^E	10 ± 2^E	3.7 ± 1.1^A	1.0 ± 0.3^A	104 ± 9^D	$> S^{SI}$	20 ± 10^I	1.3 ± 0.6^A	146 ± 88^H	> 10
10x	2-OMe, 5-Et	63 ± 23	48 ± 46	n. d.	n. d.	90 ± 12	n. d.	29 ± 10	5.4	273 ± 27	> 10
10y	2-Et, 5-Ac	56 ± 11	32 ± 12	n. d.	n. d.	103 ± 2	n. d.	44 ± 6	n. d.	233 ± 45	n. d.
10z	2-OMe, 3-Ac	91 ± 19	48 ± 37	n. d.	n. d.	99 ± 3	n. d.	86 ± 8	n. d.	170 ± 10	n. d.
10aa	2-OMe, 4-Ac	62 ± 12	8 ± 0	> 10 ~ 13.3	2.1	103 ± 4	> 20	31 ± 11	4.9	193 ± 58	> 10
10ab	2-OMe, 6-Ac	109 ± 50	42 ± 13	n. d.	n. d.	101 ± 5	n. d.	49 ± 11	n. d.	267 ± 53	n. d.
10ac	3-OMe, 5-Ac	81 ± 22	48 ± 12	n. d.	n. d.	105 ± 5	n. d.	46 ± 9	n. d.	277 ± 50	n. d.
10ad	4-OMe, 5-Ac	78 ± 8	49 ± 1	n. d.	n. d.	101 ± 4	n. d.	29 ± 6	2.7	211 ± 44	> 10

[e]Infectivity (Inf) and cell viabilitiy (CV) as well as half-maximal inhibitory (IC$_{50}$) and cytotoxic concentrations (CC$_{50}$) of the tested compounds are listed. For the RSV assay the cells were infected in two rounds, round 1 (I) and round 2 (II). If not stated otherwise, impact on cell viability of Huh-7.5 cells was determined using FLuc activity measurement. Single-point measurements (counts (n) = 3) were performed at 10 µM compound concentration, otherwise the counts of experiments are marked according to the following legend: A: n = 2, B: n = 4, C: n = 5, D: n = 6, E: n = 7, F: n = 8, G: n = 9, H: n = 10, J: n = 11. Mean values and corresponding standard deviations (SD) of these single-point measurements are given. Dose-response analyses were done once if not described differently; for their counts the same legend as for the single-point measurements was used. Furthermore, the following abbreviations were used: *: commercial compound; +: impact on viability of Huh-7.5 was determined using MTT assay instead of FLuc activity; S: kinetic solubility in µM; SI: see supporting information (Table S45); n. d.: not determined; Ph: phenyl, Pyr: pyridyl.
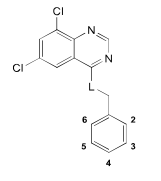
initial hit compound **8a** (Table 5). First, we checked relevance of oxygen atoms for the activity and replaced the corresponding functionalities consecutively by an ethyl group (**10x** and **10y**). In both cases, we figured out that the oxygen is important for the activity either because of electronic or proton-accepting reasons. In accordance to the results from the *ortho*- and *meta-mono*-substitutions, the first reason is the more probable one. Next, we performed a scrambling of the acetyl and methoxy group keeping constant the respective other group to evaluate the most promising directions for *di*-substitution patterns (**10z–10ad**, Table 5). This analysis led to the result, that the original 2-methoxy-5-acetyl-substitution pattern (**8a**) is the most favored one to address RSV. For hCoV-229E, we observed that all these tested combinations of the acetyl-methoxy-scrambling were less active than the starting point, but did not lead to such a clear disacceptance as against RSV. This finding speaks for a stronger direct interaction on RSV than on hCoV-229E and underlined the announced differentiated profile of RSV and hCoV-229E.
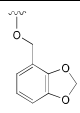
Taking our knowledge from the *mono-* and *di*-substitution studies into account, we created a couple of combi-derivatives around the benzylic moiety (Table 6).

To address RSV selectively, we used the observed activity-improving tendency from the *mono*-substitution patterns (see Table 4) for the design of a *di*-substitution pattern. Since the 3-pyridyl group in position two of the benzylic moiety was the most promising one among the 2-modifications, we combined this functionality with the original acetyl group (**10ae**, Table 5). Unfortunately, this combi-derivative was inactive either because the additional 5-acteyl group is not accepted in a different mode of action that was maybe induced by the 3-pyrodinyl group (**10k**) or because tendencies of *mono*-substitution patterns cannot be translated to *di*-substitution patterns. Furthermore, we investigated the inhibitors' behavior combining different moieties that showed promising tendencies in single-substitution patterns against hCoV-229E. Adding a second methoxy group in 6-position (**10ab**) to the 2-methoxy-substituted derivative **10b** resulted in no improvement compared to the *mono*-substituted version. Instead, the 229E selective profile was even weaker for compound **10ab** than for **10b**.

8

Table 6. Activity and cell viability profiles of combi derivatives from most promising *mono*-substitution patterns compared to initial hit 8a.[f]

| | | RSV | | | | HEp-2 | | hCoV-229E | | Huh-7.5 | |
| | | % Inf | | IC$_{50}$ [μM] | | | | | | | |
		I	II	I	II	% CV	CC$_{50}$ [μM]	% Inf	IC$_{50}$ [μM]	% CV	CC$_{50}$ [μM]
8a[+]	2-OMe, 3-Ac	22 ± 5[E]	10 ± 2[E]	3.7 ± 1.1[A]	1.0 ± 0.3[A]	104 ± 9[D]	> S[SI]	20 ± 10[I]	1.3 ± 0.6[A]	146 ± 88[H]	> 10
10ae	2-(3-Pyr), 5-Ac	53 ± 8	63 ± 34	n. d.	n. d.	101 ± 1	n. d.	91 ± 2	n. d.	119 ± 5	n. d.
10af	L = O, 2-OMe, 6-OMe	63 ± 20	40 ± 4	n. d.	n. d.	100 ± 5	n. d.	18 ± 11	1.9	374 ± 94	> 10
10ag	(structure)	86 ± 27	65 ± 8	n. d.	n. d.	87 ± 6	n. d.	15 ± 9	0.7	307 ± 79	> 10
10b2	L = S, 2-OMe	61 ± 11	35 ± 10	n. d.	n. d.	93 ± 2	n. d.	1 ± 0	0.3	333 ± 50	> 10

[f]Infectivity (Inf) and cell viability (CV) as well as half-maximal inhibitory (IC$_{50}$) and cytotoxic concentrations (CC$_{50}$) of the tested compounds are listed. For the RSV assay the cells were infected in two rounds, round 1 (I) and round 2 (II). If not stated otherwise, impact on cell viability of Huh-7.5 cells was determined using FLuc activity measurement. Single-point measurements (counts (n) = 3) were performed at 10 μM compound concentration, otherwise the counts of experiments are marked according to the following legend A: $n = 2$, B: $n = 4$, C: $n = 5$, D: $n = 6$, E: $n = 7$, F: $n = 8$, G: $n = 9$, H: $n = 10$, J: $n = 11$. Mean values and corresponding standard deviations (SD) of these single-point measurements are given. Dose-response analyses were done once if not described differently; for their counts the same legend as for the single-point measurements was used. Furthermore, the following abbreviations were used: *: commercial compound; +: impact on viability of Huh-7.5 was determined using MTT assay instead of FLuc activity; S: kinetic solubility in μM; SI: see supporting information (Table S45); n. d.: not determined.

Since positions two and three were accepted for the methoxy group (see derivatives **10b** and **10m**, Table 4) a combined derivative was created having a rigid, cyclic dimethoxy moiety (**10am**, Table 6). This compound showed a slight improvement in terms of anti-hCoV-229E activity compared to the *mono*-substituted 2-methoxy analogue **10b** and preserved its selective profile. Merging the promising thio-linker with the 2-methoxy-*mono*-substituted benzyl derivative (**10b2**) confirmed the strong influence of the sulfide on hCoV-229E since it led to an improved activity towards starting point **8a** but did not overcome 229E frontrunner **9a**. Therefore, we excluded an additive SAR at this point.

SARS-CoV-2 activity. To evaluate the potential inhibitory effects of the most promising hCoV-229E inhibitors, including the initial hit **8a**, against SARS-CoV-2, we conducted tests on Calu-3 cells infected with SARS-CoV-2. Unfortunately, our findings revealed that neither the dual RSV/hCoV-229E inhibitor **8a** nor its highly active analogue **9a**, which is selective for hCoV-229E, exhibited efficacy against the novel coronavirus (data not shown). Nevertheless, this scaffold presents an intriguing avenue for the development of inhibitors targeting other coronaviruses.

Absorption, distribution, metabolism, and excretion (ADME) studies. In order to assess the concentration limits of the compounds for conducting the biological assays, as well as their solubility as a physicochemical property within the multiparametric optimization approach, we determined the kinetic solubilities of all substances tested in this study (Tables S45-S50).

The solubility results of selective RSV inhibitors that reached an infection maximum of 25% are additionally summarized and compared to parent compound **8a** in Table 7. Interestingly, two (**8f** and **8k**) of our three (**8f**, **8k** and **8t**) most active RSV inhibitors showed improved solubility of more than 100 μM in 1% DMSO/PBS. Since **8f** was in contrast to **8k** not cytotoxic on HEp-2 cells, this selective inhibitor turned out to be the most promising one in terms of four optimization parameters: activity, cytotoxicity, selectivity, and solubility.

Furthermore, we conducted a more detailed examination of the selective hCoV-229E inhibitors (see Table 8). Regrettably, the most active compounds (**9a**, **10b2**, and **10ag**) exhibited even poorer solubility compared to the starting point **8a**. Notably, none of the selective hCoV-229E inhibitors demonstrated improved solubility.

9

Table 7. Kinetic solubilities (S) and activity/cell viability profiles of selective RSV inhibitors compared to initial dual RSV/hCoV-229E inhibitor 8a.[g]

Cp	RSV		HEp-2	S [μM]
	IC$_{50}$ [μM]		CC$_{50}$ [μM]	1% DMSO/ PBS
	I	II		
8a	3.7 ± 1.1[A]	1.0 ± 0.3[A]	> S	62 ± 19
8b	0.7	0.6	> S	58 ± 1
8e	1.2	1.2	> S	54 ± 9
8f	0.3	0.9	> 100	> 100
8h	0.6	1.0	> 20	57 ± 5
8i	3.0	1.9	> 20	33 ± 2
8m	2.4	3.7	> 20	55 ± 26
8o	4.0	4.0	> 20	53 ± 9
8j	> 10	2.4	> 100	> 100
8k	0.4	0.4	73.7	> 100
8r	> 10 (~ 16.3)	0.4	> 20	35 ± 2
8t	0.3	0.3	> 20	37 ± 17
8u	4.3	1.3	> 20	41 ± 2
10k	~6.1	1.8	> 20	60 ± 9

[g]Half-maximal inhibitory (IC$_{50}$) and cytotoxic concentrations (CC$_{50}$) as well as kinetic solubilities (S) of the tested compounds (Cp) are listed. The cells were infected in two rounds, round 1 (I) and round 2 (II). Solubility experiments were performed in triplicates (*n* = 3), otherwise the count of experiments is marked with A for *n* = 2. Mean values and corresponding standard deviations (SD) of the experiments are given. Dose-response analyses were done once if not described differently; for their counts the same legend as described beforehand was applied. Furthermore, the following abbreviations were used: *: commercial compound.

Regarding the dual RSV/hCoV-229E inhibitors (Table 9) we unexpectedly enhanced the solubility by substituting both chlorine atoms with methyl groups (**8x**). This improved solubility can be attributed to the disruption of molecular planarity, resulting in easier disruption of crystal packing and consequently increasing the compounds' solubility.[36,37] Despite the improved solubility, the derivative exhibited retained activity against RSV and a slightly impaired inhibitory effect on hCoV-229E compared to the initial hit **8a**. Thus, it can be regarded as an optimized dual inhibitor. Additionally, compound **9b**, which maintained activity against hCoV-229E, exhibited higher solubility than the starting point due to the presence of an amine function substituting the initial ether linkage.

Table 8. Kinetic solubilities (S) and activity/cell viability profiles of selective hCoV-229E inhibitors compared to initial dual RSV/hCoV-229E inhibitor 8a.[h]

Cp	hCoV-229E	Huh-7.5	S [μM]
	IC$_{50}$ [μM]	CC$_{50}$ [μM]	1% DMSO/ PBS
8a[+]	1.3 ± 0.6[A]	> 10	62 ± 19
8v	3.0	> 10	50 ± 6[C]
9a[+]	0.08	> 10	17 ± 4
10b[+]	2.1	> 10	32 ± 11
10m*[+]	3.1	> 10	22 ± 2
10p	7.0	> 5	18 ± 4
10s	1.7	> 5	12 ± 6
10x	5.4	> 10	34 ± 7
10af	1.9	> 10	21 ± 1
9a	0.08	> 10	17 ± 4
10b2	0.3	> 10	24 ± 10
10ag	0.7	> 10	21 ± 2

[h]Half-maximal inhibitory (IC$_{50}$) and cytotoxic concentrations (CC$_{50}$) as well as kinetic solubilities (S) of the tested compounds (Cp) are listed. The cells were infected in two rounds, round 1 (I) and round 2 (II). If not stated otherwise, impact on cell viability of Huh-7.5 cells was determined using FLuc activity measurement. Solubility experiments were performed in triplicates (*n* = 3), otherwise the counts of experiments are marked according to the following legend: A: *n* = 2, C: *n* = 4.. Mean values and corresponding standard deviations (SD) of the experiments are given. Dose-response analyses were done once if not described differently; for their counts the same legend as described beforehand was applied. Furthermore, the following abbreviations were used: *: commercial compound; +: impact on viability of Huh-7.5 was determined using MTT assay instead of FLuc activity.

Metabolic stability. In our ADME studies, we examined the metabolic stability of the most active compounds against RSV and hCoV-229E, in addition to the solubility optimization parameter. These analyses were performed using mouse liver S9 fractions, and the results are presented in Tables S7–9. To facilitate the comparison of our initial frontrunners, namely compounds **8f**, **8t**, **8k**, **9a**, **10b2**, **10ag**, and **8x**, we have summarized their respective metabolic stability results in Table 10.

The analysis conducted revealed that most of the quinazoline-modified RSV inhibitors exhibited higher metabolic stability compared to the initial hit (refer to Table S51). Notably, the *mono*-cyano-substituted analogue **8k** demonstrated the highest metabolic stability.

10

Table 9. Kinetic solubilities (S) of dual hCoV-229E/RSV inhibitors compared to dual RSV/hCoV-229E inhibitor 8a.[i]

Cp	RSV IC$_{50}$ [μM]		HEp-2 CC$_{50}$ [μM]	hCoV-229E IC$_{50}$ [μM]	Huh-7.5 CC$_{50}$ [μM]	S [μM] 1% DMSO/PBS
	I	II				
8a[+]	3.7 ± 1.1[A]	1.0 ± 0.3[A]	> S	1.3 ± 0.6[A]	> 10	62 ± 19
8g	1.0	0.9	> 20	6.4	> 10	41 ± 10
8p	1.2	0.6	88.5	12.4	> 10	> 100
8q	4.6	0.9	> 20	9.0	> 10	27 ± 4
8s[+]	1.7	0.7	> 20	8.0	> 10	32 ± 5
8w	1.3	0.7	> 20	1.6	> 10	66 ± 2
8x	2.7	0.9	> 20	2.1	> 10	> 100[B]
9b[+]	8.00	1.54	58.4	1.73	> 10	> 100
10aa	> 10 ~ 13.3	2.1	> 20	4.9	> 10	26 ± 6

[i]Half-maximal inhibitory (IC$_{50}$) and cytotoxic concentrations (CC$_{50}$) as well as kinetic solubilities (S) of the tested compounds (Cp) are listed. The cells were infected in two rounds, round 1 (I) and round 2 (II). If not stated otherwise, impact on cell viability of Huh-7.5 cells was determined using FLuc activity measurement. Solubility experiments were performed in triplicates (n = 3), otherwise the count of experiments is marked with A for n = 2. Mean values and corresponding standard deviations SD of these single-point measurements are given. Dose-response analyses were done once if not described differently; for their counts the same legend as described beforehand was applied. Furthermore, the following abbreviations were used: *: commercial compound; [+]: impact on viability of Huh-7.5 was determined using MTT assay instead of FLuc activity
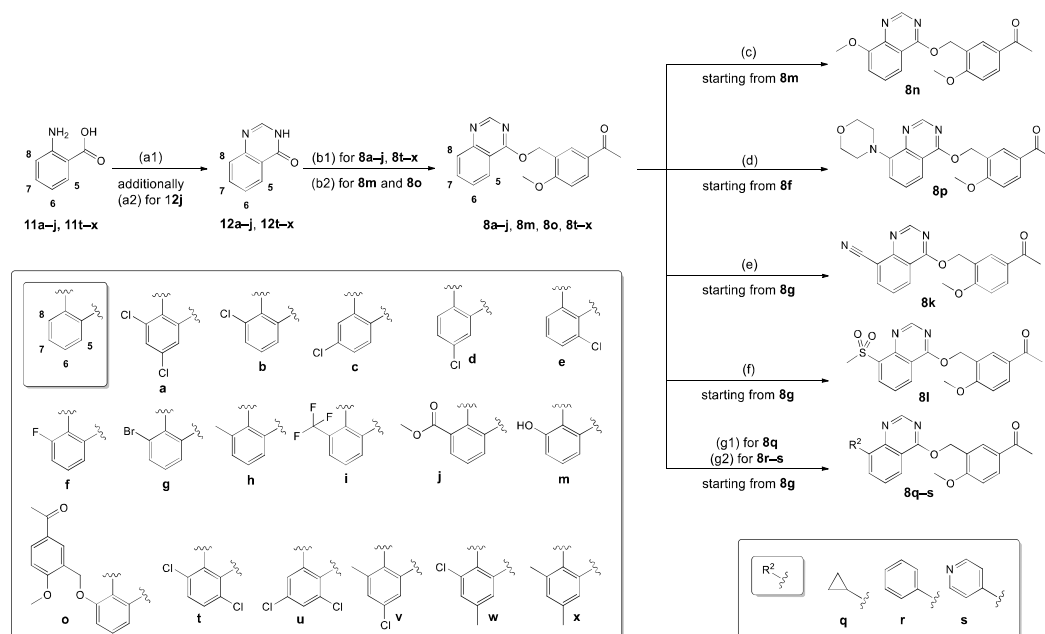
Table 10. Metabolic stability of most promising selective and dual inhibitors against RSV and hCoV-229E.

Cp	t$_{1/2}$ [min]	Cl$_{int}$ [μL/mg/min]
8a	3.4 ± 0.3	203.0 ± 15.0
Selective RSV inhibitors		
8f	24.8 ± 4.7	28.6 ± 5.4
8k	55.9 ± 6.7	12.5 ± 1.6
8t	11.0 ± 1.2	63.7 ± 7.1
Selective hCoV-229E inhibitors		
9a	7.1 ± 0.7	98.6 ± 10.2
10b2	9.9 ± 6.2	88.0 ± 55.0
10ag	5.9 ± 0.4	118.0± 6.6
Dual RSV/hCoV-229E inhibitor		
8x	7.0 ± 0.4	99.8 ± 3.1

[a]Half-life (t$_{1/2}$) and intrinsic clearance (Cl$_{int}$) of the tested compounds (Cp) are listed. Duplicates were performed. Mean values and corresponding SD are given.
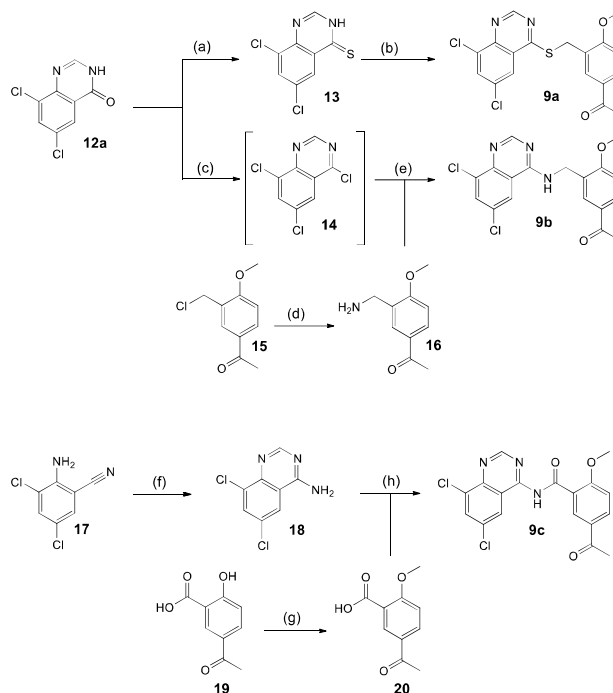
However, this compound was found to be cytotoxic. Therefore, we designated RSV inhibitor **8f** as the primary frontrunner in this study due to its improved activity against RSV, good cell viability, selectivity towards hCoV-229E, high solubility, and moderate yet enhanced metabolic stability. For the selective and highly active hCoV-229E inhibitor **9a**, only a minimal improvement in metabolic stability was achieved by introducing the thioether moiety, as this functional group can be susceptible to oxidation and thus decrease metabolic stability.[38] In our efforts to address the issues of poor solubility and metabolic stability, we attempted to convert the thioether moiety to a sulfonyl group. However, the desired product could not be obtained in sufficient quantities at this stage and requires further investigation. Our attempts to use oxone® as an oxidation reagent resulted in product degradation, and isolation of the desired product was not achieved even with *meta*-chloroperoxybenzoic acid (*m*CPBA, data not shown). Additionally, compound **10f** (Table S53), which features a 2-*mono*-substituted fluorine benzyl pattern, exhibited high metabolic stability. Unfortunately, this derivative was only moderately active against hCoV-229E. Nevertheless, the motif observed in compound **10f** can serve as inspiration for enhancing the metabolic stability of our inhibitors in future studies as fluorine has been described to enhance metabolic stability.[39] The dual RSV/hCoV-229E inhibitor **8x** exhibited two-fold improved metabolic stability compared to the starting point **8a**, but it still demonstrated poor metabolic stability and requires further optimization in future investigations.
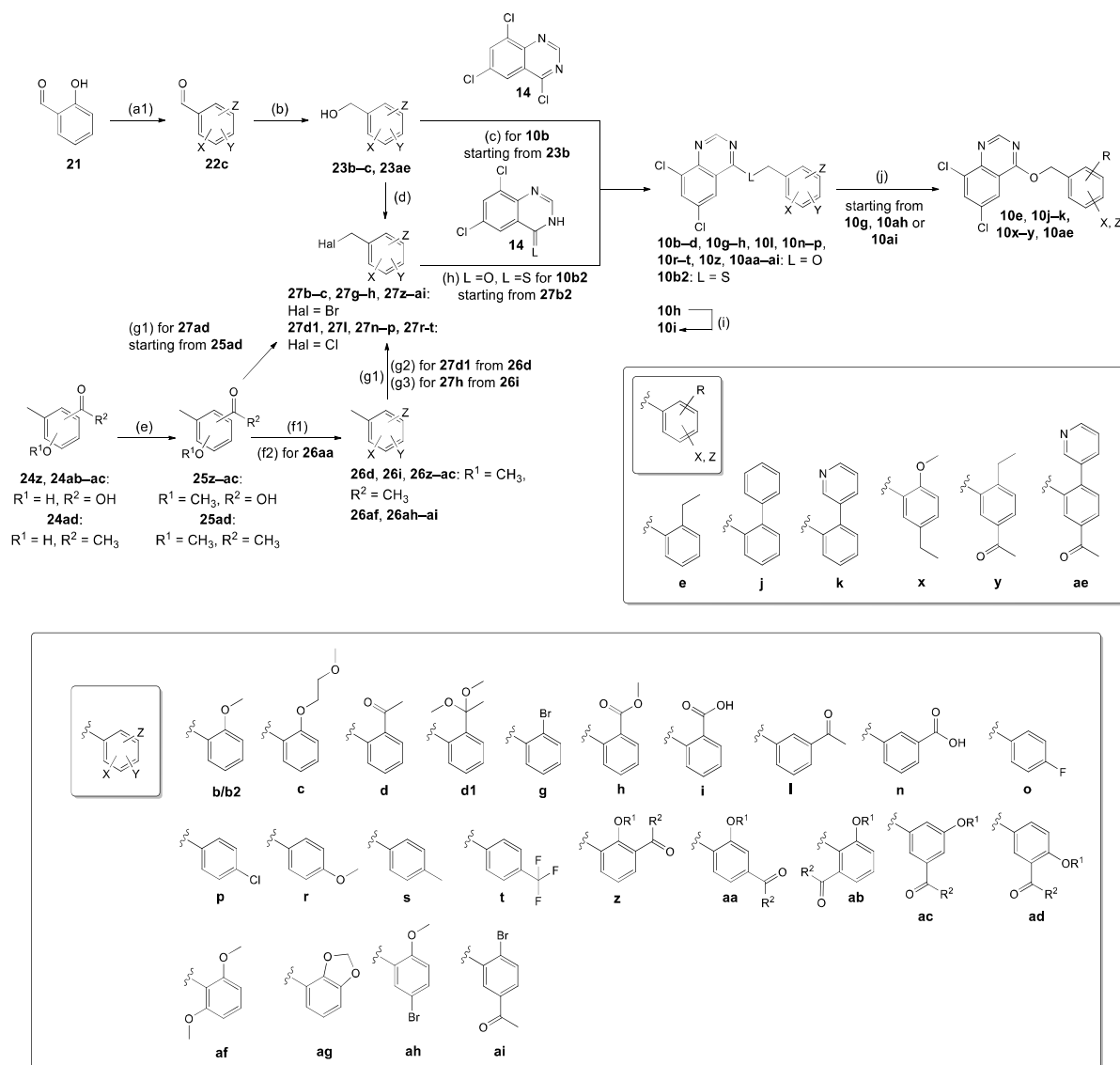
11

Scheme 1. Reagents and conditions to modify quinazoline in single-molecule syntheses.

(a1) formamide/acetic acid (v/v: 10:1), 150 °C, overnight (o/n), closed vessel (c. v.), 35–98%; (a2) methyl iodide (MeI), K_2CO_3, dimethylformamide (DMF), room temperature (r. t.), o/n, 68%; (b1) 3-(chloromethyl)-4-methoxy acetophenone, K_2CO_3, acetonitrile (MeCN), reflux, 2 h – o/n, c. v., 47–91%; (b2) 3-(chloromethyl)-4-methoxy acetophenone, K_2CO_3, DMF, r. t., o/n, 17–19%. (c) MeI, K_2CO_3, DMF, r. t., o/n, 23%; (d) Morpholine (4.0 equiv), 120 °C, c. v., o/n, 5%; (e) $Zn(CN)_2$ (3.0 equiv), $[Pd(PPh_3)_4]$ (10 mol%), DMF, 100 °C, 1 d, 7%; (f) Cu_2O (10 mol%), Na^tBuO (3 equiv), dimethyl sulfoxide (DMSO), acetylacetone, 7%; (g1) K_3PO_4, $[Pd(OAc)_2]$, PCy_3, toluene/H_2O (100:1), 100 °C, 73%; (g2) K_2CO_3, $[Pd(PPh_3)_4]$ (5 mol%), 1,4-dioxane/H_2O (6:1), 100 °C, 8–17%.

Scheme 2. Reagents and conditions for the syntheses of linker modifications.

(a) Lawesson's reagent, pyridine, reflux, c. v., o/n, 70%; (b) 3-(chloromethyl)-4-methoxy acetophenone, K_2CO_3, MeCN, reflux, o/n, c. v., 73%; (c) $SOCl_2$, $DMF_{cat.}$, reflux, 2 h, crude; (d) NH_3 (7 N in methanol (MeOH)), mw, standard method, 50 °C, 2 h, crude; (e) Cs_2CO_3, MeCN, reflux, c. v., o/n, 39%; (f) formamide/acetic acid (v/v: 10:1), 150 °C, c. v., o/n; crude; (g) 1.) MeI, K_2CO_3, DMF, r. t., o/n; 2.) NaOH (1 M), tetrahydrofuran (THF)/H_2O, r. t. o/n, 71%; (h) DIPEA, Hexafluorophosphate Azabenzotriazole Tetramethyl Uronium (HATU), DMF, r. t., o/n, 17%.

12

Scheme 3. Reagents and conditions for the syntheses of benzyl-modified derivatives.

(a1) $CH_3O(CH_2)_2Br$, K_2CO_3, DMF, r. t. o/n, quant.; (a2) 1.) sodium hydride (NaH), bromomethyl methyl ether, THF, *tert*-butyl lithium (tBuLi), Et_2O, then DMF, 0 °C – r. t., 2 h, 2.) tBuLi, diethyl ether (Et_2O). – 40 °C, 2 h, then DMF, 0 °C – r. t., quant. (b) 1.) sodium borohydride ($NaBH_4$), MeOH, 0 °C – r.t., 2.) 1 h, r. t., 65%; (c) **8**, Cs_2CO_3, MeCN, reflux, c. v., o/n, 10%; (d) PBr_3, dichloromethane (DCM), 0 °C – r. t., 3 h, 91%; (e) 1.) MeI, K_2CO_3, DMF, r., o/n; 2.) NaOH (1 M), THF/H_2O, o/n, 71% – quant.; (f1) MeLi, Et_2O, 0°C – r. t., o/n, 42–90%; (f2) 1.) oxalyl chloride, $DMF_{cat.}$, DCM, 50 °C, 2 h, 2.) triethylamine (NEt_3), *N,O*-dimethylammonium chloride, THF, r. t., 2 h, 3.) MeMgBr, (1.0 M in THF), THF, 0 °C – r. t., 2 h, quant.; (g1) *N*-bromosuccinimide (NBS), azobisisobutyronitrile (AIBN), CCl_4, 4 h, 11% – quant.; (g2) 1.) $CH(OMe)_3$, hydrochloric acid (HCl, cat.)., MeOH, r. t., o/n, 2.) NBS, AIBN, CCl_4, reflux, 4 h, 68%; (g3) 1.) K_2CO_3, MeI, DMF, rt, o/n; 2.) NBS, AIBN, CCl_4, reflux, 4 h, crude; (h) K_2CO_3, MeCN, reflux, c. v., o/n, 10–97%; (i) LiOH, THF/H_2O, r. t., o/n, 25%; (j) K_2CO_3, $[Pd(PPh_3)_4]$ (5 mol%), 1,4-dioxane/H_2O (6:1), 100 °C, 6–34%.

Chemistry. In our studies, we utilized commercially available derivatives in the vicinity of inhibitor 8a (Table S1) and synthesized additional 53 close derivatives applying single-molecule syntheses and late-stage modifications on certain building blocks (Schemes 1–3).

Starting with the modification of the quinazoline moiety, we synthesized 23 close derivatives. For this, we prepared different quinazolinones applying our recently published procedure[35]. To combine them with 1-(3-(chloromethyl)-4-methoxyphenyl)ethan-1-one in an *O*-alkylation reaction we optimized our published procedure[35] in terms of the yield

(data not shown) resulting in **GPB-1**. Additionally, we performed late-stage modifications, such as methylation (a), nucleophilic aromatic substitution (b), cyanation[40] (c), sulfonylation[41] (d), and Suzuki reaction[42,43] (e) following common and literature-known protocols.(Scheme 1)

As previously mentioned, we conducted linker modifications as part of our study. Due to the unavailability of commercially accessible compounds for these specific modifications, we synthesized several compounds with a specific focus on ether replacement. Their synthetic routes are displayed in Scheme 2 and consisted of two to four steps each.

13

The thio-linked derivative **9a** could be achieved by transformation of quinazolinone **12a** to thio analogue **13** using the Lawesson's reagent[44] and an additional nucleophilic substitution. The amine linker (**9b**) was synthesized using the same starting material, **12a**. In this case, the starting material was converted into the 4-chloro intermediate **14** by employing thionyl chloride, DMF, and dry conditions. This intermediate facilitated a nucleophilic attack by the previously synthesized benzyl amine **16**, resulting in the formation of the desired amine linker (**9b**). For the synthesis of the amide-linked derivative **9c**, starting material **17** was cyclized to the 4-amino analogue **18** adapting a literature-known procedure[45]. Then, compound **18** was coupled to benzoic acid **20**.

To investigate the benzyl moiety, we expanded a small commercial library (refer to SI, Table S1) by synthesizing additional derivatives using the synthetic pathways outlined in Scheme 3. Many of these derivatives required single-molecule syntheses of multiple building blocks, such as benzylic alcohols **23** and halogenides **27**. These building blocks were subsequently utilized for the *O*-alkylation of intermediate **12a** (as shown in Scheme 3). Since benzylic alcohol **23c** was not commercially available, it was synthesized from the corresponding aldehyde **22c** *via* reduction with sodium borohydride, following a known method.[46] Aldehyde **22c** had been prepared adapting a literature-known procedure[47]. Benzylic halogenides were either commercially available (**27g**, **27l**, **27n–p**, **27r–t**, **27am**) or synthesized from the corresponding benzylic alcohols or tolyl derivatives **21/22** following common methods[48,49]. In case of **10b**, the benzyl alcohol was directly converted to the final product by using intermediate **14** as starting material. Some combi-derivatives and alkylations as well as arylations were performed according to Scheme 3 by late-stage modifications applying Suzuki reactions according to literature-known conditions.[42,43]

CONCLUSIONS

In summary, we have observed a distinct modification-dependent profile against RSV and hCoV-229E within the compound class centered around the starting point **8a**, revealing intriguing SARs for both viruses (refer to Figures 4 and 5).

RSV was selectively targeted by introducing modifications to the quinazoline moiety at the 8-position. Notably, electron-withdrawing groups proved to be advantageous for activity, with fluorine being the most active and selective *mono*-substituent (**8f**). Another substitution, the 8-nitrile group (**8p**), exhibited high activity; however, it was unfortunately cytotoxic. Depending on the intended application, the 8-nitrile substituent may be considered, as it demonstrated good metabolic stability, outperforming all other *mono*-substituted quinazoline derivatives. Nevertheless, the cytotoxic effect of the 8-nitrile group would require further detailed analysis and mitigation. Generally, various functionalities were found to be tolerated at this position, offering control over drug properties and selectivity Remarkably, even larger motifs such as the 4-pyridyl group (**8t**) were well-tolerated, demonstrating a broad versatility for introducing additional functionalities and facilitating further expansion. Notably, the 5,8-dichloro derivative (**8u**) exhibited favorable selectivity and RSV inhibition, albeit

with lower solubility compared to the leading candidate **8f**. It is worth noting that the discussed quinazoline modifications did not yield improvements in terms of hCoV-229E inhibition, failing to provide selectivity against this virus. In summary, RSV selectivity could be effectively controlled by the choice of *mono*-substitution patterns or by altering the position of the chlorine atom from six to five. Interestingly, neither linker nor benzyl modifications resulted in improvements in RSV inhibition. However, the flexibility of the linker may play a crucial role and warrants further investigation. To gain deeper insights into the linker region, plans are underway to explore inverse linkers. Additionally, in future analyses, the interaction between the linker and the binding pocket could be examined by introducing a ketone group instead of the ether at both linker positions. Among the *mono*-substituted benzyl modifications, the 2-(3-pyridyl) group (**10k**) was the only one showing some activity against RSV, but only in the second infection round, which could speak for another mode of action. When the initial acetyl group was combined with the aforementioned functionality in a *di*-substitution pattern (**10ae**), it resulted in inactivity. Hence, we deduce that tendencies observed in *mono*-substituted derivatives cannot be directly applied to *di*-substitution patterns, at least in the case of RSV. Through simplifications of the 2-methoxy and 3-acetyl groups within the *di*-substitution pattern, we discovered the necessity of oxygen in both groups, likely due to their electronic influence or proton-accepting function. Interestingly, the original 2-methoxy-5-acetyl substitution pattern exhibited the best results in addressing both RSV and hCoV-229E. However, other positions showed stronger disfavor towards RSV, which might be attributed to the direct interaction of the corresponding functionalities with the binding pocket.

In our pursuit of achieving selectivity against hCoV-229E (as depicted in Figure 5), no success was attained through quinazoline modifications. However, future investigations should focus on exploring potential synergistic effects, such as the combination of the 6,7-dichloro substitution. Additionally, we discovered that a sulfide-ether exchange in the linker region (**9a**) yielded the most active and selective inhibitor in our study, exhibiting an activity of 80 nM. Nonetheless, this compound exhibited low solubility and poor metabolic stability. The flexibility of the linker region appears to be crucial for targeting hCoV-229E, similar to what was described for RSV-selective inhibitors. Benzyl modifications with *mono*-substitution patterns generally exhibited greater acceptance against hCoV-229E compared to RSV, thereby reinforcing the previously observed differentiated profile of the two viruses. Both the 2-methoxy (**10b**) and 4-methyl (**10s**) groups displayed a comparable inhibitory effect on hCoV-229E as the starting point **8a**, demonstrating selectivity against this virus. Further investigation is required to evaluate the combinatorial impact of these two modifications. In addition, weak or moderately electron-donating functionalities should be considered for designing combi-derivatives to target hCoV-229E, particularly if the combination of the 2-methoxy and 4-methyl groups proves promising. Unfortunately, the anticipated synergistic effect of combining the 2-methoxy group with the best linker against hCoV-229E (**10b2**) could not be confirmed. We observed a slight improvement in the *mono*-methoxy substituted derivative **10b** by imitating the previously
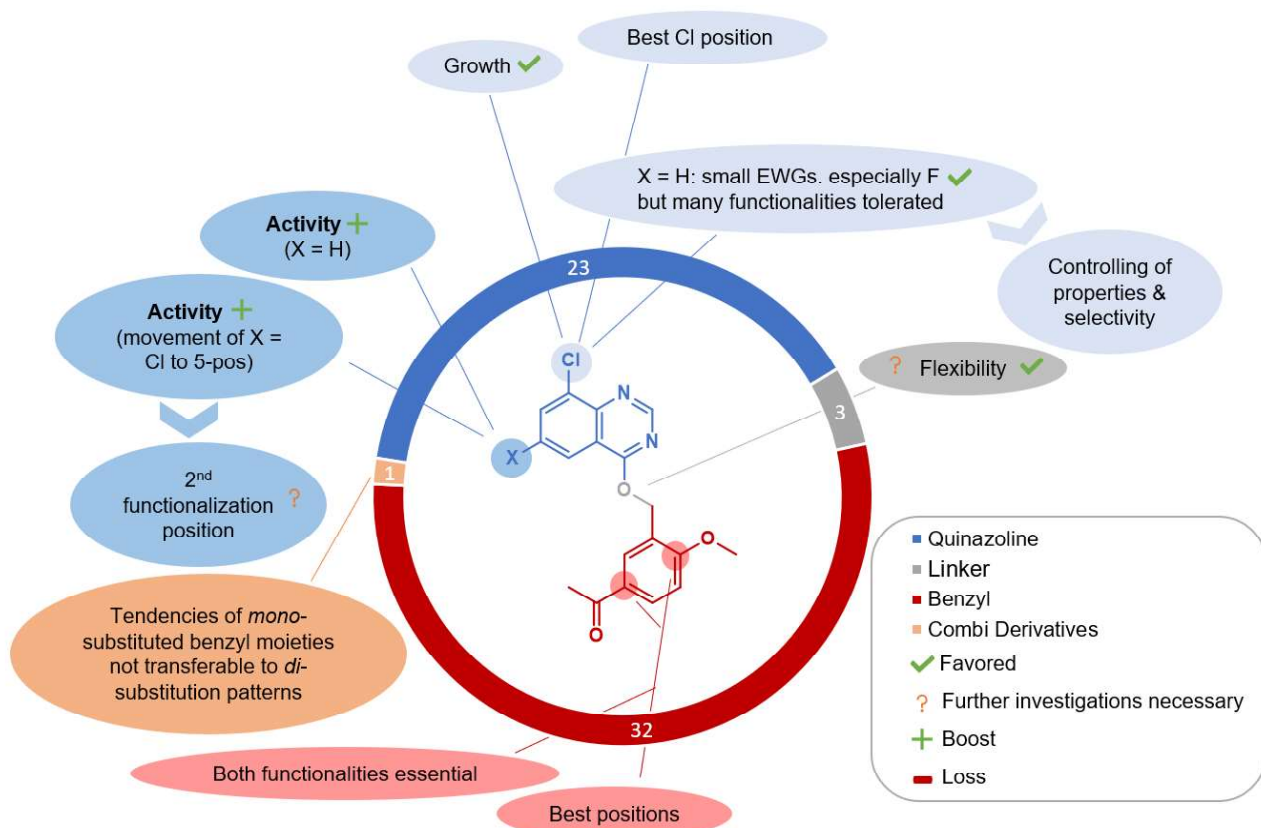
14

Figure 4. Structure–activity relationships for selective RSV inhibitors. Numbers in the ring give the total count of corresponding derivatives for each modification class.
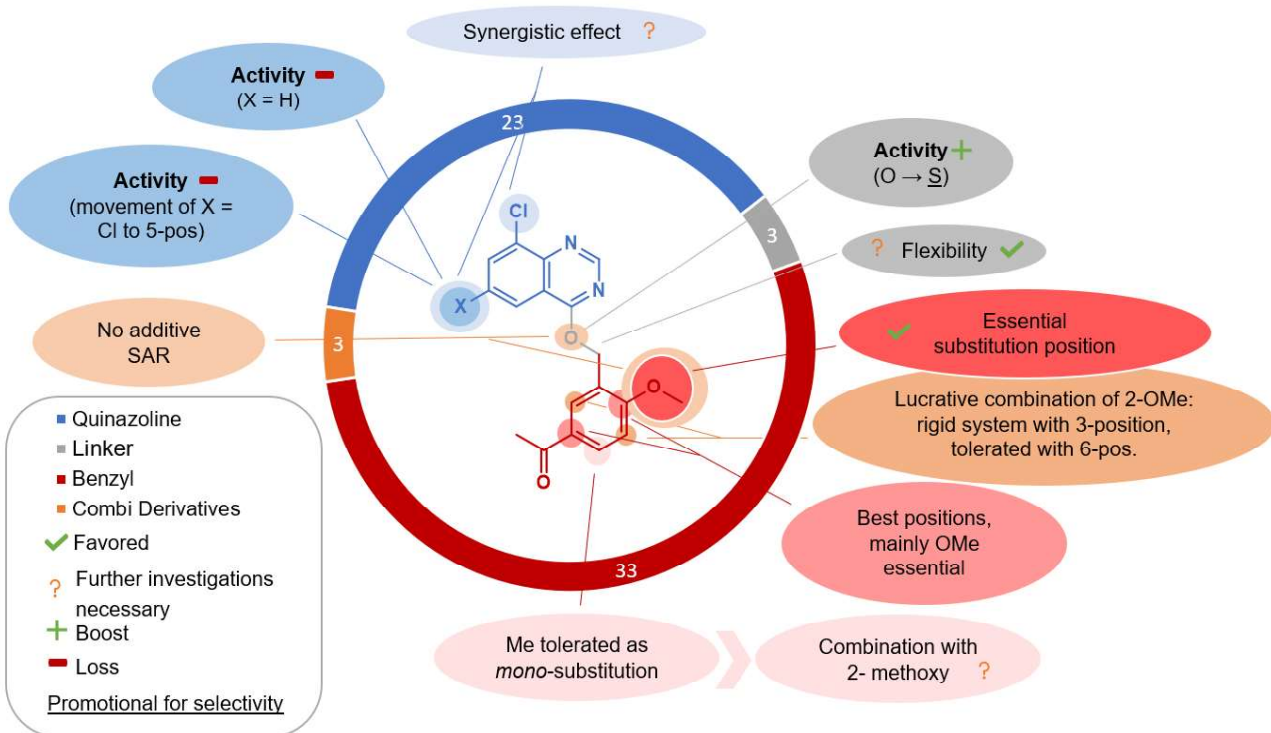

Figure 5. Structure–activity relationships for selective hCoV-229E inhibitors. Numbers in ring give the total count of corresponding derivatives for each modification class.

planned rigid 2,3-dimethoxy motif with compound **10ag**. To maintain the dual inhibitory nature of the starting point **8a**, a 6,8-di-substitution pattern in the quinazoline moiety appears to be crucial. Replacing both chlorine atoms with methyl groups (**8x**) resulted in a slight decrease in activity against hCoV-229E but significantly improved the compound's solubility. Among the performed linker modifications, none was beneficial in terms of dual inhibition, except amine-linked compound **9b** would turn out to be an inhibitor with a different mode of action against RSV in the future.Overall, the 8-fluoro quinazoline substitution pattern (**8f**) emerged as the most favorable in terms of RSV inhibition, solubility, cytotoxicity, and selectivity.Furthermore, it displayed improved, albeit moderate metabolic stability in mouse liver S9 fractions.

Consequently, it can be regarded as a promising starting point for future combinations involving the quinazoline moiety and other parts of the molecule. Moreover, we have developed a highly active inhibitor of hCoV-229E (**9a**) that serves as a promising starting point for further optimization. Additionally, we enhanced the solubility of the dual inhibitor by creating compound **8x**. Unfortunately, neither the starting point **8a** nor the highly active hCoV-229E inhibitor demonstrated activity against SARS-CoV-2. Nevertheless, these novel scaffolds could be valuable in drug-development efforts, targeting other coronaviruses.

EXPERIMENTAL SECTION

Chemistry – General information. All chemicals were used as obtained from commercial suppliers without further purification.

^{1}H and ^{13}C nuclear magnetic resonance (NMR) spectra were recorded on a Bruker Fourier 500 [500 MHz (^{1}H), 126 MHz (^{13}C)] spectrometer. Chemical shifts are given in parts per million (ppm) and referenced against the residual dimethyl sulfoxide-d_6 (DMSO-d_6), Chloroform-d (CDCl$_3$), or acetone-d_6 peak. J stands for coupling constants. Multiplicities are described with singlet (s), broad singlet (br s), doublet (d), doublet of a doublet (dd), doublet of a doublet of a doublet (ddd), triplet (t), doublet of a triplet (dt), quartet (q), doublet of a quartet (dq), sextet (sxt), septet (sept), and multiplet (m).

For reaction controls, thin layer chromatography (TLC) and/or liquid chromatography-mass spectrometry (LC-MS) were used. Low-resolution mass analytics and purity control of final compounds were performed by applying a SpectraSystems-MSQ LC-MS system (Thermo Fisher Scientific) consisting of pump, Hypersil Gold column (100 mm x 2.1 mm, particle size 3 μm), autosampler, VWD detector and an ESI quadrupole mass spectrometer. For LC-MS measurements, the following method was used: positive/negative mode, acetonitrile (MeCN) + 0.1% formic acid (FA)/water (H$_2$O) + 0.1% FA, 5 – 100% MeCN + 0.1% FA over 5.8 min, 0.7 mL/min, wavelength (λ) = 254 nm.

Microwave-assisted (mw) syntheses were carried out in a Discover microwave synthesis system from CEM. For column chromatography, either the automated flash column chromatography (AFC) system CombiFlash Rf 150 (Teledyne Isco) equipped with RediSepRf silica columns was used or manual flash column chromatography (MFC) with

Silica 60M, 0.04 – 0.063 mm or 0.063 – 0.2 mm, (Macherey Nagel) was performed.

Final products were dried under high vacuum. In case the final compound was purified with semi-preparative high-performance liquid chromatography (semi-prep HPLC), the corresponding isolated fraction was lyophilized using a Christ Alpha 2-4 LD plus freeze-dryer connected to Chemistry Hybrid Pump RC6 (Vacuubrand). For semi-prep HPLC, an Ultimate 3000 ultra-high-performance liquid chromatography (UHPLC) system (Thermo Fisher Scientific) equipped with Dionex RS Pump, Diode Array Detector, Automated Fraction Collector, Nucleodur C18 Gravity column (250 mm x 10 mm (column A) or 16 mm (column B), particle size 5 μm) was used.[35] All final and tested compounds are at least 95% pure by HPLC (see LC-MS UV/Vis chromatograms, SI 1-2).

High-resolution mass spectrometry (HRMS) measurements were conducted with a Q Exactive Focus (Thermo Fischer Scientific) connected to Dionex Ultimate 3000 RS Pump and Autosampler as well as UHPLC system Column compartment with Nucleodur C18 Pyramid column (150mm x 2 mm, particle size 3 μm) and Diode Array Detector.[35]

Characterizations of some compounds have partly already been published in different journals but resulted sometimes from other procedures. To give a complete overview of their characterizations and to confirm synthesized structures by the performed method we showed all details referencing also the other sources for comparison.

If not described differently, reactions have not been optimized.

General procedures. General procedure A (GP A): **Cyclization to quinazolinone.** For the cyclization, we applied our recently published procedure for the synthesis of 6,8-dichloroquinazolin-4(3H)-one.[35]

General procedure B, Method 1 (GP B-1): *O*-**Alkylation of quinazolinones.** To optimize the yields of the second step, we changed our recently published procedure[35] to the following one: The corresponding quinazoline was mixed with K$_2$CO$_3$ (1.0 equiv), the related benzyl halogenide (1.0 equiv), and MeCN (0.08 M) in a closed vessel (c. v., Crimp vial). This mixture was heated to reflux for a certain time. After full conversion of the starting material, the solvent was removed *in vacuo.* Then, the residue was suspended in water, filtered, and washed with water. If not described differently, no further purification *via* AFC and/or semi-prep HPLC was necessary.

General procedure B, Method 2 (GP B-2): *O*-**Alkylation of quinazolinones using caesium carbonate and potassium iodide.** Adapting method 1 (**GP B-1**), compound **12a**, corresponding benzylic halogenide (1.0 equiv), Cs$_2$CO$_3$ (1.0 equiv) and a catalytic amount of KI were suspended in anhydrous MeCN (0.1 M). The resulting suspension was degassed by bubbling nitrogen gas through it. The reaction mixture was heated up to 60 °C, stirred at this temperature o/n and concentrated *in vacuo.* The residue was taken up into saturated, aqueous NaHCO$_3$ solution, which was subsequently extracted with ethyl acetate (EtOAc). The combined organic fractions were washed with saturated, aqueous NaCl solution, dried over anhydrous Na$_2$SO$_4$, filtered,

16

concentrated *in vacuo* and subjected to flash chromatography to obtain the desired compound.

General procedure B, Alternative 3 (GP B-3): *O*-Alkylation of quinazolinone at room temperature for sensitive starting materials. Applying our recently published procedure[35], the corresponding quinazolinone, K_2CO_3 (1.0 equiv), and benzyl halogenide (1.0 equiv) were stirred in DMF (0.1 M) at room temperature until full consumption of the starting material was reached. After concentrating the reaction mixture *in vacuo*, water or aqueous, saturated NH_4Cl solution was added to the crude product which was then extracted with a suitable organic solvent depending on the product's polarity. The combined organic layers were combined, washed with water, and dried over Na_2SO_4. After filtration, the filtrate was dried *in vacuo*. If necessary, the resulting crude product was purified by AFC and/or prep-HPLC.

General procedure B, Alternative 4 (GP B-4): *O*-**Modification of quinazolinones with nucleophiles.** Performing a literature-known procedure[50], the quinazoline was converted to the corresponding chloroquinazoline. The resulting crude was directly used for the nucleophilic substitution following **GP B-1** under inert conditions and usage of Cs_2CO_3 as a base, a nucleophile instead of benzyl halogenide as well as dry MeCN.

General procedure C (GP C): Methylation. The corresponding starting material and K_2CO_3 (1.0 – 2.0 equiv) were suspended in DMF (0.5 – 1.0 M). After stirring for 10 min at r. t., MeI (1.0 – 2.5 equiv) was added. The mixture was stirred o/n at r. t. in a closed system. Then, MeI was quenched with aqueous saturated NH_4Cl solution and concentrated *in vacuo*. After treating the resulting residue with water, the crude product was extracted using dichloromethane (DCM). The combined organic layers were dried over Na_2SO_4, filtered and concentrated to dryness *in vacuo*. For final products, the crude was purified by semi-prep HPLC. Otherwise, the resulting residue was used without further purification.

General procedure D (GP D): Sulfonylation. Applying the literature-known procedure[41], a mixture of the corresponding brominated starting material, $[Cu_2O]$ (0.1 equiv), Na^tBuO (3.0 equiv), and acetylacetone (1.0 equiv) in DMSO (0.13 M) was heated to 100 °C o/n under inert conditions in a c. v.. The reaction mixture was then diluted with DCM, filtered and concentrated *in vacuo* to isolate the desired product using semi-prep HPLC.

General procedure E (GP E): Suzuki reaction as late-stage modification. For this reaction, commonly known conditions[42] were adapted. The brominated starting material, boronic acid (1.2 – 5.0 equiv) and K_2CO_3 (2.5 equiv) were weighed into a c. v., flushed with nitrogen and mixed with degassed solvents, 1,4-dioxane (0.05 M) and water (0.3 M). After adding $[Pd(PPh_3)_4]$ (0.05 – 0.01 equiv), the mixture was heated to 100 °C in a c. v. o/n. Then, the reaction mixture was diluted with DCM, filtered *via* Celite, and concentrated *in vacuo*. The resulting crude was purified by semi-prep HPLC.

General procedure F (GP F): Hydrolysis. The corresponding starting material was stirred in a mixture of aqueous NaOH solution and tetrahydrofuran (THF) (*v/v* (NaOH (1 M)/ THF) = 1:1 – 1:3; 0.2 – 0.5 M) at r. t. o/n. Then, the reaction mixture was acidified using aqueous hydrochloric

acid (HCl) solution (1 M) to extract the crude product with EtOAc. After extraction, the combined organic layers were washed with water, dried over Na_2SO_4, filtered, and dried *in vacuo*.

General procedure G (GP G): Ketone formation from carboxylic acid using methyl lithium. Adapting the literature-known procedure[51] slightly, a mixture of carboxylic acid and diethyl ether (Et_2O, 0.13 M) was cooled to 0 °C under dry conditions. To this mixture, a solution of methyl lithium (MeLi) (1.6 M in Et_2O, 4.0 equiv) was added dropwise. The resulting mixture was stirred o/n reaching r. t. and then quenched with aqueous, saturated NH_4Cl solution. After extraction with DCM, the resulting organic layers were combined, washed with saturated, aqueous NaCl solution and dried over Na_2SO_4. Lastly, it was filtered and dried *in vacuo*. The resulting crude was purified by AFC if necessary.

General procedure H (GP H): Alcohol-halogen transformation using PBr_3. Following the literature-known procedure[48] (REF), the corresponding alcohol was stirred at 0 °C in DCM (0.5 M). After adding PBr_3 (1.5 equiv) dropwise at this temperature, the mixture was stirred for 3 h reaching r. t.. Then, it was quenched with cold water. The organic layer was washed with saturated, aqueous NaCl solution and dried over Na_2SO_4. Filtration and drying *in vacuo* to gave the desired product.

General procedure I (GP I): Radicalic alkyl-bromination using *N*-Bromosuccinimde and AIBN. Adapting a literature-known procedure[49], *N*-bromosuccinimide (NBS, 1.00 – 1.05 equiv) and AIBN (0.05 – 0.20 equiv) were added to a mixture of alkylic starting material and CCl_4 (0.5 M), and heated to reflux for 4 h. The mixture was then filtered and concentrated in *vacuo*. The resulting crude product was either used without further purification or purified by AFC.**1-(3-(((6,8-Dichloroquinazolin-4-yl)oxy)methyl)-4-methoxyphenyl)ethan-1-one (8a).** Starting from **12a** (50.0 mg, 0.23 mmol), K_2CO_3 (32.2 mg, 0.23 mmol), and 1-(3-(chloromethyl)-4-methoxyphenyl)ethan-1-one (46.2 mg, 0.23 mmol), **8a** (75.6 mg, 0.20 mmol, 86%) was obtained as a beige solid. Characterization measurements showed the same data describing the desired product as for **3s** from our recently published procedure[35] (REF). Herein, the NMR spectra were recorded in $CDCl_3$ instead of DMSO-d_6. **^{1}H NMR** (500 MHz, $CDCl_3$) δ = 8.40 (s, 1H), 8.17 (dd, *J* = 2.1, 9.5 Hz, 2H), 7.98 (dd, *J* = 2.1, 8.7 Hz, 1H), 7.79 (d, *J* = 2.3 Hz, 1H), 6.95 (d, *J* = 8.7 Hz, 1H), 5.17 (s, 2H), 3.95 (s, 3H), 2.58 (s, 3H). **^{13}C NMR** (126 MHz, $CDCl_3$) δ = 196.4, 161.3, 159.6, 147.9, 143.4, 134.5, 132.8, 132.7, 131.2, 130.4, 125.2, 124.3, 122.7, 110.4, 56.0, 46.4, 26.4 (overlap of two quaternary carbon signals in $CDCl_3$, no overlap in HSQC spectrum (Figure S117) visible).

1-(3-(((8-Chloroquinazolin-4-yl)oxy)methyl)-4-methoxyphenyl)ethan-1-one (8b). Applying **GP B-1** with **12b** (50.0 mg, 0.28 mmol), K_2CO_3 (38.3 mg, 0.28 mmol), and 1-(3-(chloromethyl)-4-methoxyphenyl)ethan-1-one (55.0 mg, 0.28 mmol) in MeCN (3.5 mL), **8b** (77.1 mg, 0.22 mmol, 81%) was obtained as a beige solid. **LC-MS** *m/z* ([M+H]$^+$) = 343.08, t_r = 3.91 min, *purity*: 98%. **^{1}H NMR** (500 MHz, $CDCl_3$) δ = 8.44 (s, 1H), 8.22 (dd, *J* = 1.4, 7.8 Hz, 1H), 8.17 (d, *J* = 2.3 Hz, 1H), 7.98 (dd, *J* = 2.3, 8.7 Hz, 1H), 7.83 (dd, *J* = 1.4, 7.8 Hz, 1H), 7.41 (t, *J* = 7.8 Hz, 1H), 6.95 (d, *J* = 8.7 Hz, 1H), 5.18 (s, 2H), 3.96 (s, 3H), 2.58 (s, 3H). **^{13}C NMR** (126 MHz, $CDCl_3$) δ = 196.5, 161.4, 160.6, 147.9,

17

144.6, 134.5, 132.8, 131.6, 131.1, 130.4, 127.3, 125.7, 123.8, 122.9, 110.3, 56.0, 46.3, 26.4. **HRMS** *calculated: m/z* ([M+H]⁺) = 343.0844, *found: m/z* ([M+H]⁺) = 343.0839.

1-(3-(((7-Chloroquinazolin-4-yl)oxy)methyl)-4-methoxyphenyl)ethan-1-one (8c). According to **GP B-1**, **8c** (80.9 mg, 0.23 mmol, 85%) was synthesized and isolated as a beige solid. For this reaction **12c** (50.0 mg, 0.28 mmol), K₂CO₃ (38.3 mg, 0.28 mmol), and 1-(3-(chloromethyl)-4-methoxyphenyl)ethan-1-one (55.0 mg, 0.28 mmol) were mixed in MeCN (3.5 mL). **LC-MS** *m/z* ([M+H]⁺) = 343.08, t_r = 4.06 min, *purity*: 97%. **¹H NMR** (500 MHz, CDCl₃) δ = 8.29 (s, 1H), 8.21 (d, J = 8.6 Hz, 1H), 8.13 (d, J = 2.2 Hz, 1H), 7.97 (dd, J = 2.2, 8.6 Hz, 1H), 7.68 (d, J = 1.8 Hz, 1H), 7.43 (dd, J = 1.8, 8.6 Hz, 1H), 6.95 (d, J = 8.6 Hz, 1H), 5.15 (s, 2H), 3.95 (s, 3H), 2.57 (s, 3H). **¹³C NMR** (126 MHz, CDCl₃) δ = 196.5, 161.3, 160.5, 148.8, 148.3, 140.4, 132.5, 131.0, 130.3, 128.2, 127.8, 126.9, 123.1, 120.7, 110.3, 55.9, 46.1, 26.4. **HRMS** *calculated: m/z* ([M+H]⁺) = 343.0844, *found: m/z* ([M+H]⁺) = 343.0838.

1-(3-(((6-Chloroquinazolin-4-yl)oxy)methyl)-4-methoxyphenyl)ethan-1-one (8d). Following **GP B-1** under usage of **12d** (50.0 mg, 0.28 mmol), K₂CO₃ (38.3 mg, 0.28 mmol), and 1-(3-(chloromethyl)-4-methoxyphenyl)ethan-1-one (55.0 mg, 0.28 mmol) in MeCN (3.5 mL), **8d** (44.2 mg, 0.13 mmol, 47%) was synthesized and isolated as a colorless solid after additional washing with methyl tert-butyl ether. **LC-MS** *m/z* ([M+H]⁺) = 343.08, 163.04, t_r = 4.04 min, *purity*: 96%. **¹H NMR** (500 MHz, CDCl₃) δ = 8.27 (s, 1H), 8.26 (d, J = 2.3 Hz, 1H), 8.14 (d, J = 2.3 Hz, 1H), 7.98 (dd, J = 2.3, 8.7 Hz, 1H), 7.69 - 7.65 (m, 1H), 7.63 (d, J = 8.7 Hz, 1H), 6.95 (d, J = 8.7 Hz, 1H), 5.17 (s, 2H), 3.95 (s, 3H), 2.58 (s, 3H). **¹³C NMR** (126 MHz, CDCl₃) δ = 196.5, 161.3, 160.2, 147.3, 146.5, 134.6, 133.0, 132.6, 131.0, 130.4, 129.1, 126.2, 123.3, 123.1, 110.4, 55.9, 46.2, 26.5. **HRMS** *calculated: m/z* ([M+H]⁺) = 343.0844, *found: m/z* ([M+H]⁺) = 343.0837.

1-(3-(((5-Chloroquinazolin-4-yl)oxy)methyl)-4-methoxyphenyl)ethan-1-one (8e). Colorless solid **8e** (53.1 mg, 0.16 mmol, 56%) was synthesized using **GP B-1** by stirring **12e** (50.0 mg, 0.28 mmol), K₂CO₃ (38.3 mg, 0.28 mmol), and 1-(3-(chloromethyl)-4-methoxyphenyl)ethan-1-one (55.0 mg, 0.28 mmol) in MeCN (3.5 mL). **LC-MS** *m/z* ([M+H]⁺) = 343.08, t_r = 3.79 min, *purity*: > 98%. **¹H NMR** (500 MHz, CDCl₃) δ = 8.30 (s, 1H), 8.15 (d, J = 2.1 Hz, 1H), 7.99 (dd, J = 2.1, 8.7 Hz, 1H), 7.63 - 7.57 (m, 2H), 7.48 (dd, J = 2.4, 6.6 Hz, 1H), 6.96 (d, J = 8.7 Hz, 1H), 5.14 (s, 2H), 3.95 (s, 3H), 2.59 (s, 3H). **¹³C NMR** (126 MHz, CDCl₃) δ = 196.6, 161.4, 159.1, 150.1, 147.9, 134.2, 133.7, 132.6, 131.0, 130.4, 130.0, 126.6, 123.0, 119.4, 110.3, 55.9, 46.3, 26.5. **HRMS** *calculated: m/z* ([M+H]⁺) = 343.0844, *found: m/z* ([M+H]⁺) = 343.0840.

1-(3-(((8-Fluoroquinazolin-4-yl)oxy)methyl)-4-methoxyphenyl)ethan-1-one (8f). Following **GP B-1**, light-brown solid **8f** (51.6 mg, 0.16 mmol, 86%) was prepared by heating **12f** (30.0 mg, 0.18 mmol,), K₂CO₃ (25.3 mg, 0.18 mmol), and 1-(3-(chloromethyl)-4-methoxyphenyl)ethan-1-one (36.3 mg, 0.18 mmol) in MeCN (2.3 mL) to reflux. **LC-MS** *m/z* ([M+H]⁺) = 327.2, t_r = 2.94 min, *purity*: > 98%. **¹H NMR** (500 MHz, DMSO-*d₆*) δ = 8.55 (s, 1H), 7.97 (dd, J = 2.1, 8.5 Hz, 1H), 7.93 (d, J = 8.0 Hz, 1H), 7.81 (d, J = 2.1 Hz, 1H), 7.75 - 7.66 (m, 1H), 7.53 (dt, J = 4.8, 8.0 Hz, 1H), 7.14 (d, J = 8.5 Hz, 1H), 5.16 (s, 2H), 3.92 (s,

3H), 2.49 (s, 3H). **¹³C NMR** (126 MHz, DMSO-*d₆*) δ = 196.3, 161.1, 159.3 (d, $^4J_{CF}$ = 2.8 Hz), 156.4 (d, J_{CF} = 253.7 Hz), 149.2, 137.1 (d, $^2J_{CF}$ = 11.9 Hz), 131.0, 129.7, 129.4, 127.6 (d, $^3J_{CF}$ = 8.3 Hz, 1C), 123.8, 123.6, 121.9 (d, $^4J_{CF}$ = 3.7 Hz), 119.9 (d, $^2J_{CF}$ = 18.4 Hz), 110.8, 56.1, 46.0, 26.4. **HRMS** *calculated: m/z* ([M+H]⁺) = 327.1139, *found: m/z* ([M+H]⁺) = 327.1126.

1-(3-(((8-Bromoquinazolin-4-yl)oxy)methyl)-4-methoxyphenyl)ethan-1-one (8g). According to **GP B-1**, light-brown solid **8g** (237.7 mg, 0.61 mmol, 89%) was synthesized using **12g** (155.7 mg, 0.69 mmol), K₂CO₃ (95.6 mg, 0.69 mmol), 1-(3-(chloromethyl)-4-methoxyphenyl)ethan-1-one (137.5 mg, 0.69 mmol), and MeCN (8.7 mL). **LC-MS** *m/z* ([M+H]⁺) = 387.14, t_r = 4.04 min, *purity*: 96%. **¹H NMR** (500 MHz, CDCl₃) δ = 8.45 (s, 1H), 8.26 (d, J = 7.9 Hz, 1H), 8.19 - 8.15 (m, 1H), 8.06 - 7.93 (m, 2H), 7.34 (t, J = 7.9 Hz, 1H), 6.95 (d, J = 8.7 Hz, 1H), 5.18 (s, 2H), 3.96 (s, 3H), 2.58 (s, 3H). **¹³C NMR** (126 MHz, CDCl₃) δ = 196.5, 161.4, 160.5, 148.0, 145.6, 137.9, 132.8, 131.2, 130.4, 127.8, 126.5, 123.8, 122.9, 122.0, 110.4, 56.0, 46.3, 26.5. **HRMS** *calculated: m/z* ([M+H]⁺) = 387.0339, *found: m/z* ([M+H]⁺) = 387.0335.

1-(4-Methoxy-3-(((8-methylquinazolin-4-yl)oxy)methyl)phenyl)ethan-1-one (8h). The synthesis of **8h** was performed according to **GP B-1** giving beige solid **8h** (54.5 mg, 0.17 mmol, 90%). For this reaction, **12h** (30.0 mg, 0.19 mmol), K₂CO₃ (25.8 mg, 0.19 mmol), 1-(3-(chloromethyl)-4-methoxyphenyl)ethan-1-one (37.2 mg, 0.19 mmol), and MeCN (2.3 mL) were used. **LC-MS** *m/z* ([M+H]⁺) = 323.21, t_r = 3.92 min, *purity*: 98%. **¹H NMR** (500 MHz, CDCl₃) δ = 8.33 (s, 1H), 8.15 (d, J = 7.5 Hz, 1H), 8.14 (d, J = 2.2 Hz, 1H), 7.97 (dd, J = 2.2, 8.7 Hz, 1H), 7.59 (d, J = 7.5 Hz, 1H), 7.37 (t, J = 7.5 Hz, 1H), 6.95 (d, J = 8.7 Hz, 1H), 5.18 (s, 2H), 3.96 (s, 3H), 2.62 (s, 3H), 2.57 (s, 3H). **¹³C NMR** (126 MHz, CDCl₃) δ = 196.6, 161.4, 161.3, 146.3, 146.1, 135.6, 135.0, 132.5, 130.8, 130.3, 126.8, 124.5, 123.4, 122.2, 110.3, 55.9, 45.8, 26.4, 17.5. **HRMS** *calculated: m/z* ([M+H]⁺) = 323.1390, *found: m/z* ([M+H]⁺) = 323.1384.

1-(4-Methoxy-3-(((8-(trifluoromethyl)quinazolin-4-yl)oxy)methyl)phenyl)ethan-1-one (8i). Compound **8i** was prepared applying **GP B-1**. Thereby, **12i** (50.0 mg, 0.14 mmol), K₂CO₃ (19.3 mg, 0.14 mmol), and 1-(3-(chloromethyl)-4-methoxyphenyl)ethan-1-one (27.8 mg, 0.14 mmol) were mixed in MeCN (1.8 mL) to afford **8j** (47.9 mg, 0.13 mmol, 91%) as a light-yellow solid. **LC-MS** *m/z* ([M+H]⁺) = 377.3, t_r = 4.35 min, *purity*: >98%. **¹H NMR** (500 MHz, DMSO-*d₆*) δ = 8.64 (s, 1H), 8.41 (d, J = 8.5 Hz, 1H), 8.22 (d, J = 7.8 Hz, 1H), 7.98 (dd, J = 2.2, 8.5 Hz, 1H), 7.83 (d, J = 2.2 Hz, 1H), 7.68 (t, J = 7.8 Hz, 1H), 7.15 (d, J = 8.5 Hz, 1H), 5.17 (s, 2H), 3.93 (s, 3H), 2.50 (s, 3H). **¹³C NMR** (126 MHz, DMSO-*d₆*) δ = 159.9, 146.9, 146.2, 145.9 (q, $^2J_{CF}$ = 19.2 Hz), 131.97 (q, $^4J_{CF}$ = 5.2 Hz), 130.6, 126.1, 124.8 (q, $^3J_{CF}$ = 8.3 Hz), 125.02 (q, J_{CF} = 284.0 Hz). **HRMS** *calculated: m/z* ([M+H]⁺) = 377.1108, *found: m/z* ([M+H]⁺) = 377.1102.

4-((5-Acetyl-2-methoxybenzyl)oxy)-8-(methoxycarbonyl)quinazolin-1-ium formate (8j). Following **GP B-1** under usage of **12j** (100.0 mg, 0.49 mmol), K₂CO₃ (67.7 mg, 0.49 mmol), 1-(3-(chloromethyl)-4-methoxyphenyl)ethan-1-one (97.4 mg, 0.49 mmol), and MeCN (6.1 mL), **8j** (1.5 mg, 4 μmol, 1%) was obtained as a colorless solid after purification *via* semi-prep HPLC (MeCN + 0.05% formic acid (FA) / H₂O + 0.05% FA, 15 – 100% MeCN + 0.05% FA over 30 min, 10 mL/min, column B, **8j** at 63% MeCN + 0.05% FA). **LC-MS** *m/z* ([M-H]⁻) = 366.41, t_r = 2.76 min, *purity*: > 98%.

18

¹H NMR (500 MHz, DMSO-*d₆*) δ = 9.86 (br d, *J* = 4.6 Hz, 1H), 8.63 (s, 1H), 8.47 (s, 1H), 8.45 (dd, *J* = 1.6, 7.8 Hz, 1H), 8.28 (dd, *J* = 1.6, 7.8 Hz, 1H), 7.99 (dd, *J* = 2.2, 8.6 Hz, 1H), 7.84 (d, *J* = 2.2 Hz, 1H), 7.63 (t, *J* = 7.8 Hz, 1H), 7.16 (d, *J* = 8.6 Hz, 1H), 7.01 (br s, 2H), 5.19 (s, 2H), 3.93 (s, 3H), 2.91 (d, *J* = 4.6 Hz, 3H), 2.50 (s, 3H). **¹³C NMR** (126 MHz, DMSO-*d₆*) δ = 196.3, 165. 7, 164.9, 161.1, 159.8, 148. 9, 144.9, 135.7, 131.0, 129.8, 129.4, 129.4, 129.2, 126.8, 123.7, 122.0, 110.8, 56.2, 45.8, 26.4, 26.2. **HRMS** *calculated: m/z* ([M+H]⁺) = 368.1498, *found: m/z* ([M+H]⁺) = 367.1367.

4-((5-Acetyl-2-methoxybenzyl)oxy)quinazoline-8-carbonitrile (8k). According to a published procedure[40], a mixture of **8g** (30.0 mg, 77 µmol, 1.0 equiv), [Pd(PPh₃)₄] (9.2 mg, 8 µmol, 0.1 equiv) and [Zn(CN)₂] (27.1 mg, 231 µmol, 3.0 equiv) in DMF (0.3 mL, 0.3 M) was heated to 100 °C o/n giving the corresponding product **8k** (2.0 mg, 6 µmol, 7%) after filtering the reaction mixture, concentrating the filtrate *in vacuo* and purifying the resulting crude *via* semi-prep-HPLC (MeCN + 0.05% FA/H₂O + 0.05% FA, 5 – 100% MeCN + 0.05% FA over 30 min, 10 mL/min, column B, **8k** at 59% MeCN + 0.05% FA). **LC-MS** *m/z* ([M+H]⁺) = 334.20, *t_r* = 2.98 min, *purity*: > 98%. **¹H NMR** (500 MHz, DMSO-*d₆*) δ = 8.71 (s, 1H), 8.38 (dd, *J* = 1.2, 7.9 Hz, 1H), 8.35 (dd, *J* = 1.2, 7.9 Hz, 1H), 7.98 (dd, *J* = 2.1, 8.6 Hz, 1H), 7.86 (d, *J* = 2.1 Hz, 1H), 7.67 (t, *J* = 7.9 Hz, 1H), 7.15 (d, *J* = 8.6 Hz, 1H), 5.17 (s, 2H), 3.93 (s, 3H), 2.51 (s, 3H). **¹³C NMR** (126 MHz, DMSO-*d₆*) δ = 196.3, 161.1, 159.3, 151.1, 149.0, 139.4, 131.3, 131.0, 130.1, 129.4, 127.1, 123.4, 122.3, 116.5, 110.8, 109.9, 56.2, 46.3, 26.4. **HRMS** *calculated: m/z* ([M+H]⁺) = 334.1186, *found: m/z* ([M+H]⁺) = 334.1173.

1-(4-Methoxy-3-(((8-(methylsulfonyl)quinazolin-4-yl)oxy)methyl)phenyl)ethan-1-one (8l). Applying **GP D** on **8g** (50.0 mg, 0.13 mmol), [Cu₂O] (1.9 mg, 13 µmol), Nat-BuO (8.3 mg, 0.39 mmol), acetylacetone (13 µL, 0.13 mmol), and DMSO (1.0 mL, 0.13 m), colorless solid **8l** (3.78 mg, 8 µmol, 7%) was isolated from the resulting crude product by purification *via* semi-prep HPLC (MeCN + 0.05% FA/H₂O + 0.05% FA, 5 – 100% MeCN + 0.05% FA over 30 min, 10 mL/min, column B, **8l** at 59% MeCN + 0.05% FA). **LC-MS** *m/z* ([M+H]⁺) = 387.39, *t_r* = 2.76 min, *purity*: > 98%. **¹H NMR** (500 MHz, DMSO-*d₆*) δ = 8.71 (s, 1H), 8.45 (dd, *J* = 1.3, 7.9 Hz, 1H), 8.39 (dd, *J* = 1.3, 7.9 Hz, 1H), 7.99 (dd, *J* = 2.1, 8.7 Hz, 1H), 7.86 (d, *J* = 2.1 Hz, 1H), 7.74 (t, *J* = 7.9 Hz, 1H), 7.16 (d, *J* = 8.7 Hz, 1H), 5.19 (s, 2H), 3.93 (s, 3H), 3.53 (s, 3H), 2.50 (s, 3H). Contains 28 mol% FA according to ¹H NMR spectrum. **¹³C NMR** (126 MHz, DMSO-*d₆*) δ = 196.3, 161.1, 159.3, 150.0, 145.0, 136.2, 133.7, 132.1, 131.1, 130.0, 129.4, 126.7, 123.5, 123.0, 110.9, 56.2, 45.9, 43.6, 26.4. **HRMS** *calculated: m/z* ([M+H]⁺) = 387.1009, *found: m/z* ([M+H]⁺) = 387.0994.

1-(3-(((8-Hydroxyquinazolin-4-yl)oxy)methyl)-4-methoxyphenyl)ethan-1-one (8m) and 1,1'-(((quinazoline-4,8-diylbis(oxy))bis(methylene))bis(4-methoxy-3,1-phenylene))bis(ethan-1-one) (8o). Both compounds, **8m** and **8o**, were obtained at the same time by performing **GP B-3** on **12m** (50.0 mg, 0.31 mmol), K₂CO₃ (42.6 mg, 0.31 mmol), and 1-(3-(chloromethyl)-4-methoxyphenyl)ethan-1-one (60.4 mg, 0.31 mmol) in DMF (3.1 mL). For the extraction EtOAc was used. The crude product was purified by semi-prep HPLC (MeCN + 0.05% formic acid (FA) / H₂O + 0.05% FA, 5 – 100% MeCN + 0.05% FA over 30 min, 10 mL/min, column B, **8m** at 57% MeCN + 0.05% FA,

8o at 70% MeCN + 0.05% FA) isolating colorless solid **8m** (16.7 mg, 0.05 mmol, 17%) and light-yellow solid **8o** (12.9 mg, 27 µmol, 9%). **8m**: **LC-MS** *m/z* ([M+H]⁺) = 325.27, *t_r* = 3.18 min, *purity*: > 98%. **¹H NMR** (500 MHz, DMSO-*d₆*) δ = 9.93 (br s, 1H), 8.44 (s, 1H), 7.97 (dd, *J* = 2.1, 8.5 Hz, 1H), 7.74 (d, *J* = 2.1 Hz, 1H), 7.53 (dd, *J* = 1.1, 7.9 Hz, 1H), 7.34 (t, *J* = 7.9 Hz, 1H), 7.20 (dd, *J* = 1.1, 7.8 Hz, 1H), 7.15 (d, *J* = 8.5 Hz, 1H), 5.15 (s, 2H), 3.93 (s, 3H), 2.48 (s, 3H). **¹³C NMR** (126 MHz, DMSO-*d₆*) δ = 196.2, 161.0, 160.2, 153.1, 146.6, 136.9, 130.8, 129.4, 129.2, 127.7, 124.2, 122.5, 118.6, 115.6, 110.7, 56.1, 45.5, 26.3. **HRMS** *calculated: m/z* ([M+H]⁺) = 325.1183, *found: m/z* ([M+H]⁺) = 325.1170. **8o**: **LC-MS** *m/z* ([M+H]⁺) = 487.42, *t_r* = 4.01 min, *purity*: > 98%. **¹H NMR** (500 MHz, DMSO-*d₆*) δ = 8.43 (s, 1H), 8.13 (d, *J* = 2.1 Hz, 1H), 8.02 (dd, *J* = 2.1, 8.7 Hz, 1H), 7.97 (dd, *J* = 2.1, 8.7 Hz, 1H), 7.76 (d, *J* = 1.9 Hz, 1H), 7.69 (dd, *J* = 1.9, 7.2 Hz, 1H), 7.51 - 7.43 (m, 2H), 7.20 (d, *J* = 8.7 Hz, 1H), 7.14 (d, *J* = 8.7 Hz, 1H), 5.24 (s, 2H), 5.14 (s, 2H), 3.92 (s, 6H), 2.53 (s, 3H), 2.48 (s, 3H). **¹³C NMR** (126 MHz, DMSO-*d₆*) δ = 196.3, 196.2, 161.0, 160.9, 160.0, 153.6, 147.2, 138.6, 130.9, 129.7, 129.6, 129.4, 129.4, 127.5, 124.6, 124.1, 122.8, 117.4, 116.5, 110.8, 110.7, 65.5, 56.1, 56.1, 45.5, 26.4, 26.3 (according to HSQC spectrum (see Figure S146): overlap of two signals belonging to two different carbons, signal at 130.9 ppm). **HRMS** *calculated: m/z* ([M+H]⁺) = 487.1864, *found: m/z* ([M+H]⁺) = 487.1850.

1-(4-Methoxy-3-(((8-methoxyquinazolin-4-yl)oxy)methyl)phenyl)ethan-1-one (8n). Performing **GP C** with **8m** (8.1 mg, 25 µmol), K₂CO₃ (4.2 mg, 30 µmol), MeI (2 µL, 38 µmol), and DMF (0.3 mL) led to the colorless solid **8n** (1.93 mg, 6 µmol, 23%) after purification of the crude product *via* semi-prep HPLC (MeCN + 0.05% FA/H₂O + 0.05% FA, 15 – 100% MeCN + 0.05% FA over 30 min, 10 mL/min, column B, **8n** at 55% MeCN + 0.05% FA). **LC-MS** *m/z* ([M+H]⁺) = 339.40, *t_r* = 2.75 min, *purity*: > 98%. **¹H NMR** (500 MHz, DMSO-*d₆*) δ = 8.42 (s, 1H), 7.97 (dd, *J* = 2.2, 8.7 Hz, 1H), 7.74 (d, *J* = 2.2 Hz, 1H), 7.66 (dd, *J* = 1.1, 8.0 Hz, 1H), 7.46 (t, *J* = 8.0 Hz, 1H), 7.38 (dd, *J* = 1.1, 8.0 Hz, 1H), 7.14 (d, *J* = 8.7 Hz, 1H), 5.14 (s, 2H), 3.92 (s, 3H), 3.91 (s, 3H), 2.48 (s, 3H). **¹³C NMR** (126 MHz, DMSO-*d₆*) δ = 196.2, 161.0, 160.0, 154.5, 147.1, 138.3, 130.9, 129.4, 129.3, 127.5, 124.1, 122.7, 116.9, 114.9, 110.7, 56.1, 56.0, 45.6, 26.3. **HRMS** *calculated: m/z* ([M+H]⁺) = 339.1339, *found: m/z* ([M+H]⁺) = 339.1327.

1-(4-Methoxy-3-(((8-morpholinoquinazolin-4-yl)oxy)methyl)phenyl)ethan-1-one (8p). Compound **8f** (20.0 mg, 61 µmol) and morpholine (0.02 mL, 245 µmol, 4.0 equiv) were heated to 120 °C in a c. v. o/n to give **8p** (1.6 mg, 4 µmol, 5%) as a colorless solid after purification by semi-prep HPLC (MeCN + 0.05% FA/H₂O + 0.05% FA, 30 – 100% MeCN + 0.05% FA over 30 min, 10 mL/min, column B, **8p** at 57% MeCN + 0.05% FA). **LC-MS** *m/z* ([M+H]⁺) = 394.27, *t_r* = 2.93 min, *purity*: > 98%. **¹H NMR** (500 MHz, DMSO-*d₆*) δ = 8.43 (s, 1H), 7.97 (dd, *J* = 2.1, 8.5 Hz, 1H), 7.73 (d, *J* = 2.1 Hz, 1H), 7.73 - 7.69 (m, 1H), 7.43 (t, *J* = 7.9 Hz, 1H), 7.28 (dd, *J* = 1.0, 7.9 Hz, 1H), 7.15 (d, *J* = 8.7 Hz, 1H), 5.13 (s, 2H), 3.93 (s, 3H), 3.83 - 3.76 (m, 4H), 3.27 - 3.24 (m, 4H), 2.48 (s, 3H). **¹³C NMR** (126 MHz, DMSO-*d₆*) δ = 196.3, 161.1, 159.3, 149.1, 147.9, 145.9, 130.9, 129.2, 127.5, 124.1, 123.8, 122.9, 121.3, 118.5, 110.8, 66.3, 56.1, 51.5, 45.3, 26.4. **HRMS** *calculated: m/z* ([M+H]⁺) = 394.1748, *found: m/z* ([M+H]⁺) = 339.1761.

19

1-(3-(((8-Cyclopropylquinazolin-4-yl)oxy)methyl)-4-methoxyphenyl)ethan-1-one (8q). Applying known conditions[52] on the brominated quinazolinone **8g** (30.0 mg, 77 μmol) under usage of cyclopropylboronic acid (10.0 mg, 0.12 mmol, 1.5 equiv), K₃PO₄ (49.2 mg, 0.23 mmol, 3.0 equiv), [Pd(OAc)₂] (1.8 mg, 8 μmol, 0.1 equiv), PCy₃ (4.5 mg, 16 μmol, 0.2 equiv), toluene (0.4 mL, 0.2 M), and water (4 μL, 20 M), **8q** was synthesized. After purification *via* MFC (DCM/methanol (MeOH), 99:1) the colorless solid **8q** (19.5 mg, 0.06 mmol, 73%) was isolated. **R$_f$** (DCM/MeOH, 99:1) = 0.13. **LC-MS** *m/z* ([M+H]⁺) = 349.19, t_r = 3.82 min, *purity*: > 98%. **¹H NMR** (500 MHz, CDCl₃) δ = 8.39 (br s, 1H), 8.14 (d, *J* = 2.3 Hz, 1H), 8.11 (dd, *J* = 1.4, 7.7 Hz, 1H), 7.98 (dd, *J* = 2.3, 8.7 Hz, 1H), 7.39 (t, *J* = 7.7 Hz, 1H), 7.22 (d, *J* = 7.7 Hz, 1H), 6.96 (d, *J* = 8.7 Hz, 1H), 5.20 (s, 2H), 3.97 (s, 3H), 2.87 - 2.79 (m, 1H), 2.58 (s, 3H), 1.17 - 1.10 (m, 2H), 0.82 - 0.76 (m, 2H). **¹³C NMR** (126 MHz, CDCl₃) δ = 196.6, 161.4, 146.4, 146.3, 146.3, 132.5, 131.0, 130.4, 128.7, 128.7, 128.7, 127.2, 123.9, 123.3, 122.0, 110.3, 56.0, 45.9, 26.5, 10.4, 9.4. **HRMS** *calculated: m/z* ([M+H]⁺) = 349.1547, *found: m/z* ([M+H]⁺) = 349.1542.

1-(4-Methoxy-3-(((8-phenylquinazolin-4-yl)oxy)methyl)phenyl)ethan-1-one (8r). Performing **GP E** on **8g** (30.0 mg, 77 μmol) under usage of K₂CO₃ (26.8 mg, 0.19 mmol), [Pd(PPh₃)₄] (4.6 mg, 4 μmol), 1,4-dioxane (1.5 mL) and water (0.3 mL), **8r** (2.3 mg, 6 μmol, 8%) was isolated as a colorless solid after purification by semi-prep HPLC (MeCN + 0.05% FA/H₂O + 0.05% FA, 5 –100% MeCN + 0.05% FA over 30 min, 10 mL/min, column B, **8r** at 81% MeCN + 0.05% FA). **LC-MS** *m/z* ([M+H]⁺) = 385.33, t_r = 4.65 min, *purity*: > 98%. **¹H NMR** (500 MHz, DMSO-*d₆*) δ = 8.45 (s, 1H), 8.17 (dd, *J* = 1.4, 7.6 Hz, 1H), 7.97 (dd, *J* = 2.1, 8.7 Hz, 1H), 7.84 (dd, *J* = 1.4, 7.6 Hz, 1H), 7.80 (d, *J* = 2.1 Hz, 1H), 7.65 - 7.55 (m, 3H), 7.46 (t, *J* = 7.5 Hz, 2H), 7.43 - 7.36 (m, 1H), 7.15 (d, *J* = 8.7 Hz, 1H), 5.16 (s, 2H), 3.92 (s, 3H), 2.49 (s, 3H). **¹³C NMR** (126 MHz, DMSO-*d₆*) δ = 196.3, 161.0, 160.3, 147.8, 144.9, 138.8, 138.1, 135.0, 130.9, 130.4, 129.5, 129.4, 127.8, 127.3, 127.0, 125.6, 124.0, 122.2, 110.8, 56.1, 45.5, 26.4. **HRMS** *calculated: m/z* ([M+H]⁺) = 385.1547, *found: m/z* ([M+H]⁺) = 385.1541.

1-(4-Methoxy-3-(((8-(pyridin-4-yl)quinazolin-4-yl)oxy)methyl)phenyl)ethan-1-one (8s). Following **GP E** under usage of **8g** (30.0 mg, 77 μmol), K₂CO₃ (26.8 mg, 0.19 mmol), [Pd(PPh₃)₄] (4.6 mg, 4 μmol), 1,4-dioxane (1.5 mL), and water (0.3 mL), **8s** (5.0 mg, 10 μmol, 17%) was isolated as a colorless solid after purification by semi-prep HPLC (MeCN + 0.05% FA/ H₂O + 0.05% FA, 5 – 100% MeCN + 0.05% FA over 30 min, 10 mL/min, column B, **8s** at 43% MeCN + 0.05% FA). **LC-MS** *m/z* ([M+H]⁺) = 386.26, t_r = 2.85 min, *purity*: > 98%. **¹H NMR** (500 MHz, DMSO-*d₆*) δ = 8.67 - 8.65 (m, 2H), 8.50 (s, 1H), 8.24 (dd, *J* = 1.4, 7.6 Hz, 1H), 7.97 (dd, *J* = 2.2, 8.7 Hz, 1H), 7.93 (dd, *J* = 1.4, 7.6 Hz, 1H), 7.81 (d, *J* = 2.2 Hz, 1H), 7.67 - 7.61 (m, 3H), 7.15 (d, *J* = 8.7 Hz, 1H), 5.16 (s, 2H), 3.92 (s, 3H), 2.49 (s, 3H). **¹³C NMR** (126 MHz, DMSO-*d₆*) δ = 196.3, 161.0, 160.1, 149.2, 148.4, 145.6, 144.9, 135.9, 135.0, 130.9, 129.6, 129.4, 127.2, 126.9, 125.2, 123.9, 122.3, 110.8, 56.1, 45.6, 26.4. **HRMS** *calculated: m/z* ([M+H]⁺) = 386.1499, *found: m/z* ([M+H]⁺) = 386.1495.

1-(3-(((5,8-Dichloroquinazolin-4-yl)oxy)methyl)-4-methoxyphenyl)ethan-1-one (8t). According to **GP B-1**, beige solid **8t** (57.30 mg, 0.15 mmol, 65%) was prepared from **12t** (50.0 mg, 0.23 mmol), K₂CO₃ (32.2 mg,

0.23 mmol), 1-(3-(chloromethyl)-4-methoxyphenyl)ethan-1-one (46.3 mg, 0.23 mmol), and MeCN (2.9 mL), **LC-MS** *m/z* ([M+H]⁺) = 377.07, t_r = 3.80 min, *purity*: > 98%. **¹H NMR** (500 MHz, DMSO-*d₆*) δ = 8.65 (s, 1H), 7.97 (dd, *J* = 2.1, 8.7 Hz, 1H), 7.91 (d, *J* = 8.5 Hz, 1H), 7.84 (d, *J* = 2.1 Hz, 1H), 7.52 (d, *J* = 8.5 Hz, 1H), 7.13 (d, *J* = 8.7 Hz, 1H), 5.10 (s, 2H), 3.92 (s, 3H), 2.50 (s, 3H). **¹³C NMR** (126 MHz, DMSO-*d₆*) δ = 196.3, 161.2, 157.8, 150.2, 146.4, 134.2, 131.4, 131.0, 130.0, 130.0, 129.6, 129.4, 123.5, 119.9, 110.8, 56.1, 46.3, 26.4. **HRMS** *calculated: m/z* ([M+H]⁺) = 377.0454, *found: m/z* ([M+H]⁺) = 377.0450.

1-(3-(((5,7-Dichloroquinazolin-4-yl)oxy)methyl)-4-methoxyphenyl)ethan-1-one (8u). Based on **GP B-1**, **12u** (50.0 mg, 0.23 mmol), K₂CO₃ (32.1 mg, 0.23 mmol), 1-(3-(chloromethyl)-4-methoxyphenyl)ethan-1-one (46.1 mg, 0.23 mmol), and MeCN (2.9 mL) were used for the synthesis of beige solid **8u** (71.8 mg, 0.19 mmol, 82%). **LC-MS** *m/z* ([M+H]⁺) = 377.10, t_r = 4.00 min, *purity*: 98%. **¹H NMR** (500 MHz, CDCl₃) δ = 8.29 (s, 1H), 8.14 (d, *J* = 1.7 Hz, 1H), 7.99 (dd, *J* = 1.7, 8.5 Hz, 1H), 7.58 (d, *J* = 1.6 Hz, 1H), 7.46 (d, *J* = 1.6 Hz, 1H), 6.96 (d, *J* = 8.5 Hz, 1H), 5.11 (s, 2H), 3.95 (s, 3H), 2.59 (s, 3H). **¹³C NMR** (126 MHz, CDCl₃) δ = 196.6, 161.4, 158.7, 150.9, 148.8, 139.3, 135.3, 132.7, 131.1, 130.4, 129.9, 126.3, 122.8, 118.0, 110.3, 55.9, 46.4, 26.6. **HRMS** *calculated: m/z* ([M+H]⁺) = 377.0454, *found: m/z* ([M+H]⁺) = 377.0451.

1-(3-(((6-Chloro-8-methylquinazolin-4-yl)oxy)methyl)-4-methoxyphenyl)ethan-1-one (8v). According to **GP B-1**, light-beige solid **8w** (82.5 mg, 0.23 mmol, 91%) was synthesized according to **GP B-1** using **12v** (49.2 mg, 0.25 mmol) with K₂CO₃ (34.9 mg, 0.25 mmol), 1-(3-(chloromethyl)-4-methoxyphenyl)ethan-1-one (50.3 mg, 0.25 mmol), and MeCN (3.2 mL). **LC-MS** *m/z* ([M+H]⁺) = 357.14, t_r = 4.09 min, *purity*: 98%. **¹H NMR** (500 MHz, DMSO-*d₆*) δ = 8.53 (s, 1H), 7.97 (dd, *J* = 2.2, 8.7 Hz, 1H), 7.90 (d, *J* = 2.2 Hz, 1H), 7.80 - 7.74 (m, 2H), 7.14 (d, *J* = 8.7 Hz, 1H), 5.14 (s, 2H), 3.92 (s, 3H), 2.54 (s, 3H), 2.49 (s, 3H). **¹³C NMR** (126 MHz, DMSO-*d₆*) δ = 196.3, 161.0, 159.5, 148.0, 145.2, 138.6, 134.5, 130.9, 130.9, 129.5, 129.4, 123.8, 122.7, 122.6, 110.8, 56.1, 45.7, 26.4, 16.8. **HRMS** *calculated: m/z* ([M+H]⁺) = 357.1000, *found: m/z* ([M+H]⁺) = 357.0995.

1-(3-(((8-Chloro-6-methylquinazolin-4-yl)oxy)methyl)-4-methoxyphenyl)ethan-1-one (8w). This beige solid (83.1 mg, 0.23 mmol, quant.) was synthesized according to **GP B-1** converting **12w** (45.2 mg, 0.23 mmol) with K₂CO₃ (32.1 mg, 0.23 mmol), and 1-(3-(chloromethyl)-4-methoxyphenyl)ethan-1-one (46.1 mg, 0.23 mmol) in MeCN (2.9 mL). **LC-MS** *m/z* ([M+H]⁺) = 357.14, t_r = 3.78 min, *purity*: 98%. **¹H NMR** (500 MHz, DMSO-*d₆*) δ = 8.53 (s, 1H), 7.97 (dd, *J* = 2.1, 8.7 Hz, 1H), 7.88 (s, 1H), 7.85 (s, 1H), 7.78 (d, *J* = 2.1 Hz, 1H), 7.14 (d, *J* = 8.7 Hz, 1H), 5.14 (s, 2H), 3.92 (s, 3H), 2.49 (s, 3H), 2.42 (s, 3H). **¹³C NMR** (126 MHz, DMSO-*d₆*) δ = 196.3, 161.0, 159.6, 148.5, 142.3, 137.9, 135.6, 131.0, 130.5, 129.6, 129.4, 124.8, 123.9, 123.0, 110.8, 56.2, 45.8, 26.4, 20.5. **HRMS** *calculated: m/z* ([M+H]⁺) = 357.1000, *found: m/z* ([M+H]⁺) = 357.0996.

1-(3-(((6,8-Dimethylquinazolin-4-yl)oxy)methyl)-4-methoxyphenyl)ethan-1-one (8x). For this compound, **GP B-1** was performed under usage of **12x** (26.2 mg, 0.15 mmol) with K₂CO₃ (19.3 mg, 0.15 mmol), 1-(3-

(chloromethyl)-4-methoxyphenyl)ethan-1-one (27.8 mg, 0.15 mmol), and MeCN (1.9 mL) giving **8x** (43.1 mg, 0.13 mmol, 85%) as a light-yellow solid. **LC-MS** *m/z* ([M+H]⁺) = 337.19, t_r = 3.73 min, *purity*: 98%. **¹H NMR** (500 MHz, CDCl₃) δ = 8.27 (s, 1H), 8.12 (d, *J* = 2.0 Hz, 1H), 8.01 - 7.90 (m, 2H), 7.42 (s, 1H), 6.94 (d, *J* = 8.5 Hz, 1H), 5.17 (s, 2H), 3.95 (s, 3H), 2.58 (s, 3H), 2.57 (s, 3H), 2.43 (s, 3H). **¹³C NMR** (126 MHz, CDCl₃) δ = 196.6, 161.4, 161.3, 145.3, 144.3, 137.0, 136.5, 135.3, 132.5, 130.8, 130.3, 123.9, 123.5, 121.9, 110.3, 55.9, 45.7, 26.4, 21.3, 17.4. **HRMS** *calculated: m/z* ([M+H]⁺) = 337.1540, *found: m/z* ([M+H]⁺) = 357.1547.

1-(3-(((6,8-Dichloroquinazolin-4-yl)thio)methyl)-4-methoxyphenyl)ethan-1-one (9a).

According to **GP B-1**, thione **13** (100.0 mg, 0.43 mmol) was converted to beige solid **9a** (123.4 mg, 0.31 mmol, 73%) under usage of K₂CO₃ (59.8 mg, 0.43 mmol), 1-(3-(chloromethyl)-4-methoxy-phenyl)ethan-1-one (86.0 mg, 0.43 mmol), and MeCN (2.9 mL). **LC-MS** *m/z* ([M+H]⁺) = 392.97, t_r = 5.44 min, *purity*: 96%. **¹H NMR** (500 MHz, CDCl₃) δ = 9.15 (s, 1H), 8.17 (s, 1H), 7.98 (s, 1H), 7.95 - 7.89 (m, 2H), 6.95 (d, *J* = 8.5 Hz, 1H), 4.70 (s, 2H), 3.98 (s, 3H), 2.56 (s, 3H). **¹³C NMR** (126 MHz, CDCl₃) δ = 196.5, 171.4, 161.4, 153.8, 143.6, 134.4, 134.1, 132.5, 131.5, 130.4, 130.1, 125.0, 124.9, 121.9, 110.1, 56.0, 29.1, 26.3. **HRMS** *calculated: m/z* ([M+H]⁺) = 393.0226, *found: m/z* ([M+H]⁺) = 393.0220.

1-(3-(((6,8-Dichloroquinazolin-4-yl)amino)methyl)-4-methoxyphenyl)ethan-1-one (9b).

Following **GP B-4**, first, intermediate **14** was synthesized using **12a** (100.0 mg, 0.47 mmol), thionyl chloride (1.5 mL, 0.3 M), and DMF (5 drops). After removing thionyl chloride *in vacuo*, one part of the resulting crude product (50.0 mg, 0.21 mmol) was heated to reflux with intermediate **16** (44.7 mg, 0.21 mmol, purity: 87%, 1.0 equiv) and Cs₂CO₃ (69.7 mg, 0.21 mmol, 1.0 equiv) in dry MeCN (2.7 mL, 0.08 M). The resulting reaction mixture was concentrated *in vacuo*, suspended in water and filtered off, giving **9b** (31.2 mg, 82 μmol, 39%) as a colorless solid after purification by semi-prep HPLC (MeCN + 0.05% FA/H₂O + 0.05% FA, 5 – 100% MeCN + 0.05% FA over 50 min, 5 mL/min, column A, **9b** at 58% MeCN + 0.05% FA). **LC-MS** *m/z* ([M+H]⁺) = 376.02, t_r = 3.27 min, *purity*: > 98%. **¹H NMR** (500 MHz, DMSO-*d₆*) δ = 8.95 (t, *J* = 5.4 Hz, 1H), 8.54 (s, 1H), 8.53 (d, *J* = 2.3 Hz, 1H), 8.12 (d, *J* = 2.1 Hz, 1H), 7.95 (dd, *J* = 2.3, 8.5 Hz, 1H), 7.79 (d, *J* = 2.1 Hz, 1H), 7.14 (d, *J* = 8.7 Hz, 1H), 4.75 (d, *J* = 5.4 Hz, 2H), 3.93 (s, 3H), 2.46 (s, 3H). **¹³C NMR** (126 MHz, DMSO-*d₆*) δ = 196.4, 160.9, 158.9, 156.1, 144.7, 132.8, 132.6, 130.1, 129.4, 129.3, 127.5, 126.2, 121.5, 116.5, 110.4, 56.0, 40.1, 26.4. **HRMS** *calculated: m/z* ([M+H]⁺) = 376.0614, *found: m/z* ([M+H]⁺) = 376.0610.

5-Acetyl-*N*-(6,8-dichloroquinazolin-4-yl)-2-methoxybenzamide (9c).

Carboxylic acid **20** (30.0 mg, 0.15 mmol) and DIPEA (30 μL, 0.17 mmol, 1.1 equiv) were stirred for 10 min at r. t. in DMF (0.6 mL, 0.25 M). Then, *O*-(7-Azabenzotriazol-1-yl)-*N*,*N*,*N′*,*N′*-tetramethyluronium-hexafluorphosphat (HATU, 70.3 mg, 0.19 mmol, 1.2 equiv) was added. After stirring the reaction mixture for further 10 min at r. t., the corresponding amine **18** (32.0 mg, 0.15 mmol, 1.0 equiv) was added and the mixture was stirred at the same temperature o/n. To extract the crude product with EtOAc, the reaction mixture was concentrated *in vacuo* and suspended in aqueous, saturated NH₄Cl solution. The combined organic layers were dried over Na₂SO₄, filtered, and

concentrated to dryness *in vacuo*. Purification by semi-prep HPLC (MeCN + 0.05% FA/H₂O + 0.05% FA, 5 – 100% MeCN + 0.05% FA over 30 min, 10 mL/min, column B, **9c** at 68% MeCN + 0.05% FA) gave **9c** (10.4 mg, 27 μmol, 17%) as a colorless solid. **LC-MS** *m/z* ([M+H]⁺) = 390.22, t_r = 3.89 min, *purity*: > 98%. **¹H NMR** (500 MHz, DMSO-*d₆*) δ = 11.39 (br s, 1H), 8.99 (s, 1H), 8.45 (d, *J* = 2.1 Hz, 1H), 8.35 (d, *J* = 2.1 Hz, 1H), 8.21 (d, *J* = 2.1 Hz, 1H), 8.14 (dd, *J* = 2.1, 8.8 Hz, 1H), 7.25 (d, *J* = 8.8 Hz, 1H), 3.78 (s, 3H), 2.59 (s, 3H). **¹³C NMR** (126 MHz, DMSO-*d₆*) δ = 196.1, 165.9, 160.1, 157.1, 154.8, 146.0, 134.0, 133.2, 133.0, 131.2, 130.4, 129.6, 124.7, 123.2, 119.1, 111.9, 56.3, 26.5. **HRMS** *calculated: m/z* ([M+H]⁺) = 390.0407, *found: m/z* ([M+H]⁺) = 390.0394.

6,8-Dichloro-4-((2-methoxybenzyl)oxy)quinazoline (10b).

Following **GP B-4** under usage of intermediate **14** (50.0 mg, 0.21 mmol), Cs₂CO₃ (69.7 mg, 0.21 mmol), 2-methoxybenzyl alcohol (27 μL, 021 mmol) an MeCN (2.7 mL). Instead of filtering the crude product off, it was extracted from the aqueous layer with EtOAc (3 x 20 mL). The combined organic layers were dried over MgSO₄, filtered, and dried *in vacuo*. For purification, AFC (Cyclohexane/EtOAc, 0 – 100% EtOAc over 20 min, **10b** at 30% EtOAc, 4 g silica) was performed to give **10b** (7.2 mg, 21 μmol, 10%) as a colorless solid. **LC-MS** *m/z* ([M+H]⁺) = 335.04, t_r = 5.61 min, *purity*: 98%. **¹H NMR** (500 MHz, CDCl₃) δ = 8.95 (s, 1H), 8.11 (d, *J* = 2.3 Hz, 1H), 7.92 (d, *J* = 2.3 Hz, 1H), 7.48 (dd, *J* = 1.6, 7.6 Hz, 1H), 7.39 (dt, *J* = 1.6, 7.6 Hz, 1H), 7.02 (t, *J* = 7.6 Hz, 1H), 6.97 (d, *J* = 7.6 Hz, 1H), 5.69 (s, 2H), 3.88 (s, 3H). **¹³C NMR** (126 MHz, CDCl₃) δ = 166.2, 157.8, 155.2, 146.4, 134.0, 133.4, 132.1, 130.0, 129.9, 123.6, 121.8, 120.5, 118.3, 110.6, 65.2, 55.5. **HRMS** *calculated: m/z* ([M+H]⁺) = 335.0349, *found: m/z* ([M+H]⁺) = 335.0342.

6,8-Dichloro-4-((2-methoxybenzyl)thio)quinazoline (10b2)

According to **GP B-1**, **5** (50.0 mg, 0.22 mmol), K₂CO₃ (29.9 mg, 0.22 mmol), 2-methoxybenzyl bromide **27b** (43.4 mg, 0.22 mmol), and MeCN (11.6 mL) were used. Thereby, **10b2** (61.4 mg, 0.18 mmol, 81%) was obtained as a light-brown solid after filtration. **LC-MS** *m/z* ([M+H]⁺) = 350.81, t_r = 5.45 min, *purity*: 97%. **¹H NMR** (500 MHz, CDCl₃) δ = 9.12 (s, 1H), 7.98 (d, *J* = 0.8 Hz, 1H), 7.89 (d, *J* = 0.8 Hz, 1H), 7.49 (d, *J* = 7.2 Hz, 1H), 7.28 (t, *J* = 7.2 Hz, 1H), 6.98 - 6.85 (m, 2H), 4.69 (s, 2H), 3.91 (s, 3H). **¹³C NMR** (126 MHz, CDCl₃) δ = 171.8, 157.7, 153.9, 143.6, 134.3, 134.0, 132.3, 130.9, 129.2, 125.0, 124.5, 122.0, 120.5, 110.6, 55.5, 29.3. **HRMS** *calculated: m/z* ([M+H]⁺) = 351.0120, *found: m/z* ([M+H]⁺) = 351.0115.

6,8-Dichloro-4-((2-(2-methoxyethoxy)benzyl)oxy)quinazoline (10c).

To a solution of **23c** (25.5 mg, 0.14 mmol) in DCM (0.22 m), NBS (49.8 mg, 0.28 mmol, 2.0 equiv) and PPh₃ (55.1 mg, 0.21 mmol, 1.5 equiv) were added at 0 °C. This mixture was stirred o/n reaching r. t.. Then, it was concentrated in *vacuo*. Following **GP B-1**, the resulting residue, containing benzyl bromide **23c**, was mixed with K₂CO₃ (19.3 mg, 0.14 mmol) and **12a** (30.0 mg, 0.14 mmol) in MeCN (1.8 mL, 0.08 m) to obtain **10c** (14.1 mg, 0.04 mmol, 27%) as a colorless solid after purification *via* AFC (PB/EtOAc, 0 –100% EtOAc over 22 min, 4 g silica, 18 mL/min, **10c** at 40% EtOAc). **LC-MS** *m/z* ([M+H]⁺) = 379.19, t_r = 4.90 min, *purity*: 97%. **¹H NMR** (500 MHz, CDCl₃) δ = 8.47 (s, 1H), 8.18 (d, *J* = 2.3 Hz, 1H), 7.78 (d, *J* = 2.3 Hz, 1H), 7.53 (dd, *J* = 1.6, 7.6 Hz, 1H), 7.30 (dt, *J* = 1.6, 7.6 Hz, 1H), 6.97 (t, *J* = 7.6 Hz, 1H), 6.89 (d, *J* = 7.6 Hz, 1H), 5.18

(s, 2H), 4.20 - 4.14 (m, 2H), 3.80 - 3.75 (m, 2H), 3.46 (s, 3H). **^{13}C NMR** (126 MHz, CDCl$_3$) δ = 159.7, 156.9, 148.5, 143.5, 134.3, 132.8, 132.4, 132.0, 130.2, 125.1, 124.4, 123.1, 121.1, 111.6, 70.7, 67.3, 59.1, 46.4. **HRMS** *calculated: m/z* ([M+H]$^+$) = 379.0611, *found: m/z* ([M+H]$^+$) = 379.0599.

1-(2-(((6,8-Dichloroquinazolin-4-yl)oxy)methyl)phenyl)ethan-1-one (10d). *Acetal installation on 2'-methylacetophenone (step 1).* To a stirred solution of 2'-methylacetophenone (1.34 g, 10.0 mmol) in MeOH (20.0 mL) methyl orthoformate (1.28 g, 12.0 mmol. 1.2 equiv) was added followed by two drops of HCl (4.0 M solution in 1,4-dioxane). The reaction mixture was then stirred at r. t. o/n and concentrated *in vacuo* to yield the crude product (1.78 g) as a colorless liquid that was used in the next step without additional purification. **R$_f$** (Hex/EtOAc, 9:1) = 0.25.

Bromination to 1-(Bromomethyl)-2-(1,1-dimethoxyethyl)benzene (step 2). According to **GP I**, one part of the previously synthesized 2'-methylacetophenone dimethyl-ketal (288.1 mg, 1.60 mmol), AIBN (13.0 mg, 79 µmol), NBS (299.0 mg, 1.68 mmol), and CCl$_4$ (8.0 mL, 0.2 M) were used for the synthesis of **27d1**. Differently to **GP I**, NBS was added in two equal portions with 30 min break in between. After concentrating the reaction mixture *in vacuo*, the oily residue was resuspended in ether, the white precipitate was filtered off and the mother liquor was concentrated. The resulting benzyl bromide (280.0 mg) **R$_f$** (Hex/DCM = 10:1) = 0.4.

O-Akylation to final compound (step 3). Applying **GP B-2** on **12a** (9.0 mg, 0.04 mmol), **27d1** (11.0 mg, 0.04 mmol), Cs$_2$CO$_3$ (14.0 mg, 0.04 mmol), and MeCN (0.5 mL) the final compound **27d** was obtained. It was isolated as a white solid (12.0 mg, 0.03 mmol, 80%) using AFC (DCM/MeOH, 0 –10% MeOH over 15 min, 4 g silica, 18 mL/min, **27d** at 5% MeOH). **LC-MS** *m/z* ([M+H]$^+$) = 347.12, t_r = 3.84 min, *purity*: 95%. **^{1}H NMR** (500 MHz, DMSO-d_6) δ = 8.51 (s, 1H), 8.22 (d, J = 2.3 Hz, 1H), 8.09 (d, J = 2.3 Hz, 1H), 8.03 (d, J = 7.6 Hz, 1H), 7.56 (t, J = 7.5 Hz, 1H), 7.44 (t, J = 7.6 Hz, 1H), 7.39 (d, J = 7.5 Hz, 1H), 5.54 (s, 2H), 2.44 (s, 3H). **^{13}C NMR** (126 MHz, DMSO-d_6) δ = 195.3, 158.8, 149.6, 143.6, 138.3, 134.4, 134.3, 132.6, 132.5, 132.0, 131.4, 129.1, 126.2, 124.4, 123.7, 54.1, 20.8. **HRMS** *calculated: m/z* ([M+H]$^+$) = 347.0349, *found: m/z* ([M+H]$^+$) = 347.0337.

6,8-Dichloro-4-((2-ethylbenzyl)oxy)quinazoline (10e). **GP E** was used for the synthesis of **10e** starting from **10g** (30.0 mg, 78 µmol), ethyl boronic acid (6.9 mg, 94 µmol), K$_2$CO$_3$ (27.0 mg, 195 µmol), and [Pd(PPh$_3$)$_4$] (4.5 mg, 4 µmol) in 1,4-dioxane (1.5 mL) and water (0.3 mL). Thereby, the desired product **10e** (4.7 mg, 14 µmol, 18%) was isolated as a colorless solid *via* semi-prep HPLC (MeCN + 0.05% FA/H$_2$O + 0.05% FA, 5 – 100% MeCN + 0.05% FA over 30 min, 10 mL/min, column B, **10e** at 95% MeCN + 0.05% FA). **LC-MS** *m/z* ([M+H]$^+$) = 333.20, t_r = 5.32 min, *purity*: > 98%. **^{1}H NMR** (500 MHz, DMSO-d_6) δ = 8.60 (s, 1H), 8.19 (d, J = 2.4 Hz, 1H), 8.07 (d, J = 2.4 Hz, 1H), 7.29 - 7.22 (m, 2H), 7.16 - 7.10 (m, 1H), 6.93 (d, J = 7.6 Hz, 1H), 5.25 (s, 2H), 2.74 (q, J = 7.5 Hz, 2H), 1.19 (t, J = 7.6 Hz, 3H). **^{13}C NMR** (126 MHz, DMSO-d_6) δ = 158.8, 149.4, 143.5, 141.4, 134.2, 133.4, 132.4, 131.3, 128.5, 127.7, 126.4, 126.1, 124.5, 124.0, 46.7, 24.8, 14.7. **HRMS** *calculated: m/z* ([M+H]$^+$) = 333.0556, *found: m/z* ([M+H]$^+$) = 333.0552.

4-((2-Bromobenzyl)oxy)-6,8-dichloroquinazoline (10g). Its synthesis was performed according to **GP B-1** using **12a** (200.0 mg, 0.93 mmol), K$_2$CO$_3$ (128.5 mg, 0.93 mmol), 2-bromobenzyl bromide (0.13 mL, 0.93 mmol), and MeCN (11.6 mL). Thereby, **10g** (356.9 mg, 0.93 mmol, quant.) was obtained as a yellow solid and used for further reaction without additional purification. **LC-MS** *m/z* ([M+H]$^+$) = 383.09, t_r = 5.15 min, *purity*: 79%. For testing, one part of this crude (30.0 mg) was additionally purified by semi-prep HPLC (MeCN + 0.05% FA/H$_2$O + 0.05% FA, 5 – 100% MeCN + 0.05% FA over 30 min, 10 mL/min, column B, **10g** at 94% MeCN + 0.05% FA) to isolate **10g** (15.5 mg, 0.04 mmol) as a colorless solid. **LC-MS** *m/z* ([M+H]$^+$) = 383.11, t_r = 5.16 min, *purity*: > 98%. **^{1}H NMR** (500 MHz, DMSO-d_6) δ = 8.64 (s, 1H), 8.19 (d, J = 2.3 Hz, 1H), 8.06 (d, J = 2.3 Hz, 1H), 7.69 (d, J = 7.6 Hz, 1H), 7.32 (t, J = 7.6 Hz, 1H), 7.27 (dt, J = 1.4, 7.6 Hz, 1H), 7.08 (d, J = 7.6 Hz, 1H), 5.24 (s, 2H). **^{13}C NMR** (126 MHz, DMSO-d_6) δ = 159.3, 150.0, 144.0, 135.2, 134.7, 133.2, 132.9, 131.8, 130.1, 129.0, 128.5, 125.0, 124.5, 122.5, 50.5. **HRMS** *calculated: m/z* ([M+H]$^+$) = 382.9348, *found: m/z* ([M+H]$^+$) = 382.9335.

Methyl 2-(((6,8-dichloroquinazolin-4-yl)oxy)methyl)benzoate (10h). Starting from *o*-toluic acid **26i** (200.0 mg, 1.47 mmol), K$_2$CO$_3$ (243.6 mg, 1.76 mmol), MeI (312.8 mg, 0.14 mmol), and DMF (14.7 mL), methyl 2-methylbenzoate (217.3 mg, 1.44 mmol, 99%, light-yellow oil) was synthesized according to **GP C** and directly used without further purification to synthesize **27h**. For this, one part of previously synthesized methyl 2-methylbenzoate (100.0 mg, 0.67 mmol) was converted by performing **GP I** under usage of AIBN (21.9 mg, 0.13 mmol), NBS (118.5 mg, 0.67 mmol), and CCl$_4$ (1.3 mL). Thereby, **27h** (95.1 mg) was obtained as a yellow oil and also directly used without further purification. **R$_f$** (PB/EtOAc, 9:1) = 0.56. Applying **GP B** under usage of **12a** (71.6 mg, 0.33 mmol), K$_2$CO$_3$ (45.6 mg, 0.33 mmol), benzyl bromide **27h** (47.1 mg, crude), and MeCN (4.2 mL). Thereby, crude product **10h** (11.5 mg) was obtained. One part of this crude product (6.0 mg) was used without further purification, while the other part (5.5 mg) was purified by semi-prep HPLC (MeCN + 0.05% FA/H$_2$O + 0.05% FA, 5 – 100% MeCN + 0.05% FA over 30 min, 10 mL/min, column B, **10h** at 79% MeCN + 0.05% FA) isolating pure **10h** (1.38 mg, 4 µmol, 1%) as a colorless solid. **LC-MS** *m/z* ([M+H]$^+$) = 363.22, t_r = 3.85 min, *purity*: 97%. **^{1}H NMR** (500 MHz, DMSO-d_6) δ = 8.62 (s, 1H), 8.20 (d, J = 2.4 Hz, 1H), 8.06 (d, J = 2.4 Hz, 1H), 7.96 (d, J = 7.7 Hz, 1H), 7.55 - 7.50 (m, 1H), 7.45 (t, J = 7.7 Hz, 1H), 7.09 (d, J = 7.7 Hz, 1H), 5.55 (s, 2H), 3.90 (s, 3H). **^{13}C NMR** (126 MHz, DMSO-d_6) δ = 166.8, 159.0, 149.6, 143.6, 137.1, 134.2, 132.9, 132.4, 131.2, 130.6, 128.3, 127.7, 127.1, 124.5, 124.1, 52.4, 48.3. **HRMS** *calculated: m/z* ([M+H]$^+$) = 363.0298, *found: m/z* ([M+H]$^+$) = 363.0283.

2-(((6,8-Dichloroquinazolin-4-yl)oxy)methyl)benzoic acid (10i). Starting from **10h** (6.0 mg, crude), compound **10i** was synthesized according to **GP F** under usage of aqueous LiOH solution (20 µL, 1.0 M) instead of NaOH, and THF (50 µL). After purifying the resulting crude by semi-prep HPLC (MeCN + 0.05% FA/H$_2$O + 0.05% FA, 5 – 100% MeCN + 0.05% FA over 30 min, 10 mL/min, column B, **10i** at 72% MeCN + 0.05% FA), **10i** (1.5 mg, 4 µmol, ~25%) was obtained as a colorless solid. **LC-MS** *m/z* ([M-OH]$^+$) = 348.99, t_r = 3.43 min, *purity*: > 98%. **^{1}H NMR** (500 MHz, DMSO-d_6) δ

= 8.76 (s, 1H), 8.27 (s, 1H), 8.16 (d, J = 2.4 Hz, 1H), 8.07 (d, J = 2.4 Hz, 1H), 7.87 - 7.72 (m, 1H), 7.32 - 7.25 (m, 2H), 7.06 - 7.01 (m, 1H), 5.58 (s, 2H). **¹³C NMR** (126 MHz, DMSO-d_6) δ = 169.7, 167.0, 164.2, 159.0, 150.0, 147.5, 143.5, 134.0, 132.4, 131.0, 130.1, 127.4, 127.2, 124.5, 124.1, 48.3. **HRMS** *calculated: m/z* ([M-OH]⁺) = 349.0141, *found: m/z* ([M-OH]⁺) = 349.0131.

4-([1,1'-Biphenyl]-2-ylmethoxy)-6,8-dichloroquinazoline (10j). According to **GP E**, **10g** (30.0 mg, 78 µmol), phenyl boronic acid (11.5 mg, 94 µmol), K₂CO₃ (27.0 mg, 195 µmol), and [Pd(PPh₃)₄] (4.5 mg, 4 µmol) in 1,4-dioxane (1.5 mL) and water (0.3 mL) were used for this synthesis. The purification *via* semi-prep HPLC (MeCN + 0.05% FA/H₂O + 0.05% FA, 5 –100% MeCN + 0.05% FA over 30 min, 10 mL/min, column B, **10j** at 98% MeCN + 0.05% FA) led to **10j** (7.9 mg, 21 µmol, 26%) as a colorless solid (7.9 mg, 21 µmol, 26%). **LC-MS** *m/z* ([M+H]⁺) = 381.24, t_r = 5.50 min, *purity*: > 98%. **¹H NMR** (500 MHz, DMSO-d_6) δ = 8.30 (s, 1H), 8.14 (d, J = 2.3 Hz, 1H), 7.98 (d, J = 2.3 Hz, 1H), 7.50 - 7.44 (m, 2H), 7.43 - 7.30 (m, 5H), 7.26 (dd, J = 1.3, 7.4 Hz, 1H), 7.10 (d, J = 7.4 Hz, 1H), 5.16 (s, 2H). **¹³C NMR** (126 MHz, DMSO-d_6) δ = 158.6, 149.3, 143.4, 140.8, 139.9, 134.1, 133.2, 132.3, 131.1, 130.1, 128.9, 128.5, 127.8, 127.6, 127.5, 126.7, 124.4, 124.0, 48.1. **HRMS** *calculated: m/z* ([M+H]⁺) = 381.0556, *found: m/z* ([M+H]⁺) = 381.0552.

6,8-Dichloro-4-((2-(pyridin-3-yl)benzyl)oxy)quinazoline (10k). Following **GP E**, **10g** (30.0 mg, 78 µmol), 3-pyridyl boronic acid (11.5 mg, 94 µmol), K₂CO₃ (27.0 mg, 195 µmol), and [Pd(PPh₃)₄] (4.5 mg, 4 µmol) in 1,4-dioxane (1.5 mL) and water (0.3 mL) were used for this synthesis affording colorless solid **10k** (8.2 mg, 22 µmol, 28%) after purification *via* semi-prep HPLC (MeCN + 0.05% FA/H₂O + 0.05% FA, 5 – 100% MeCN + 0.05% FA over 30 min, 10 mL/min, column B, **10k** at 72% MeCN + 0.05% FA). **LC-MS** *m/z* ([M+H]⁺) = 382.24, t_r = 3.83 min, *purity*: > 98%.**¹H NMR** (500 MHz, DMSO-d_6) δ = 8.66 - 8.59 (m, 2H), 8.40 (s, 1H), 8.15 (d, J = 2.3 Hz, 1H), 7.97 (d, J = 2.3 Hz, 1H), 7.88 (td, J = 1.8, 7.8 Hz, 1H), 7.51 (dd, J = 4.9, 7.8 Hz, 1H), 7.43 - 7.35 (m, 2H), 7.31 (dd, J = 1.4, 7.2 Hz, 1H), 7.16 (d, J = 7.8 Hz, 1H), 5.16 (s, 2H). ¹³C NMR (126 MHz, DMSO-d_6) δ = 158.6, 149.3, 148.6, 143.4, 137.3, 136.5, 135.6, 134.1, 133.7, 132.4, 131.2, 130.4, 128.5, 127.8, 127.0, 124.4, 124.0, 123.5, 47.8, 22.8; overlap of two signals at 149.3 ppm (see HSQC spectrum Figure S192). **HRMS** *calculated: m/z* ([M+H]⁺) = 382.0508, *found: m/z* ([M+H]⁺) = 382.0506.

1-(3-(((6,8-Dichloroquinazolin-4-yl)oxy)methyl)phenyl)ethan-1-one (10l). Applying **GP B-1** under usage of **12a** (50.0 mg, 0.23 mmol), K₂CO₃ (32.2 mg, 0.23 mmol), 3-acetylbenzyl chloride (39.3 mg, 0.23 mmol), and MeCN (2.9 mL) led to **10l** (20.9 mg, 0.06 mmol, 22%) as a beige solid. **LC-MS** *m/z* ([M+H]⁺) = 346.95, t_r = 4.53 min, *purity*: 96%. **¹H NMR** (500 MHz, CDCl₃) δ = 8.16 (s, 1H), 8.14 (d, J = 2.3 Hz, 1H), 7.89 (s, 1H), 7.84 (d, J = 7.8 Hz, 1H), 7.76 (d, J = 2.3 Hz, 1H), 7.49 (d, J = 7.6 Hz, 1H), 7.41 (t, J = 7.6 Hz, 1H), 5.17 (s, 2H), 2.53 (s, 3H). **¹³C NMR** (126 MHz, CDCl₃) δ = 197.4, 159.5, 146.7, 143.4, 137.8, 135.6, 134.8, 133.2, 133.1, 132.6, 129.5, 128.7, 127.7, 125.3, 124.2, 50.0, 26.7. **HRMS** *calculated: m/z* ([M+H]⁺) = 347.0349, *found: m/z* ([M+H]⁺) = 347.0344.

3-(((6,8-Dichloroquinazolin-4-yl)oxy)methyl)benzoic acid (10n). Following **GP B-3** under usage of **12a** (50.0 mg, 0.28 mmol), K₂CO₃ (32.2 mg, 0.23 mmol), 3-(chloromethyl)benzoic acid (39.7 mg, 0.28 mmol), and DMF (2.9 mL) **10n** was synthesized. After full consumption of the starting material, the reaction mixture was acidified with HCl (1.0 M). Thereby, a colorless solid precipitated that was filtered off and washed with acetone. The acetone solution was dried in *vacuo* and purified by semi-prep HPLC (MeCN + 0.05% FA/H₂O + 0.05% FA, 5 – 100% MeCN + 0.05% FA over 50 min, 5 mL/min, column A, **10n** at 60% MeCN + 0.05% FA) affording **10n** (12.7 mg, 0.04 mmol, 16%) as a colorless solid. **LC-MS** *m/z* ([M+H]⁺) = 346.95, t_r = 4.53 min, *purity*: 96%. **¹H NMR** (500 MHz, DMSO-d_6) δ = 13.05 (br s, 1H), 8.79 (s, 1H), 8.17 (d, J = 2.3 Hz, 1H), 8.06 (d, J = 2.3 Hz, 1H), 7.96 (s, 1H), 7.87 (d, J = 7.8 Hz, 1H), 7.64 (d, J = 7.8 Hz, 1H), 7.48 (t, J = 7.8 Hz, 1H), 5.27 (s, 2H). **¹³C NMR** (126 MHz, DMSO-d_6) δ = 167.0, 158.8, 149.3, 143.5, 136.7, 134.2, 132.4, 132.3, 131.3, 129.0, 128.7, 128.7, 124.5, 124.0, 49.2, 14.9. **HRMS** *calculated: m/z* ([M+H]⁺) = 349.0134, *found: m/z* ([M+H]⁺) = 349.0141.

6,8-Dichloro-4-((4-fluorobenzyl)oxy)quinazoline (10o). According to **GP B-1**, **10o** was synthesized starting from **12a** (20.0 mg, 93 µmol), K₂CO₃ (12.9 mg, 93 µmol), 4-fluorobenzyl chloride (11 µL, 93 µmol) in MeCN (1.2 mL). After purification of the crude product using semi-prep HPLC (MeCN + 0.05% FA/H₂O + 0.05% FA, 5 – 100% MeCN + 0.05% FA over 30 min, 10 mL/min, column B, **10o** at 87% MeCN + 0.05% FA) **10o** (18.0 mg, 56 µmol, 60%) was isolated as a colorless solid. **LC-MS** *m/z* ([M+H]⁺) = 323.06, t_r = 3.87 min, *purity*: > 98%. **¹H NMR** (500 MHz, DMSO-d_6) δ = 8.74 (s, 1H), 8.15 (d, J = 2.3 Hz, 1H), 8.04 (d, J = 2.3 Hz, 1H), 7.48 - 7.43 (m, 2H), 7.21 - 7.15 (m, 2H), 5.18 (s, 2H). **¹³C NMR** (126 MHz, DMSO-d_6) δ = 161.7 (d, J = 243.6 Hz, 1C), 158.8, 149.2, 143.4, 134.1, 132.4 (d, J = 3.2 Hz, 1C), 132.4, 131.2, 130.1 (d, J = 9.2 Hz, 1C), 124.4, 124.1, 115.4 (d, J = 21.1 Hz, 1C), 48.8. **HRMS** *calculated: m/z* ([M+H]⁺) = 323.0137, *found: m/z* ([M+H]⁺) = 323.0149.

6,8-Dichloro-4-((4-chlorobenzyl)oxy)quinazoline (10p). Applying **GP B-1** under usage of **12a** (20.0 mg, 93 µmol), K₂CO₃ (12.9 mg, 93 µmol), 4-chlorobenzyl chloride (12 µL, 93 µmol), and MeCN (1.2 mL) led to **10p** (14.6 mg, 43 µmol, 46%) as a colorless solid after purification *via* semi-prep HPLC (MeCN + 0.05% FA/H₂O + 0.05% FA, 5 – 100% MeCN + 0.05% FA over 30 min, 10 mL/min, column B, **10p** at 97% MeCN + 0.05% FA). **LC-MS** *m/z* ([M+H]⁺) = 339.05, t_r = 4.07 min, *purity*: > 98%. **¹H NMR** (DMSO-d_6, 500 MHz) δ = 8.73 (s, 1H), 8.17 (d, 1H, J=2.3 Hz), 8.05 (d, 1H, J=2.3 Hz), 7.42 (s, 4H), 5.20 (s, 2H). **¹³C NMR** (DMSO-d_6, 126 MHz) δ = 158.8, 149.2, 143.5, 135.2, 134.2, 132.5, 132.4, 131.2, 129.8, 128.6, 124.4, 124.1, 48.8. **HRMS** *calculated: m/z* ([M+H]⁺) = 338.9853, *found: m/z* ([M+H]⁺) = 338.9844.

6,8-Dichloro-4-((4-methoxybenzyl)oxy)quinazoline (10r). Following **GP B-1** by using **12a** (20.0 mg, 93 µmol), K₂CO₃ (12.9 mg, 93 µmol), 4-methoxybenzyl chloride (13 µL, 93 µmol), and MeCN (1.2 mL), **10r** (1.7 mg, 5 µmol, 5%) was obtained as a colorless solid after purification by semi-prep HPLC (MeCN + 0.05% FA/H₂O + 0.05% FA, 5 – 80% MeCN + 0.05% FA over 30 min, 10 mL/min, column B, **10r** at 53% MeCN + 0.05% FA). **LC-MS** *m/z* ([M+H]⁺) = 335.10, t_r = 3.81 min, *purity*: > 98%. **¹H NMR** (DMSO-d_6, 500 MHz) δ = 8.72 (s, 1H), 8.16 (d, 1H, J=2.3 Hz), 8.06 (d, 1H, J=2.3 Hz), 7.35 (d, 2H, J=8.5 Hz), 6.90 (d, 2H, J=8.5 Hz), 5.13 (s, 2H), 3.72 (s, 3H). **¹³C NMR** (DMSO-d_6, 126 MHz) δ = 158.9,

23

158.7, 149.2, 143.4, 134.1, 132.4, 131.2, 129.5, 128.2, 124.4, 114.0, 113.8, 55.1, 48.9. **HRMS** *calculated: m/z* ([M+H]⁺) = 335.0349, *found: m/z* ([M+H]⁺) = 335.0336.

6,8-Dichloro-4-((4-methylbenzyl)oxy)quinazoline (10s). According to **GP B-1**, **10s** (127.6 mg, 0.40 mmol, 86%) was synthesized and isolated after washing with DCM as a yellow solid. For this reaction, **12s** (100.0 mg, 0.47 mmol), K₂CO₃ (64.3 mg, 0.47 mmol), 4-methylbenzyl chloride (62 μL, 0.47 mmol), and MeCN (5.8 mL) were used. **LC-MS** *m/z* ([M+H]⁺) = 319.04, t_r = 4.70 min, *purity*: > 98%. **¹H NMR** (DMSO-d_6, 500 MHz) δ = 8.71 (s, 1H), 8.16 (d, 1H, *J*=2.4 Hz), 8.05 (d, 1H, *J*=2.4 Hz), 7.2-7.3 (m, 2H, *J*=8.1 Hz), 7.1-7.2 (m, 2H, *J*=7.9 Hz), 5.15 (s, 2H), 2.26 (s, 3H). **¹³C NMR** (DMSO-d_6, 126 MHz) δ = 159.2, 149.7, 143.9, 137.6, 134.6, 133.7, 132.9, 131.7, 129.6, 128.3, 124.9, 124.5, 49.6, 21.1. **HRMS** *calculated: m/z* ([M+H]⁺) = 319.0399, *found: m/z* ([M+H]⁺) = 319.0396.

1-(4-Methoxy-3-(((8-(trifluoromethyl)quinazolin-4-yl)oxy)methyl)phenyl)ethan-1-one (10t). Starting from **12a** (20.0 mg, 93 μmol), K₂CO₃ (12.9 mg, 93 μmol), 4-tri-fluoromethylbenzyl chloride (14 μL, 93 μmol), and MeCN (5.8 mL), **10t** was synthesized according to **GP B-1**. After purification *via* semi-prep HPLC (MeCN + 0.05% FA/H₂O + 0.05% FA, 5 – 100% MeCN + 0.05% FA over 30 min, 10 mL/min, column B, **10t** at 92% MeCN + 0.05% FA), **10t** (0.06 mmol, 64%) was isolated as a colorless solid. **LC-MS** *m/z* ([M+H]⁺) = 373.08, t_r = 4.11 min, *purity*: > 98%. **¹H NMR** (500 MHz, DMSO-d_6) δ = 8.75 (s, 1H), 8.17 (d, *J* = 2.3 Hz, 1H), 8.04 (d, *J* = 2.3 Hz, 1H), 7.71 (d, *J* = 8.2 Hz, 2H), 7.59 (d, *J* = 8.2 Hz, 2H), 5.30 (s, 2H). **¹³C NMR** (126 MHz, DMSO-d_6) δ = 196.3, 161.1, 149.8, 145.2, 132.1 (q, $^4J_{CF}$ = 5.2 Hz), 131.2, 130.9 (q, $^3J_{CF}$ = 15.6 Hz), 129.8, 129.4, 126.6, 124.7, 124.9 (q, $^2J_{CF}$ = 30.0 Hz), 123.6, 122.8, 121.4 (q, J_{CF} = 261.0 Hz), 110.8, 56.2, 45.8, 26.4. **HRMS** *calculated: m/z* ([M+H]⁺) = 373.0117, *found: m/z* ([M+H]⁺) = 373.0103.

6,8-Dichloro-4-((5-ethyl-2-methoxyben-zyl)oxy)quinazoline (10x). According to **GP E**, starting material **10ae** (30.0 mg, 72 μmol) was converted under usage of ethyl boronic acid (26.7 mg, 362 μmol), K₂CO₃ (0.180 μmol), and [Pd(PPh₃)₄] (4.6 mg, 4 μmol) in 1,4-diox-ane (1.4 mL) and water (0.2 mL) to give **10x** (1.7 mg, 5 μmol, 6%) as a colorless solid after purification of the crude product *via* semi-prep HPLC (MeCN + 0.05% FA/H₂O + 0.05% FA, 75 – 100% MeCN + 0.05% FA over 30 min, 10 mL/min, column B, **10x** at 85% MeCN + 0.05% FA). **LC-MS** *m/z* ([M+H]⁺) new = 363.13, t_r = 4.27 min, *purity*: > 98%. **¹H NMR** (500 MHz, DMSO-d_6) δ = 8.58 (s, 1H), 8.15 (d, *J* = 2.4 Hz, 1H), 8.05 (d, *J* = 2.4 Hz, 1H), 7.13 (dd, *J* = 2.0, 8.3 Hz, 1H), 7.07 (d, *J* = 2.0 Hz, 1H), 6.94 (d, *J* = 8.3 Hz, 1H), 5.08 (s, 2H), 3.79 (s, 3H), 1.11 (t, *J* = 7.6 Hz, 3H); quartet overlapped by DMSO peak (see HSQC spectrum Figure S210). **¹³C NMR** (126 MHz, DMSO-d_6) δ = 158.8, 155.3, 149.8, 143.5, 135.5, 134.1, 132.3, 131.1, 129.3, 128.4, 124.5, 124.1, 123.0, 111.0, 55.6, 46.1, 27.2, 15.9. **HRMS** *cal-culated: m/z* ([M+H]⁺) = 363.0662, *found: m/z* ([M+H]⁺) = 363.0652.

1-(3-(((6,8-Dichloroquinazolin-4-yl)oxy)methyl)-4-ethylphenyl)ethan-1-one (10y). According to **GP E**, **10ao** (30.0 mg, 70 μmol), ethyl boronic acid (13.0 mg, 352 μmol), K₂CO₃ (24.3 mg, 176 μmol), [Pd(PPh₃)₄] (8.0 mg, 8 μmol), 1,4-dioxane (1.4 mL), and water (0.2 mL) were used for the synthesis of **10y** (8.9 mg, 24 μmol, 34%) that was obtained

as a colorless solid after purification *via* semi-prep HPLC (MeCN + 0.05% FA/H₂O + 0.05% FA, 5 – 100% MeCN + 0.05% FA over 30 min, 10 mL/min, column B, **10y** at 87% MeCN + 0.05% FA). **LC-MS** *m/z* ([M+H]⁺) = 375.26, t_r = 4.91 min, *purity*: > 98%. **¹H NMR** (500 MHz, DMSO-d_6) δ = 8.66 (s, 1H), 8.18 (d, *J* = 2.4 Hz, 1H), 8.06 (d, *J* = 2.4 Hz, 1H), 7.86 (dd, *J* = 1.4, 7.9 Hz, 1H), 7.54 (d, *J* = 1.4 Hz, 1H), 7.42 (d, *J* = 7.9 Hz, 1H), 5.30 (s, 2H), 2.82 (q, *J* = 7.6 Hz, 2H), 2.48 (s, 3H), 1.19 (t, *J* = 7.6 Hz, 3H). **¹³C NMR** (126 MHz, DMSO-d_6) δ = 197.4, 158.8, 149.4, 147.4, 143.4, 134.9, 134.3, 134.0, 132.5, 131.4, 129.0, 128.2, 126.3, 124.5, 123.9, 46.8, 26.6, 25.0, 14.4. **HRMS** *calculated: m/z* ([M+H]⁺) = 375.0662, *found: m/z* ([M+H]⁺) = 375.0659.

1-(3-(((6,8-Dichloroquinazolin-4-yl)oxy)methyl)-2-methoxyphenyl)ethan-1-one (10z). Applying **GP I** under usage of **26z** (243.0 mg, 1.48 mmol), NBS (263.4 mg, 1.48 mmol), AIBN (48.6 mg, 0.30 mmol), and CCl₄ (3.0 mL) gave **27z** (183.4 mg, 0.75 mmol, 51%) as a yellow oil. **R_f** (PB/EtOAc, 9:1) = 0.23. One part of this oil (31.6 mg, 0.13 mmol) was directly converted under usage of **12a** (27.1 mg, 0.13 mmol), K₂CO₃ (17.4 mg, 0.13 mmol), and MeCN (1.6 mL). Thereby, **10z** (20.8 mg, 55 μmol, 44%) was obtained as a colorless solid after purification by semi-prep HPLC (MeCN + 0.05% FA/H₂O + 0.05% FA, 5 – 100% MeCN + 0.05% FA over 30 min, 10 mL/min, column B, **10z** at 83% MeCN + 0.05% FA). **LC-MS** *m/z* ([M+H]⁺) = 377.21, t_r = 4.60 min, *purity*: > 98%. **¹H NMR** (500 MHz, DMSO-d_6) δ = 8.66 (s, 1H), 8.17 (d, *J* = 2.4 Hz, 1H), 8.03 (d, *J* = 2.4 Hz, 1H), 7.56 (dd, *J* = 1.5, 7.7 Hz, 1H), 7.37 (dd, *J* = 1.5, 7.7 Hz, 1H), 7.16 (t, *J* = 7.7 Hz, 1H), 5.24 (s, 2H), 3.78 (s, 3H), 2.57 (s, 3H). **¹³C NMR** (126 MHz, DMSO-d_6) δ = 199.8, 158.8, 156.7, 149.7, 143.5, 134.1, 132.9, 132.7, 132.4, 131.2, 129.8, 129.4, 124.4, 124.1, 123.9, 62.6, 45.7, 30.1. **HRMS** *calculated: m/z* ([M+H]⁺) = 377.0454, *found: m/z* ([M+H]⁺) = 377.0441.

1-(4-(((6,8-Dichloroquinazolin-4-yl)oxy)methyl)-3-methoxyphenyl)ethan-1-one (10aa). To synthesize **10aa**, **GP B-2** was applied using **12a** (24.0 mg, 0.11 mmol), **27aa** (26.5 mg, 0.11 mmol), Cs₂CO₃ (36.0 mg, 0.11 mmol), and MeCN (1.0 mL). The product **10aa** (31.0 mg, 82 μmol, 75%) was isolated by AFC (DCM/MeOH, 0 – 10% MeOH over 15 min, 13 mL/min, 4 g silica, **10aa** at 6% MeOH) as a white solid. **LC-MS** *m/z* ([M+H]⁺) = 377.03, t_r = 3.69 min, *purity*: > 98%. **¹H NMR** (500 MHz, DMSO-d_6) δ = 8.64 (s, 1H), 8.17 (d, *J* = 2.3 Hz, 1H), 8.03 (d, *J* = 2.3 Hz, 1H), 7.53 (dd, *J* = 1.3, 7.9 Hz, 1H), 7.50 - 7.47 (m, 1H), 7.30 (d, *J* = 7.9 Hz, 1H), 5.17 (s, 2H), 3.92 (s, 3H), 2.57 (s, 3H). **¹³C NMR** (126 MHz, DMSO-d_6) δ = 197.9, 159.3, 157.5, 150.3, 143.9, 138.3, 134.6, 132.8, 131.6, 129.9, 129.2, 124.9, 124.5, 121.4, 109.9, 56.2, 46.5, 27.3. **HRMS** *calculated: m/z* ([M+H]⁺) = 377.0454, *found: m/z* ([M+H]⁺) = 377.0442.

1-(2-(((6,8-Dichloroquinazolin-4-yl)oxy)methyl)-3-methoxyphenyl)ethan-1-one (10ab). The application of **GP B-1** on **12a** (30.0 mg, 0.14 mmol) with K₂CO₃ (19.3 mg, 0.14 mmol), benzyl bromide **27ab** (34.0 mg, 0.14 mmol), and MeCN (1.8 mL) led to pure orange solid **10ab** (41.2 mg, 0.11 mmol, 78%) after filtration. **LC-MS** *m/z* ([M+H]⁺) = 377.23, t_r = 4.83 min, *purity*: > 98%. **¹H NMR** (500 MHz, CDCl₃) δ = 8.28 (s, 1H), 8.13 (s, 1H), 7.75 (s, 1H), 7.39 (t, *J* = 7.7 Hz, 1H), 7.27 (d, *J* = 7.7 Hz, 1H), 7.01 (d, *J* = 7.7 Hz, 1H), 5.29 (s, 2H), 3.84 (s, 3H), 2.72 (s, 3H). **¹³C NMR** (126 MHz, CDCl₃) δ = 202.5, 159.5, 158.8, 148.3, 143.4, 142.6, 134.2, 132.5, 132.2, 129.8, 125.0, 124.3, 120.4, 119.9, 113.2, 55.8,

24

42.8, 29.6. **HRMS** *calculated: m/z* ([M+H]⁺) = 377.0454, *found: m/z* ([M+H]⁺) = 377.0450.

1-(3-(((6,8-Dichloroquinazolin-4-yl)oxy)methyl)-5-methoxyphenyl)ethan-1-one (10ac). The alkyl bromination was performed according to **GP I** using **26ac** (211.1 mg, 1.29 mmol), AIBN (42.2 mg, 0.26 mmol), NBS (228.8 mg, 1.29 mmol), and CCl₄ (2.6 mL). One part (34.0 mg) of resulting **27ac** (75.7 mg, crude) was directly used for the next step without further purification. **R_f** (PB/EtOAc, 9:1) = 0.44. Performing **GP B-1** on **12a** (30.0 mg, 0.14 mmol) with K₂CO₃ (19.3 mg, 0.14 mmol), benzyl bromide **27ac** (34.0 mg, crude), and MeCN (1.8 mL) led to pure yellow solid **10ac** (46.6 mg, 0.12 mmol, 88%) after filtration. **LC-MS** *m/z* ([M+H]⁺) = 377.23, *t_r* = 4.66 min, *purity*: 96%. **¹H NMR** (500 MHz, CDCl₃) δ = 8.14 (s, 2H), 7.76 (s, 1H), 7.45 (s, 1H), 7.36 (s, 1H), 7.01 (s, 1H), 5.13 (s, 2H), 3.77 (s, 3H), 2.51 (s, 3H). **¹³C NMR** (126 MHz, CDCl₃) δ = 197.2, 160.4, 159.5, 146.7, 143.4, 139.2, 136.9, 134.8, 133.2, 125.3, 124.2, 120.3, 118.9, 113.0, 55.7, 49.8, 26.7. **HRMS** *calculated: m/z* ([M+H]⁺) = 377.0454, *found: m/z* ([M+H]⁺) = 377.0450.

1-(5-(((6,8-Dichloroquinazolin-4-yl)oxy)methyl)-2-methoxyphenyl)ethan-1-one (10ad). Following **GP B-1**, quinazoline **12a** (14.0 mg, 65 µmol) was converted with K₂CO₃ (9.0 mg, 65 µmol) and benzyl bromide **27ad** (7.8 mg, crude) in MeCN (0.8 mL) to **10ad** (18.1 mg, 48 µmol, 74%) which was obtained as a beige solid after filtration. **LC-MS** *m/z* ([M+H]⁺) = 377.24, *t_r* = 4.65 min, *purity*: > 98%. **¹H NMR** (500 MHz, CDCl₃) δ = 8.22 (s, 1H), 8.21 (d, *J* = 2.4 Hz, 1H), 7.82 (d, *J* = 2.4 Hz, 1H), 7.74 (d, *J* = 2.4 Hz, 1H), 7.51 (dd, *J* = 2.4, 8.5 Hz, 1H), 6.97 (d, *J* = 8.7 Hz, 1H), 5.14 (s, 2H), 3.91 (s, 3H), 2.60 (s, 3H). **¹³C NMR** (126 MHz, CDCl₃) δ = 199.1, 159.5, 159.1, 146.8, 143.4, 134.7, 133.8, 133.1, 133.0, 130.3, 128.5, 127.2, 125.2, 124.3, 112.4, 55.7, 49.5, 31.8. **HRMS** *calculated: m/z* ([M+H]⁺) = 377.0454, *found: m/z* ([M+H]⁺) = 377.0449.

1-(3-(((6,8-dichloroquinazolin-4-yl)oxy)methyl)-4-(pyridin-3-yl)phenyl)ethan-1-one (10ae). Following **GP E**, **10ai** (32.5 mg, 76 µmol), 3-pyridyl boronic acid (11.2 mg, 91 µmol), K₂CO₃ (26.4 mg, 191 µmol), [Pd(PPh₃)₄] (4.4 mg, 4 µmol), 1,4-dioxane (1.5 mL), and water (0.3 mL) were used for the synthesis of **10ae** (7.0 mg, 16 µmol, 21%) that was obtained as a colorless solid after purification *via* semi-prep HPLC (MeCN + 0.05% FA/H₂O + 0.05% FA, 5 – 100% MeCN + 0.05% FA over 30 min, 10 mL/min, column B, **10ae** at 62% MeCN + 0.05% FA). **LC-MS** *m/z* ([M+H]⁺) = 424.14, *t_r* = 3.15 min, *purity*: > 98%. **¹H NMR** (500 MHz, DMSO-*d₆*) δ = 8.64 (d, *J* = 4.9 Hz, 1H), 8.41 (s, 1H), 8.15 (d, *J* = 2.4 Hz, 1H), 8.00 (d, *J* = 7.9 Hz, 1H), 7.96 (d, *J* = 2.4 Hz, 1H), 7.90 (br d, *J* = 7.8 Hz, 1H), 7.74 (s, 1H), 7.52 (dd, *J* = 4.9, 7.8 Hz, 2H), 7.48 (d, *J* = 7.9 Hz, 1H), 5.21 (s, 2H), 2.56 (s, 3H). **¹³C NMR** (126 MHz, DMSO-*d₆*) δ = 197.5, 158.6, 149.2, 149.1, 149.0, 143.3, 142.1, 136.6, 136.4, 134.8, 134.4, 134.2, 132.4, 131.2, 131.0, 128.0, 126.7, 124.4, 123.9, 123.5, 47.9, 26.8. **HRMS** *calculated: m/z* ([M+H]⁺) = 424.0614, *found: m/z* ([M+H]⁺) = 424.0601.

6,8-Dichloro-4-((2,6-dimethoxybenzyl)oxy)quinazoline (10af). *Preparation of methyl bromide (step 1).* Starting from 2,6-dimethoxytoluene (457.0 mg, 3.00 mmol), **GP I** was performed using AIBN (50.0 mg, 0.15 mmol), NBS (535.0 mg, 3.00 mmol), and CCl₄ (6.0 mL). A full conversion was reached already after 3 h. After concentration *in vacuo*,

the resulting oily residue was re-suspended in ether. A white solid precipitated and was filtered off. The mother liquor, containing **27af**, was concentrated *in vacuo* and used without further purification in the next step. **R_f** (Hex/DCM, 4:1) = 0.50.⁵³

O-Alkylation of quinazolinone (step 2). Following **GP B-2** under usage of **12a** (21.5 mg, 0.10 mmol), **27af** (23.0 mg, crude), Cs₂CO₃ (33.0 mg, 0.10 mmol), and MeCN (1.0 mL). The resulting crude product was purified by AFC (DCM/MeOH, 0 – 10% MeOH over 15 min, 13 mL/min, 4 g silica, **10af** at 5% MeOH) to give white solid **10af** (22 mg, 60 µmol, 60%). **LC-MS** *m/z* ([M+H]⁺) = 365.45, *t_r* = 3.92 min, *purity*: 98%. **¹H NMR** (500 MHz, CDCl₃) δ = 8.24 (d, *J* = 2.3 Hz, 1H), 8.08 (s, 1H), 7.78 (d, *J* = 2.3 Hz, 1H), 7.32 (t, *J* = 8.4 Hz, 1H), 6.59 (d, *J* = 8.4 Hz, 2H), 5.24 (s, 2H), 3.83 (s, 6H). **¹³C NMR** (126 MHz, CDCl₃) δ = 159.5, 159.0, 147.6, 143.4, 134.1, 132.5, 132.2, 130.9, 125.2, 124.2, 109.9, 103.7, 55.8, 39.0. **HRMS** *calculated: m/z* ([M+H]⁺) 365.0454, *found: m/z* ([M+H]⁺) = 365.0440.

4-(Benzo[d][1,3]dioxol-4-ylmethoxy)-6,8-dichloroquinazoline (10ag). According to **GP B-2**, **12a** (24.0 mg, 0.11 mmol) was converted using 4-(bromomethyl)benzo[d][1,3]dioxole (24.0, 0.11 mmol), Cs₂CO₃ (36.0 mg, 0.11 mmol) and MeCN (1.0 mL). The product **10ag** (17.2 mg, 49 µmol, 45%) was isolated by AFC (DCM/MeOH, 0 – 10% MeOH over 15 min, 13 mL/min, 4 g silica, **10ag** at 8% MeOH) as a colorless solid. **LC-MS** *m/z* ([M+H]⁺) = 34919, *t_r* = 4.79 min, *purity*: > 98%. **¹H NMR** (500 MHz, CDCl₃) δ = 8.28 (s, 1H), 8.11 (d, *J* = 2.4 Hz, 1H), 7.73 (d, *J* = 2.4 Hz, 1H), 6.88 (dd, *J* = 1.7, 7.3 Hz, 1H), 6.77 - 6.71 (m, 2H), 5.91 (s, 2H), 5.07 (s, 2H). **¹³C NMR** (126 MHz, CDCl₃) δ = 159.4, 147.7, 147.5, 146.0, 143.4, 134.6, 132.9, 132.8, 125.2, 124.3, 123.0, 122.2, 116.3, 109.2, 101.4, 44.9. **HRMS** *calculated: m/z* ([M+H]⁺) = 349.0141, *found: m/z* ([M+H]⁺) = 349.0129.

4-((5-Bromo-2-methoxybenzyl)oxy)-6,8-dichloroquinazoline (10ah). According to **GP B-1**, **2s** (200.0 mg, 0.93 mmol), K₂CO₃ (128.5 mg, 0.93 mmol), benzyl bromide **27ah** (260.4 mg, crude), and MeCN (11.6 mL) were used for the preparation of colorless solid **10ah** (298.4 mg, 0.72 mmol, 77%). **LC-MS** *m/z* ([M+H]⁺) = 413.06, *t_r* = 5.56 min, *purity*: 98%. **¹H NMR** (500 MHz, DMSO-*d₆*) δ = 8.60 (s, 1H), 8.12 (s, 1H), 8.02 (s, 1H), 7.51 - 7.44 (m, 1H), 7.41 (s, 1H), 7.00 (d, J = 8.7 Hz, 1H), 5.08 (s, 2H), 3.83 (s, 3H). **¹³C NMR** (126 MHz, DMSO-*d₆*) δ = 158.8, 156.5, 149.7, 143.4, 134.0, 132.3, 132.3, 131.9, 131.0, 125.7, 124.4, 124.1, 113.3, 111.6, 55.9, 45.9. **HRMS** *calculated: m/z* ([M+H]⁺) = 412.9454, *found: m/z* ([M+H]⁺) = 412.0440.

1-(4-Bromo-3-(((6,8-dichloroquinazolin-4-yl)oxy)methyl)phenyl)ethan-1-one (10ai). First, **27ai** was synthesized following **GP I**. For this reaction, 1-(4-bromo-3-methylphenyl)ethan-1-one (60.0 mg, 0.28 mmol), AIBN (9.3 mg, 57 µmol), NBS (50.1 mg, 0.28 mmol), and CCl₄ (0.6 mL) were used, giving **27ai** (77.7 mg, 0.26 mmol, 94%) as a colorless oil. **R_f** (PB/EtOAc = 98:2) = 4.62. Then, **10ai** was synthesized according to **GP B-1**. Usage of **12a** (56.6 mg, 0.26 mmol), K₂CO₃ (36.3 mg, 0.26 mmol) and benzyl bromide **27ai** (76.8 mg, 0.26 mmol), and MeCN (3.3 mL) resulted in **10ai** (89.2 mg, 0.26 mmol, 80%) as a colorless solid. **LC-MS** *m/z* ([M+H]⁺) = 425.10, *t_r* = 5.09 min, *purity*: 97%. **¹H NMR** (500 MHz, CDCl₃) δ = 8.35 (s, 1H), 8.21 (d, *J* = 2.3 Hz, 1H), 8.01 (d, *J* = 1.9 Hz, 1H), 7.85 (d, *J* = 2.3 Hz, 1H),

25

7.79 (dd, J = 1.9, 8.2 Hz, 1H), 7.73 (d, J = 8.2 Hz, 1H), 5.35 - 5.31 (m, 2H), 2.58 (s, 3H), 1.26 (s, 1H). **¹³C NMR** (126 MHz, CDCl₃) δ = 196.4, 159.6, 147.1, 143.3, 136.7, 134.9, 134.4, 133.8, 133.2, 133.2, 130.9, 129.7, 129.2, 125.3, 124.2, 50.3, 26.6.

6,8-Dichloroquinazolin-4(3H)-one (12a). We have recently published this compound's synthesis.[35]

8-Chloroquinazolin-4(3H)-one (12b). According to **GP A**, 3-chloro anthranilic acid (200.0 mg, 1.17 mmol), formamide (9.8 mL), and acetic acid (1.0 mL) were used to afford **12b** (144.3 mg, 1.17 mmol, 69%) as a beige solid. **LC-MS** m/z ([M+H]⁺) = 181.04, t_r = 2.56 min, *purity*: > 98%. **¹H NMR** (500 MHz, DMSO-d_6) δ = 12.53 (br s, 1H), 8.22 (s, 1H), 8.08 (dd, J = 1.4, 7.9 Hz, 1H), 7.97 (dd, J = 1.4, 7.9 Hz, 1H), 7.50 (t, J = 7.9 Hz, 1H).[54] **¹³C NMR** (126 MHz, DMSO-d_6) δ = 160.3, 146.5, 145.3, 134.5, 130.8, 127.2, 125.1, 124.4.

7-Chloroquinazolin-4(3H)-one (12c). Following **GP A**, 4-chloro anthranilic acid (200.0 mg, 1.17 mmol) was converted using formamide (9.8 mL), and acetic acid (1.0 mL). Since only a small amount of solid was formed by pouring the reaction mixture into ice water, the aqueous solution was extracted using DCM (4 x 50 mL) after filtration. The organic layers were combined and dried over Na₂SO₄, filtered, and concentrated to dryness *in vacuo* affording the corresponding product 1**2c** (133.0 mg, 0.74 mmol, 63%) as a beige solid. **LC-MS** m/z ([M+H]⁺) = 181.04, t_r = 2.77 min, *purity*: > 98%. **¹H NMR** (500 MHz, DMSO-d_6) δ = 12.42 (br s, 1H), 8.14 (s, 1H), 8.10 (d, J = 8.5 Hz, 1H), 7.72 (d, J = 1.3 Hz, 1H), 7.55 (dd, J = 1.3, 8.5 Hz, 1H).[54] **¹³C NMR** (126 MHz, DMSO-d_6) δ = 160.2, 149.9, 147.0, 139.0, 128.0, 127.1, 126.5, 121.5.

6-Chloroquinazolin-4(3H)-one (12d). Under usage of 5-chloro anthranilic acid (200.0 mg, 1.17 mmol), formamide (9.8 mL), and acetic acid (1.0 mL) the synthesis according to **GP A** gave brown needles (141.7 mg, 0.79 mmol, 67%) that crystallized overnight from the mother liquor. **LC-MS** m/z ([M+H]⁺) = 181.05, t_r = 2.76 min, *purity*: > 98%. **¹H NMR** (500 MHz, DMSO-d_6) δ = 12.46 (br s, 1H), 8.13 (s, 1H), 8.05 (d, J = 2.5 Hz, 1H), 7.84 (dd, J = 2.5, 8.7 Hz, 1H), 7.69 (d, J = 8.7 Hz, 1H).[54] **¹³C NMR** (126 MHz, DMSO-d_6) δ = 159.8, 147.5, 146.0, 134.5, 131.1, 129.6, 124.9, 123.9.

5-Chloroquinazolin-4(3H)-one (12e). This compound was synthesized following **GP A** starting from 6-chloro anthranilic acid (200.0 mg, 1.17 mmol), formamide (9.8 mL), and acetic acid (1.0 mL). Since no solid was formed by pouring the reaction mixture into ice water, the same work-up as for **12c** was performed giving beige solid **2e** (163.2 mg, 0.90 mmol, 78%). **LC-MS** m/z ([M+H]⁺) = 181.03, t_r = 2.45 min, *purity*: 92%. **¹H NMR** (DMSO-d_6, 500 MHz) δ = 12.33 (br s, 1H), 8.09 (s, 1H), 7.73 (t, 1H, J=8.0 Hz), 7.61 (d, 1H, J=8.0 Hz), 7.53 (dd, 1H, J=1.0, 8.0 Hz).[54] **¹H NMR** (500 MHz, DMSO-d_6) δ = 12.32 (br s, 1H), 8.08 (s, 1H), 7.72 (t, J = 7.9 Hz, 1H), 7.60 (d, J = 7.9 Hz, 1H), 7.52 (dd, J = 1.0, 7.9 Hz, 1H). Contains 14 mol% formamide according to ¹H NMR spectrum. **¹³C NMR** (126 MHz, DMSO-d_6) δ = 158.9, 151.3, 146.3, 134.2, 132.4, 129.2, 126.9, 119.6.

8-Fluoroquinazolin-4(3H)-one (12f). According to **GP A**, **12f** was synthesized using 3-fluoro anthranilic acid (310.3 mg, 2.00 mmol), formamide (21.5 mL), and acetic acid (2.2 mL) and was isolated as a light-brown solid (146.3 mg, 0.89 mmol, 45%). **LC-MS** m/z ([M+H]⁺) = 165.1,

t_r = 2.11 min, *purity*: > 98%. **¹H NMR** (500 MHz, DMSO-d_6) δ = 12.45 (br s, 1H), 8.14 (s, 1H), 7.93 (d, J = 8.0 Hz, 1H), 7.69 (ddd, J = 1.2, 8.0, 10.6 Hz, 1H), 7.51 (dt, J = 4.7, 8.0 Hz, 1H).[55] **¹³C NMR** (126 MHz, DMSO-d_6) δ = 159.9 (d, $^4J_{CF}$ = 3.7 Hz), 156.5 (d, J_{CF} = 252.8 Hz), 146.0, 138.0 (d, $^2J_{CF}$ = 11.9 Hz), 127.0 (d, $^3J_{CF}$ = 8.3 Hz), 124.7, 121.6 (d, $^4J_{CF}$ = 4.6 Hz), 119.8 (d, $^2J_{CF}$ = 19.3 Hz).

8-Bromoquinazolin-4(3H)-one (12g). Following **GP A**, compound **12g** (112.1 mg, 0.50 mmol, 57%) was obtained as a yellow solid from 3-bromo anthranilic acid (200.0 mg, 0.88 mmol) heated to reflux in formamide (7.3 mL) and acetic acid (0.7 mL). **LC-MS** m/z ([M+H]⁺) = 224.96, t_r = 2.30 min, *purity*: > 98%. **¹H NMR** (500 MHz, DMSO-d_6) δ = 12.50 (br s, 1H), 8.22 (s, 1H), 8.12 (t, J = 7.5 Hz, 2H), 7.42 (t, J = 7.5 Hz, 1H). **¹³C NMR** (126 MHz, DMSO-d_6) δ = 160.3, 146.5, 146.2, 137.8, 127.6, 125.7, 124.3, 121.8.[56]

8-Methylquinazolin-4(3H)-one (12h). Under usage of 3-methyl anthranilic acid (302.3 mg, 2.00 mmol), formamide (16.7 mL), and acetic acid (1.7 mL) this synthesis was performed following **GP A** by splitting the batch into two parts due to the high reaction volume. Thereby, **12h** (210.1 mg, 1.31 mmol, 66%) was collected as a light-yellow solid**. LC-MS** m/z ([M+H]⁺) = 161.11, t_r = 2.47 min, *purity*: 90%. **¹H NMR** (500 MHz, DMSO-d_6) δ = 12.23 (br s, 1H), 8.11 (s, 1H), 7.96 (d, J = 7.6 Hz, 1H), 7.67 (d, J = 7.6 Hz, 1H), 7.39 (t, J = 7.6 Hz, 1H), 2.53 (s, 3H). **¹³C NMR** (126 MHz, DMSO-d_6) δ = 161.0, 147.2, 144.4, 135.4, 134.7, 126.2, 123.5, 122.6, 17.3.[56]

8-(Trifluoromethyl)quinazolin-4(3H)-one (12i). Applying **GP A** with 3-trifluoromethyl anthranilic acid (100.0 mg, 0.49 mmol), formamide (4.1 mL), and acetic acid (0.4 mL), light yellow solid **12i** (88.5 mg, 0.41 mmol, 85%) was synthesized. **LC-MS** m/z ([M+H]⁺) = 215.05, t_r = 3.10 min, *purity*: 97%.**¹H NMR** (500 MHz, DMSO-d_6) δ = 12.6 (br s, 1H), 8.40 (d, J = 7.6 Hz, 1H), 8.27 (s, 1H), 8.19 (d, J = 7.6 Hz, 1H), 7.66 (t, J = 7.6 Hz, 1H). **¹³C NMR** (126 MHz, DMSO-d₆) δ = 159.9, 146.9, 146.2, 145.9 (q, $^2J_{CF}$ = 19.2 Hz), 131.97 (q, $^4J_{CF}$= 5.2 Hz), 130.6, 126.1, 124.8 (q, $^3J_{CF}$ = 8.3 Hz), 125.02 (q, J_{CF} = 284.0 Hz).

8-(Methoxycarbonyl)-4-oxo-3,4-dihydroquinazolin-1-ium chloride (12j). First, the corresponding carboxy quinazoline (266.5 mg, 1.39 mmol, 70%) was synthesized following **GP A** starting from 3-carboxy anthranilic acid (362.3 mg, 2.00 mmol), formamide (16.7 mL) and acetic acid (1.7 mL). The product was precipitated by acidifying the mixture of reaction suspension and ice water with aqueous HCl (1 M). One part of the resulting pure product (200.0 mg, 1.05 mmol) were directly converted to the methyl ester **12j** by applying **GP C** under usage of K₂CO₃ (145.5 mg, 1.05 mmol) and MeI (0.1 mL, 1.58 mmol) in DMF (1.1 mL). Instead of extraction, the product was filtered off after concentrating the reaction mixture in *vacuo* and suspending the residue in water. Thereby, **12j** (141.4 mg, 0.69 mmol, 66%) was isolated as a white solid. **LC-MS** m/z ([M+H]⁺) = 205.17, t_r = 1.86 min, *purity*: 96%. **¹H NMR** (500 MHz, DMSO-d_6) δ = 9.54 (br s, 1H), 8.56 (s, 1H), 8.51 (dd, J = 1.4, 7.6 Hz, 1H), 8.34 (dd, J = 1.4, 7.6 Hz, 1H), 7.88 (br s, 1H), 7.64 (t, J = 7.6 Hz, 1H), 3.53 (s, 3H). **¹³C NMR** (126 MHz, DMSO-d_6) δ = 165.7, 160.4, 149.0, 145.5, 136.0, 129.5, 128.9, 126.5, 122.0, 33.8.

26

8-Hydroxyquinazolin-4(3*H*)-one (12m). This brown solid (233.7 mg, 1.44 mmol, 72%) was synthesized by following **GP A** under usage of 3-hydroxy anthranilic acid (306.3 mg, 2.00 mmol), formamide (16.6 mL), and acetic acid (1.7 mL). **LC-MS** m/z ([M+H]$^+$) = 163.03, t_r = 1.27 min, *purity*: > 98%. **^{1}H NMR** (500 MHz, DMSO-d_6) δ = 12.22 (br s, 1H), 9.72 (s, 1H), 8.04 (s, 1H), 7.53 (d, J = 7.6 Hz, 1H), 7.33 (t, J = 7.6 Hz, 1H), 7.18 (d, J = 7.6 Hz, 1H). **^{13}C NMR** (126 MHz, DMSO-d_6) δ = 160.7, 153.0, 143.5, 137.7, 127.3, 123.5, 118.4, 115.5.

5,8-Dichloroquinazolin-4(3*H*)-one (12t). Based on **GP A** using 3,6-dichloro anthranilic acid (200.0 mg, 0.97 mmol), formamide (8.1 mL) and acetic acid (0.8 mL), **12t** (157.9 mg, 0.73 mmol, 76%) was prepared as a beige solid. **LC-MS** m/z ([M+H]$^+$) = 215.01, t_r = 2.53 min, *purity*: > 98%. **^{1}H NMR** (500 MHz, DMSO-d_6) δ = 12.57 (br s, 1H), 8.21 (s, 1H), 7.91 (d, J = 8.5 Hz, 1H), 7.51 (d, J = 8.5 Hz, 1H). **^{13}C NMR** (126 MHz, DMSO-d_6) δ = 158.6, 147.3, 147.1, 134.1, 131.3, 130.0, 129.1, 121.0.

5,7-Dichloroquinazolin-4(3*H*)-one (12u). 4,6-Dichloro anthranilic acid (100.0 mg, 0.49 mmol), formamide (4.1 mL), and acetic acid (0.4 mL) were used for the synthesis according to **GP A**. Thereby, **12u** (85.1 mg, 0.40 mmol, 80%) was isolated as a light-beige solid. **LC-MS** m/z ([M+H]$^+$) = 215.01, t_r = 2.83 min, *purity*: > 98%. **^{1}H NMR** (500 MHz, DMSO-d_6) δ = 12.43 (br s, 1H), 8.12 (s, 1H), 7.66 (d, J = 2.0 Hz, 1H), 7.65 (d, J = 2.0 Hz, 1H). **^{13}C NMR** (126 MHz, DMSO-d_6) δ = 158.5, 151.9, 147.6, 138.1, 134.0, 128.6, 126.1, 118.6.

6-Chloro-8-methylquinazolin-4(3*H*)-one (12v). Following **GP A**, light-brown solid **12v** (84.2 mg, 0.43 mmol, 80%) was synthesized by converting 5-chloro-3-methyl anthranilic acid (100.0 mg, 0.49 mmol) with formamide (4.0 mL) and acetic acid (0.4 mL). **LC-MS** m/z ([M+H]$^+$) = 194.94, t_r = 2.88 min, *purity*: 96%. **^{1}H NMR** (500 MHz, DMSO-d_6) δ = 12.44 (br s, 1H), 8.15 (s, 1H), 7.88 (d, J = 2.1 Hz, 1H), 7.78 - 7.70 (m, 1H), 2.51 (s, 3H).[57] **^{13}C NMR** (126 MHz, DMSO-d_6) δ = 160.1, 146.1, 145.0, 138.5, 134.4, 130.5, 123.8, 122.4, 17.1.

8-Chloro-6-methylquinazolin-4(3*H*)-one (12w). According to **GP A**, this synthesis led to **12w** (55.4 mg, 0.28 mmol, 53%) as a light-brown solid. It was performed starting from 3-chloro-5-methyl anthranilic acid (100.0 mg, 0.54 mmol), formamide (4.5 mL) and acetic acid (0.5 mL). **LC-MS** m/z ([M+H]$^+$) = 194.98, t_r = 2.59 min, *purity*: > 98%. **^{1}H NMR** (500 MHz, DMSO-d_6) δ = 12.39 (br s, 1H), 8.14 (s, 1H), 8.02 - 7.94 (m, 1H), 7.88 (d, J = 1.7 Hz, 1H), 7.82 (d, J = 1.7 Hz, 1H), 2.42 (s, 3H). **^{13}C NMR** (126 MHz, DMSO-d_6) δ = 160.2, 145.5, 143.2, 137.3, 135.5, 130.5, 124.6, 124.0, 20.5.

6,8-Dimethylquinazolin-4(3*H*)-one (12x). Performing **GP A** under usage of 3,5-dimethyl anthranilic acid (200.0 mg, 1.21 mmol), formamide (10.1 mL), and acetic acid (1.0 mL) gave the corresponding product **12x** (31.0 mg, 0.18 mmol, 15%) as a light-brown solid. **LC-MS** m/z ([M+H]$^+$) = 175.12, t_r = 2.52 min, *purity*: > 98%. **^{1}H NMR** (500 MHz, DMSO-d_6) δ = 12.13 (br s, 1H), 8.05 (s, 1H), 7.75 (s, 1H), 7.50 (s, 1H), 2.50 (s, 3H), 2.39 (s, 3H).[58] **^{13}C NMR** (126 MHz, DMSO-d_6) δ = 160.9, 145.3, 143.5, 136.0, 135.7, 135.1, 122.9, 122.4, 20.8, 17.2.

6,8-Dichloroquinazoline-4(3*H*)-thione (13). According to a literature-known procedure[44], yellow solid **13**

(188.5 mg, 0.82 mmol, 70%) was synthesized using **12a** (50.0 mg, 0.23 mmol), Lawesson's reagent (69.2 mg, 0.17 mmol, 0.7 equiv), and pyridine (1.1 mL, 0.2 m). **LC-MS** m/z ([M+H]$^+$) = 230.89, t_r = 4.23 min, *purity*: 97%. **^{1}H NMR** (500 MHz, DMSO-d_6) δ = 14.21 (br s, 1H), 8.46 (d, J = 2.4 Hz, 1H), 8.30 (s, 1H), 8.23 (d, J = 2.4 Hz, 1H). **^{13}C NMR** (126 MHz, DMSO-d_6) δ = 184.5, 145.2, 140.3, 134.6, 133.4, 132.2, 131.0, 127.1.

1-(3-(Aminomethyl)-4-methoxyphenyl)ethan-1-one (16). 1-(3-(chloromethyl)-4-methoxyphenyl)ethan-1-one **15** (165.0 mg, 0.83 mmol) was dissolved in ammonia solution (7 N in MeOH) and heated to 50 °C for 2 h under microwave irradiation (standard method, CEM microwave synthesis system). The resulting mixture was concentrated in *vacuo* and washed with both, EtOAc and DCM, to obtain crude **16** (122.4 mg) as a yellow solid. **LC-MS** m/z ([M-NH$_2$+H]$^+$) = 163.03, t_r = 1.48 min, *purity*: 87%. **^{1}H NMR** (500 MHz, DMSO-d_6) δ = 8.36 (br s, 2H), 8.08 (d, J = 2.2 Hz, 1H), 8.03 (dd, J = 2.2, 8.7 Hz, 1H), 7.19 (d, J = 8.7 Hz, 1H), 4.02 (s, 2H), 3.93 (s, 3H), 2.55 (s, 3H). **^{13}C NMR** (126 MHz, DMSO-d_6) δ = 196.3, 161.0, 131.3, 130.6, 129.5, 122.0, 110.8, 56.2, 37.3, 26.5.

6,8-Dichloroquinazolin-4-amine (18). According to **GP A** and similar to a literature-known procedure[45], yellow solid **18** (363.4 mg, crude) was synthesized using commercially available nitrile **17** (374.04 mg, 2.0 mmol) instead of an anthranilic acid, formamide (16.7 mL), and acetic acid (1.7 mL). The resulting crude was used without further purification. **LC-MS** m/z ([M+H]$^+$) = 214.11, t_r = 1.94 min, *purity*: 68%. **^{1}H NMR** (500 MHz, DMSO-d_6) δ = 8.48 (s, 1H), 8.36 (d, J = 2.0 Hz, 1H), 8.15 - 8.01 (m, 3H). **^{13}C NMR** (126 MHz, DMSO-d_6) δ = 161.7, 156.9, 145.6, 133.1, 133.0, 129.2, 122.7, 116.4.

5-Acetyl-2-methoxybenzoic acid (20). First, compound **19** was methylated under usage of K$_2$CO$_3$ (138.2 mg, 1.00 mmol), MeI (62 μL, 1.0 mmol), and DMF (2.0 mL) by applying **GP C**. The obtained crude product was directly used for the hydrolysis according to **GP F** resulting in **20** (137.8 mg, 0.71 mmol, 71%) as a colorless solid. **LC-MS** m/z ([M+H]$^+$) = 195.09, t_r = 2.47 min, *purity*: > 98%. **^{1}H NMR** (500 MHz, DMSO-d_6) δ = 12.98 (br s, 1H), 8.21 (d, J = 2.2 Hz, 1H), 8.12 (dd, J = 2.2, 8.8 Hz, 1H), 7.25 (d, J = 8.8 Hz, 1H), 3.91 (s, 3H), 2.55 (s, 3H). ^{1}H NMR data published in CDCl$_3$[59] **^{13}C NMR** (126 MHz, DMSO-d_6) δ = 196.1, 166.8, 161.7, 133.5, 131.1, 129.0, 121.2, 112.4, 56.3, 26.5.

2-(2-Methoxyethoxy)benzaldehyde (22c). Similar to a literature-known procedure[47], 2-hydroxyaldehyde **21** (200.0 mg, 1.64 mmol), 1-bromo-2-methoxyethane (0.2 mL, 2.13 mmol, 1.3 equiv), and K$_2$CO$_3$ (295.9 mg, 2.13 mmol, 1.0 equiv) were stirred at 60 °C in DMF (0.7 M) o/n. Then, the resulting mixture was concentrated in *vacuo*, suspended in water and extracted with DCM (3 x 100 mL). The combined organic layers were washed with saturated, aqueous NaCl solution (100 mL) and dried over Na$_2$SO$_4$. After filtration and drying *in vacuo*, **22c** (295.7 mg, 1.64 mmol, quant.) was obtained as a brown oil that was used without further purification. **LC-MS** m/z ([M+H]$^+$) = 181.19, t_r = 4.65 min, *purity*: > 98%. **^{1}H NMR** (500 MHz, CDCl$_3$) δ = 10.54 (s, 1H), 7.84 (dd, J = 1.8, 7.8 Hz, 1H), 7.54 (s, 1H), 7.04 (t, J = 7.8 Hz, 1H), 7.00 (d, J = 7.8 Hz, 1H), 4.27 - 4.23 (m, 2H), 3.84 - 3.80 (m, 2H), 3.47 (s, 3H).[47] **^{13}C NMR**

(126 MHz, CDCl$_3$) δ = 189.8, 161.2, 135.9, 128.3, 125.0, 121.0, 112.7, 70.8, 68.1, 59.4.

(2-(2-Methoxyethoxy)phenyl)methanol (23c). Adapting a known procedure[60], compound **22c** was dissolved in MeOH (16.0 mL, 0.1 M). To this solution, NaBH$_4$ was added in small portions at 0 °C. The ice bath was removed, and the mixture allowed to stir at r. t. for 30 min. NaBH$_4$ was quenched with water. Then, the mixture was concentrated in *vacuo*, suspended in water and extracted using DCM (3 x 100 mL). After combining the organic layers, the organic phase was washed with saturated, aqueous NaCl solution (100 mL) and dried over Na$_2$SO$_4$, filtered, and concentrated to dryness *in vacuo* to give **23c** (190.6 mg, 1.05 mmol, 65%) as a brown oil. **LC-MS** *m/z* ([M-OH]$^+$) = 165.14, t_r = 2.78 min, *purity*: > 98%. **^{1}H NMR** (500 MHz, CDCl$_3$) δ = 7.28 - 7.24 (m, 1H), 6.96 (t, *J* = 7.8 Hz, 1H), 6.91 (d, *J* = 7.8 Hz, 1H), 4.68 (s, 2H), 4.24 - 4.19 (m, 2H), 3.79 - 3.73 (m, 2H), 3.44 (s, 3H). **^{13}C NMR** (126 MHz, CDCl$_3$) δ = 157.1, 130.3, 129.1, 128.9, 121.3, 112.5, 70.9, 67.9, 62.3, 59.0.

2-Methoxy-3-methylbenzoic acid (25z). Application of **GP C** on 3-methyl salicylic acid (500.0 mg, 3.28 mmol), K$_2$CO$_3$ (908.4 mg, 6.57 mmol), MeI (0.51 mL, 8.22 mmol), and DMF (3.3 mL), followed by **GPF** on the resulting yellow oil (523.5 mg), using aqueous NaOH solution (1 M, 2.9 mL) and THF (8.8 mL), led to **25z** (420.8 mg, 2.91 mmol, 89% over two steps). This compound was used without further purification. **LC-MS** *m/z* ([M-H]$^-$, [M-OH]$^+$) = 165.19, 149.14, t_r = 3.26 min, *purity*: 80%. **^{1}H NMR** (500 MHz, DMSO-*d$_6$*) δ = 12.81 (br s, 1H), 7.50 (dd, *J* = 1.7, 7.6 Hz, 1H), 7.41 - 7.37 (m, 1H), 7.08 (t, *J* = 7.6 Hz, 1H), 3.73 (s, 3H), 2.25 (s, 3H). **^{13}C NMR** (126 MHz, DMSO-*d$_6$*) δ = 167.6, 157.4, 134.4, 132.0, 128.4, 125.9, 123.4, 61.0, 15.7. NMR data only published in CDCl$_3$.[61]

3-Methoxy-2-methylbenzoic acid (25ab). Performing **GP C** under usage of 3-hydroxy-2-methylbenzoic acid (1.00 g, 6.56 mmol), K$_2$CO$_3$ (1.82 g, 13.18 mmol), MeI (1.02 mL, 16.44 mmol), and DMF (6.6 mL), resulted in a yellow solid that was directly used for the hydrolysis according to **GP F**. For that, aqueous NaOH solution (1.0 M, 5.8 mL) and THF (17.6 mL) were used to give **25ab** (1.03 g, 6.18 mmol, 94% over two steps). This compound was used without further purification. **LC-MS** *m/z* ([M-H]$^-$) = 165.17, t_r = 3.33 min, *purity*: > 98%. **^{1}H NMR** (500 MHz, DMSO-*d$_6$*) δ = 12.88 (br s, 1H), 7.30 (d, *J* = 7.6 Hz, 1H), 7.23 (t, *J* = 7.6 Hz, 1H), 7.12 (d, *J* = 7.6 Hz, 1H), 3.80 (s, 3H), 2.32 (s, 3H). **^{13}C NMR** (126 MHz, DMSO-*d$_6$*) δ = 169.6, 158.0, 133.1, 126.8, 126.8, 121.8, 113.8, 56.2, 13.1. NMR data only published in CDCl$_3$.[60]

3-Methoxy-5-methylbenzoic acid (25ac). Following **GP C**, 3-hydroxy-5-methylbenzoic acid (152.2 mg, 1.00 mmol), K$_2$CO$_3$ (276.4 mg, 2.00 mmol), MeI (0.12 mL, 2.0 mmol), and DMF (2.0 mL) were used for the methylation step. The resulting brown oil was directly used for the hydrolysis according to **GP F**. Under usage of aqueous NaOH solution (1.0 M, 3.0 mL) and THF (8.8 mL), the desired product **25ac** (118.5 mg, 0.71 mmol, 71% over two steps) was isolated as a beige solid and used without further purification. **LC-MS** *m/z* ([M-CO$_2$H]$^+$, [M-H]$^-$) = 121.07, 165.36, t_r = 3.45 min, *purity*: 95%. **^{1}H NMR** (500 MHz, DMSO-*d$_6$*) δ = 12.94 (s, 1H), 7.35 (s, 1H), 7.24 (s, 1H), 7.01 (s, 1H), 3.77 (s, 3H), 2.32 (s, 3H). **^{13}C NMR** (126 MHz, DMSO-*d$_6$*) δ = 167.2,

159.2, 139.4, 131.9, 122.3, 119.4, 111.2, 55.2, 20.9. NMR data only published in CDCl$_3$.[60]

1-(2-Methoxy-5-methylphenyl)ethan-1-one (25ad). Performing **GP C** under usage of 1-(2-hydroxy-5-methylphenyl)ethan-1-one (150.2 mg, 1.00 mmol), K$_2$CO$_3$ (138.2 mg, 1.00 mmol), MeI (62 μL, 1.00 mmol), and DMF (2.0 mL), revealed **25ad** (146.3 mg, 0.89 mmol, 89%) as a brown oil that was used without further purification. **LC-MS** *m/z* ([M+H]$^+$) = 165.13, t_r = 3.91 min, *purity*: > 98%. **^{1}H NMR** (500 MHz, DMSO-*d$_6$*) δ = 7.37 (d, *J* = 2.1 Hz, 1H), 7.34 (br d, *J* = 8.4 Hz, 1H), 7.05 (d, *J* = 8.4 Hz, 1H), 3.84 (s, 3H), 2.50 (s, 3H), 2.25 (s, 3H). ^{1}H NMR data published in CDCl$_3$.[62] **^{13}C NMR** (126 MHz, DMSO-*d$_6$*) δ = 198.9, 156.5, 134.2, 129.6, 129.2, 127.5, 112.5, 55.8, 31.6, 19.8.

1-(2-Methoxy-3-methylphenyl)ethan-1-one (26z). GP G was applied on **25z** (276.5 mg, 1.66 mmol) under usage of MeLi solution (1.9 M, in Et$_2$O, 3.5 mL, 6.65 mmol), dry Et$_2$O (12.8 mL). Extraction with DCM (3 x 40.0 mL) afforded **26z** (246.9 mg) as a light-yellow oil and was used without further purification. **LC-MS** *m/z* ([M+H]$^+$) = 165.17, t_r = 3.89 min, *purity*: 80%. **^{1}H NMR** (500 MHz, CDCl$_3$) δ = 7.37 (dd, *J* = 1.4, 7.6 Hz, 1H), 7.25 (d, *J* = 7.6 Hz, 1H), 7.00 (t, *J* = 7.6 Hz, 1H), 3.69 (s, 3H), 2.56 (s, 3H), 2.26 (s, 3H). **^{13}C NMR** (126 MHz, CDCl$_3$) δ = 201.1, 157.6, 135.0, 133.4, 132.1, 127.5, 124.0, 61.8, 30.5, 16.0.

1-(3-Methoxy-4-methylphenyl)ethan-1-one (26aa). Similar to a literature-known procedure[63] **26aa** was synthesized.

Weinreb amide formation (step 1). To a solution of commercial 3-methoxy-4-methylbenzoic acid (86.0 mg, 0.52 mmol) in dry DCM (1.5 mL, 0.34 m) one drop of anhydrous DMF was added followed by oxalyl chloride (100 μL, 1.10 mmol). The resulting reaction mixture was refluxed at 50 °C for 2 h. Then, the reaction mixture was dried in *vacuo* affording crude acid chloride (96.0 mg, 0.52 mmol, quant.), which was used in the subsequent step without additional purification. For this, the obtained acid chloride was dissolved in anhydrous THF (3.0 mL, 0.17 M) and stirred vigorously at r. t. for 2 h after addition of triethylamine (202 μL, 1.56 mmol) and *N,O*-dimethylhydroxylammoium chloride (56.0 mg, 0.57 mmol). The reaction mixture was then concentrated *in vacuo* and subjected to AFC (Hex/EtOAc 0 – 100% EtOAc over 18 min, 12 g silica, 18 mL/min, product at 45% EtOAc) to furnish the corresponding Weinreb amide (107.0 mg, 0.51 mmol, 98%) as a colorless solid. **R$_f$** (Hex/EtOAc, 3:1) = 0.40. **^{1}H NMR** (500 MHz, CDCl$_3$) δ = 7.21 (d, *J* = 7.7 Hz, 1H), 7.18 (s, 1H), 7.15 (d, *J* = 7.7 Hz, 1H), 3.86 (s, 3H), 3.59 (s, 3H), 3.36 (s, 3H), 2.25 (s, 3H). **^{13}C NMR** (126 MHz, CDCl$_3$) δ = 169.9, 157.3, 132.5, 130.0, 129.7, 120.3, 110.0, 61.0, 55.4, 34.1, 16.3.

Alkylation starting from Weinreb amide (step 2). Under nitrogen atmosphere, the previously obtained Weinreb amide (107.0 mg, 0.51 mmol) was dissolved in dry THF (5.0 mL, 0.1 M) and cooled to 0 °C. Then, the solution of MeMgBr (1.0 mL, 1.0 M in THF) was added dropwise to the reaction mixture, which was subsequently allowed to reach r. t. and stirred for 2 h. By adding aqueous, saturated solution of NH$_4$Cl, the Grignard reagent was quenched and the mixture was extracted with ether. The combined organic fractions were washed with saturated, aqueous NaCl solution, dried over anhydrous Na$_2$SO$_4$ and concentrated under reduced

pressure after filtration to give pure ketone **26aa** (83.5 mg, 0.51 mmol, quant.). **R$_f$** (Hex/EtOAc, 9:1) = 0.35. **^{1}H NMR** (500 MHz, DMSO-d$_6$) δ = 7.51 (dd, J = 1.5, 7.6 Hz, 1H), 7.40 (d, J = 1.5 Hz, 1H), 7.29 (d, J = 7.6 Hz, 1H), 3.85 (s, 3H), 2.56 (s, 3H), 2.21 (s, 3H). **^{13}C NMR** (126 MHz, DMSO-d_6) δ = 197.4, 157.4, 136.2, 131.9, 130.5, 121.1, 108.6, 55.3, 26.7, 16.2. NMR spectra published in CDCl$_3$.[64]

1-(3-Methoxy-2-methylphenyl)ethan-1-one (26ab). Starting from **25ab** (300.0 mg, 1.81 mmol) and MeLi solution (1.9 m in Et$_2$O, 3.8 mL) in dry Et$_2$O (13.8 mL), **26ab** (123.7 mg, 0.75 mmol, 42%) was synthesized according to **GP G** and isolated as a colorless solid after purification by AFC (petroleum benzine (PB)/EtOAc, 0 – 30% EtOAc over 15 min, 13 mL/min, 4 g silica, **26ab** at 13% EtOAc). **LC-MS** m/z ([M+H]$^+$) = 165.13, t_r = 3.89 min, *purity*: > 98%. **^{1}H NMR** (500 MHz, CDCl$_3$) δ = 7.22 (t, J = 7.8 Hz, 1H), 7.16 (d, J = 7.8 Hz, 1H), 6.96 (d, J = 7.8 Hz, 1H), 3.86 (s, 3H), 2.56 (s, 3H), 2.33 (s, 3H). **^{13}C NMR** (126 MHz, CDCl$_3$) δ = 203.1, 158.2, 140.5, 126.1, 125.8, 120.0, 112.6, 55.7, 30.4, 12.6.[65]

1-(3-Methoxy-5-methylphenyl)ethan-1-one (26ac). Under usage of **25ac** (300.0 mg, 1.81 mmol) and MeLi solution (1.9 m in Et$_2$O, 3.8 mL) in dry Et$_2$O (13.8 mL), **26ac** (260.1 mg, 1.58 mmol, 88%) was prepared according to **GP G** as a yellow oil and used without further purification. **LC-MS** m/z ([M+H]$^+$) = 165.14, t_r = 3.88 min, *purity*: >98%. **^{1}H NMR** (500 MHz, CDCl$_3$) δ = 7.37 (s, 1H), 7.30 (s, 1H), 6.94 (s, 1H), 3.85 (s, 3H), 2.59 (s, 3H), 2.40 (s, 3H). **^{13}C NMR** (126 MHz, CDCl$_3$) δ = 198.2, 159.8, 139.7, 138.4, 122.0, 120.2, 109.7, 55.4, 26.8, 21.4.[66]

1-(Bromomethyl)-2-methoxybenzene[48] (27b). According to **GP H**, colorless, sticky oil **27b** (290.3 mg, 1.44 mmol, quant.) was synthesized using 2-methoxybenzyl alcohol (200.0 mg, 1.45 mmol), PBr$_3$ (0.2 mL, 2.17 mmol), and DCM (2.9 mL) and used without further purification. **R$_f$** (PB/EtOAc = 9:1) = 0.63. **^{1}H NMR** (500 MHz, CDCl$_3$) δ = 7.35 (d, J = 7.6 Hz, 1H), 7.32 (t, J = 7.6 Hz, 1H), 6.95 (t, J = 7.6 Hz, 1H), 6.91 (d, J = 7.6 Hz, 1H), 4.60 (s, 2H), 3.92 (s, 3H). **^{13}C NMR** (126 MHz, CDCl$_3$) δ = 157.4, 130.8, 130.2, 126.0, 120.6, 110.9, 55.5, 29.0.

1-(4-(Bromomethyl)-3-methoxyphenyl)ethan-1-one (27aa). According to **GP I**, **23v** was synthesized under usage of 1-(3-methoxy-4-methylphenyl)ethan-1-one (328.0 mg, 2.0 mmol), AIBN (7.0 mg, 40 µmol), NBS (374.0 mg, 2.1 mmol), and CCl$_4$ (10.0 mL). The resulting mixture was stirred for 35 min. After concentrating *in vacuo*, an oily residue was obtained, that was resuspended in ether. A colorless solid precipitated and was filtered off. The mother liquor was concentrated *in vacuo* and subjected to AFC (Hex/DCM, 0 – 100% over 17 min, 20 mL/min, 12 g silica, **27aa** at 35% DCM) to yield the desired benzyl bromide **23v** (218.0 mg, 0.90 mmol, 45%). **R$_f$** (Hex/DCM= 7:3) = 0.4. **^{1}H NMR** (500 MHz, CDCl$_3$) δ = 7.53 - 7.49 (m, 2H), 7.43 (d, J = 7.6 Hz, 1H), 4.57 (s, 2H), 3.97 (s, 3H), 2.61 (s, 3H). **^{13}C NMR** (126 MHz, CDCl$_3$) δ = 197.5, 157.5, 138.6, 131.4, 130.8, 121.4, 109.6, 55.8, 27.5, 26.6.

1-(2-(Bromomethyl)-3-methoxyphenyl)ethan-1-one (27ab). For the bromination, **26ab** (218.8 mg, 1.34 mmol), AIBN (43.6 mg, 0.26 mmol), NBS (237.0 mg, 1.34 mmol), and CCl$_4$ (1.3 mL) were used following **GP I**. Herein, the crude product was purified *via* AFC (PB/EtOAc, 0 – 30% EtOAc over 20 min, 13 mL/min, 4 g silica, **27ab** at 18%

EtOAc) obtaining **27ab** as a colorless solid (290.9 mg, 1.19 mmol, 89%). **R$_f$** (PB/EtOAc, 9:1) = 0.39. **^{1}H NMR** (500 MHz, CDCl$_3$) δ = 7.36 (t, J = 8.4 Hz, 1H), 7.26 (t, J = 8.4 Hz, 1H), 7.04 (d, J = 8.4 Hz, 1H), 4.93 (s, 2H), 3.93 (s, 3H), 2.62 (s, 3H). **^{13}C NMR** (126 MHz, CDCl$_3$) δ = 202.0, 158.0, 139.4, 129.4, 125.4, 120.9, 113.9, 56.1, 30.1, 24.2.

1-(5-(Bromomethyl)-2-methoxyphenyl)ethan-1-one (27ad). Performing **GP I** under usage of **25ad** (117.2 mg, 0.71 mmol), AIBN (23.4 mg, 0.14 mmol), NBS (127.1 mg, 0.71 mmol), and CCl$_4$ (1.4 mL) led to **23x** (19.0 mg, 78 µmol, 11%) as a colorless solid after purification *via* AFC (PB/EtOAc, 0 – 40% EtOAc over 14 min, 13 mL/min, 4 g silica, **23x** at 25% EtOAc). **R$_f$** (PB/EtOAc, 9:1) = 0.27. **^{1}H NMR** (500 MHz, CDCl$_3$) δ = 7.77 (d, J = 2.4 Hz, 1H), 7.52 (dd, J = 2.4, 8.5 Hz, 1H), 6.96 (d, J = 8.5 Hz, 1H), 4.49 (s, 2H), 3.93 (s, 3H), 2.62 (s, 3H). **^{13}C NMR** (126 MHz, CDCl$_3$) δ = 199.1, 158.9, 134.4, 131.1, 130.1, 128.3, 112.1, 55.7, 32.8, 31.8.

4-Bromo-2-(bromomethyl)-1-methoxybenzene[67] (27ah). According to GP H, 3-bromo-5-methoxybenzyl alcohol (314.1 mg, 1.45 mmol), PBr$_3$ (0.2 mL, 2.17 mmol), and DCM (2.9 mL) were used for the bromination to give **27ah** (370.2 mg, 1.32 mmol, 91%) as a colorless sticky oil that was used without further purification. **R$_f$** (PB/EtOAc = 9:1) = 0.69. **^{1}H NMR** (500 MHz, CDCl$_3$) δ = 7.45 (d, J = 2.6 Hz, 1H), 7.39 (dd, J = 2.6, 8.7 Hz, 1H), 6.77 (d, J = 8.7 Hz, 1H), 4.49 (s, 2H), 3.89 (s, 3H). **^{13}C NMR** (126 MHz, CDCl$_3$) δ = 156.5, 133.4, 132.7, 128.2, 112.7, 112.5, 55.9, 29.7, 27.6.

Infection assays.

HRSV-FLuc propagation and infection assay. A recombinant hRSV encoding for a firefly luciferase reporter (kindly provided by Marie-Anne Rameix-Welti, the Institut National de la Santé et de la Recherche Médicale [INSERM], Université de Versailles St. Quentin, Montigny-le-Bretonneux, France and Jean-François Eléouët, Unité de Virologie et Immunologie Moléculaires, INRAE, France) was prepared as described previously.[68]

For the infection experiment HEp-2 cells were seeded in 96-well plates at a cell count of 1.5 x 10^4 cells/well in 100 µL advanced MEM and incubated for 24 h at 37°C and 5% CO$_2$. The cells were infected with hRSV-Luc (MOI 0.01) in the presence of compound or 1% DMSO. As a control, uninfected cells were treated with 1% DMSO. After 24 h of incubation, the cells were lysed with a lysis buffer (1% Triton-X-100, 25 mM Glycylglycine, 15 mM MgSO$_4$, 4 mM EGTA, 1mM dithiothreitol) and frozen at -20°C. Luciferase activity measurements were performed by adding 72 µL of assay buffer (25 mM Glycylglycine, 5 mM KPO$_4$, 50 mM MgSO$_4$, 10 mM EGTA, 2% ATP, 1 mM dithiothreitol) to a white 96-well plate. 20 µL of the lysed cell suspension were added to the plate and using the Berthold LB960 Centro XS3 plate luminometer, 40 µL of D-Luciferin solution was added and the RLU was measured. In order to evaluate antiviral effects of the compounds on second round infection the supernatants of infected cells were transferred to HEp-2 cells seeded the day before as described above. Those cells were incubated for 24 h and lysation and measurement were performed as described above.

HCoV-229E RLuc propagation and infection assay. Renilla luciferase reporter gene encoding hCoV-229E[69] (stock kindly provided by Volker Thiel, Institute of Virology and Immunology (IVI), Bern and Mittelhäusern, Switzerland

and Department of Infectious Diseases and Pathobiology, Vetsuisse Faculty, University of Bern, Switzerland) was propagated in Huh-7.5 cells[70] (kindly provided by Charles Rice, Laboratory of Virology and Infectious Disease, The Rockefeller University, New York, USA). Cells were seeded in 15 cm culture dishes in complete growth medium until 90% confluency. hCoV-229E RLuc primary stock was diluted 1:10 in DMEM complete and 5.5 mL used to inoculate the cells at 33 °C (5% CO_2). After 4 h the inoculum was removed, and 20 mL of fresh culture media were added. Cells were cultured for approx. another 48 h at 33 °C until cytopathic effects were visible. Then the supernatant was harvested, centrifuged at 1000 x g for 5 min. Subsequently, the supernatant was transferred to fresh Eppendorf tubes and aliquots were stored at – 80 °C. For compound testing, Huh-7.5 cells encoding for a firefly luciferase reporter gene were seeded at 1.6×10^4 cells/well in a 96-well plate in 100 µL of culture media at 37 °C. The next day, an hCoV-229E RLuc stock was diluted 1:500 in culture medium and cells were inoculated with 100 µL in the presence of compounds in the indicated concentrations or DMSO. After incubation for 48 h at 37 °C the cells were lysed by application of 0.5% Triton X-100 in PBS and frozen at – 20 °C. Renilla luciferase activity was determined as a measure of residual infectivity and firefly luciferase activity was determined as a measure for cell viability. In case of some compounds, Huh-7.5 cells without a luciferase reporter were used. In this case, the viability was assessed by using the MTT assay (described below).

Viability assay. To test possible impact of tested compounds on cell viability, HEp-2 cells or Huh-7.5 cells were seeded at a density of 1.5×10^4 in 100 µL advanced MEM or 1.6×10^4 in 100 µL DMEM respectively in a 96-well plate and incubated for 24h at 37°C and 5% CO_2. Afterwards the cells were treated with compound. As controls Puromycin and untreated cells were used. After 24h of incubation at 37°C and 5% CO_2, the supernatant was removed. Subsequently, MTT reagent (3-(4,5-dimethylthiazol-2-yl)-2,5-diphenyl tetrazolium bromide) was diluted in a 1:10 ratio in advanced MEM or DMEM and added to the cells. After 60 min incubation at 37°C the supernatant was discarded and the cells were lysed using 50 µL isopropanol. Absorbance was measured at 570 nm and 630 nm using a BioTek Synergy 2 (BioTek, Winooski, Vermont, USA).

ADME experiments.

Kinetic turbidimetric solubility. The desired compounds were sequentially diluted in DMSO in a 96-well plate. 1.5 µL of each well were transferred into another 96-well plate and mixed with 148.5 µL of PBS. Plates were shaken at 600 rpm and r. t. for 5 min. The absorbance was measured at 620 nm. Absorbance values were normalized by blank subtraction and plotted using GraphPad Prism 8.4.2 (GraphPad Software, San Diego, CA, USA). Solubility (S) was determined based on the First X value of AUC function using a threshold of 0.005.

Metabolic stability in liver S9 fractions. For the evaluation of combined phase I and phase II metabolic stability, the compound (1 µM) was incubated with 1 mg/mL pooled mouse liver S9 fraction (Xenotech, Kansas City, USA), 2 mM NADPH, 1 mM UDPGA, 10 mM $MgCl_2$, 5 mM GSH and 0.1 mM PAPS at 37 °C for 240 min. The metabolic stability of testosterone, verapamil and ketoconazole were determined in parallel to confirm the enzymatic activity of mouse S9 fractions. The incubation was stopped after defined time points by precipitation of aliquots of S9 enzymes with two volumes of cold acetonitrile containing internal standard (150 nM diphenhydramine). Samples were stored on ice until the end of the incubation and precipitated protein was removed by centrifugation (15 min, 4 °C, 4,000 g). Concentration of the remaining test compound at the different time points was analyzed by HPLC-MS/MS (TSQ Quantum Access MAX, Thermo Fisher, Dreieich, Germany) and used to determine half-life ($t_{1/2}$). Half-life and intrinsic clearance (Cl_{int}) are summarized in the corresponding tables.

AUTHOR INFORMATION

Corresponding Author

A. K. H. Hirsch https://orcid.org/0000-0001-8734-4663
*anna.hirsch@helmholtz-hips.de

Authors

C. Karhan https://orcid.org/0009-0006-8428-6692
A. F. Kiefer https://orcid.org/0000-0002-4540-6501
A. M. Kany https://orcid.org/0000-0001-7580-3658
Uladzislau Hapko https://orcid.org/0000-0003-4193-2966
T. Pietschmann https://orcid.org/0000-0001-6789-4422

Present Addresses

† htw saar – Lab of Bio and Environmental Engineering, Goebenstraße 40, 66117 Saarbrücken
†† The Herbert Wertheim UF Scripps Institute for Biomedical Innovation & Technology, 120 Scripps Way, Jupiter, FL 33458 USA

Author Contributions

The manuscript was written by C. Karhan. She also synthesized, purified and analyzed all final compounds and corresponding intermediates except commercial starting materials. The purity of commercial final compounds (**10a, 10f, 10m, 10q, 10u–w**) was analyzed by her as well. Additionally, some intermediates (**26aa**, **27d1**, **27d**. **27aa**, **27af**) and final compounds (**10d, 10aa, 10af, 10ag**) have been prepared by U. Hapko. Purity analyses of all commercial final compounds have also been performed by C. Karhan. Furthermore, she prepared all chemistry related figures/spectra/chromatograms in the supporting information. A. M. Kany supervised the performance of the solubility and metabolic stability assays. Biological infection assays were performed by S. M. Sake, A. P. Gunesch, C. Grethe and B. Hellwinkel under the supervision of T. Pietschmann. Proofreading of the manuscript was done by A. F. Kiefer and A. K. H. Hirsch as well as B. Hellwinkel and T. Pietschmann. The whole project was supervised by A. K. H. Hirsch and T. Pietschmann. The conception of this study was developed by A. K. H. Hirsch, T. Pietschmann, C. Karhan, S. Sake, A. F. Kiefer, and A. P. Gunesch. All authors have given approval to the final version of the manuscript.

ACKNOWLEDGMENT

ABBREVIATIONS

AFC, automated flash column chromatography; t_r, retention time; $t_{1/2}$: half-life; *, commercial compound; ADME, absorption, distribution, metabolism, and excretion; AIBN, azobisisobutyronitrile; br s, broad singlet; c. v., closed vessel; CC_{50}, half-maximal cytotoxic concentration; Cl_{int}, intrinsic clearance; Cp, compound; CV, cell viability; cycloPr, cyclopropyl; d, doublet; dd, doublet of a doublet; DIPEA, *N,N*-diisopropylethylamine; DMF, dimethylformamide; DMSO, dimethyl sulfoxide; dq, doublet of a quartet; EC_{50}, half-maximal effective concentration; equiv, equivalent(s); Et_2O, diethyl ether; F protein, fusion protein; FA, formic acid; G protein, attachment protein; GP, general procedure; H_2O, water; HATU, hexafluorophosphate azabenzotriazole tetramethyl uranium; HCl, hydrochloric acid; hCoV-229E, human coronavirus 229E; HRMS, high resolution mass spectrometry; Hz, Hertz; I, round 1; IC_{50}, half-maximal inhibitory concentration; II, round 2; Inf, infectivity; LC-MS, liquid chromatography-mass spectrometry; m, multiplet; mCPBA, meta-chloroperoxybenzoic acid; MeCN, acetonitrile; MeCN, acetonitrile; MeLi, methyl iodide; MeLi, methyl lithium; MeOH, methanol; MFC, manual flash column chromatography; mw, microwave-assisted; N, counts; n. d., not determined; $NaBH_4$, sodium borohydride; NaH, sodium hydride; NBS, *N*-bromosuccinimide; NEt_3, triethylamine; o/n, overnight; P, precipitation at 10 µM, measurement at 5 µM compound concentration in further analyses; Ph, phenyl; Pyr, pyridyl; q, quartet; quant., quantitative; r. t., room temperature; RSV, respiratory syncytial virus; s, singlet; S, kinetic solubility in µM; S protein, spike protein; SAR, structure-activity relationship; SARS-CoV-2, severe acute respiratory syndrome coronavirus 2; SD, standard deviations; semi-prep HPLC, semi-preparative high-performance liquid chromatography; sept, septet; SI, supporting information; so, statistical outlier, sxt, sextet; t, triplet; THF, tetrahydrofuran; TLC, thin layer chromatography; UHPLC, ultra-high-performance liquid chromatography; λ, wavelength.

ASSOCIATED CONTENT

Supporting information. Purity analysis based on LC-MS data of commercial and synthesized, tested compounds, ^{1}H and ^{13}C NMR spectra, dose response curves of all compounds showing activity in single-point measurements, data of ADME studies (kinetic solubility and metabolic stability).

REFERENCES

(1) Collins, C. L.; Pollard, A. J. Respiratory syncytial virus infections in children and adults. *Journal of Infection* **2002**, *45* (1), 10–17.

(2) Chaiwatpongsakorn, S.; Epand, R. F.; Collins, P. L.; Epand, R. M.; Peeples, M. E. Soluble respiratory syncytial virus fusion protein in the fully cleaved, pretriggered state is triggered by exposure to low-molarity buffer. *J. Virol.* **2011**, *85* (8), 3968.

(3) Battles, M. B.; McLellan, J. S. Respiratory syncytial virus entry and how to block it. *Nat. Rev. Microbiol.* **2019**, *17* (4), 233–245.

(4) Jackson, C. B.; Farzan, M.; Chen, B.; Choe, H. Mechanisms of SARS-CoV-2 entry into cells. *Nat. Rev. Mol. Cell Biol.* **2022**, *23* (1), 3–20.

(5) V'kovski, P.; Kratzel, A.; Steiner, S.; Stalder, H.; Thiel, V. Coronavirus biology and replication: implications for SARS-CoV-2. *Nat. Rev. Microbiol.* **2021**, *19* (3), 155–170.

(6) Hause, A. M.; Henke, D. M.; Avadhanula, V.; Shaw, C. A.; Tapia, L. I.; Piedra, P. A. Sequence variability of the respiratory syncytial virus (RSV) fusion gene among contemporary and historical genotypes of RSV/A and RSV/B. *PloS one* **2017**, *12* (4), e0175792.

(7) Roymans, D.; Alnajjar, S. S.; Battles, M. B.; Sitthicharoenchai, P.; Furmanova-Hollenstein, P.; Rigaux, P.; Berg, J. V.; Kwanten, L.; Ginderen, M. V.; Verheyen, N.; Vranckx, L.; Jaensch, S.; Arnoult, E.; Voorzaat, R.; Gallup, J. M.; Larios-Mora, A.; Crabbe, M.; Huntjens, D.; Raboisson, P.; Langedijk, J. P.; Ackermann; McLellan, J. S.; Vendeville, S.; Koul, A. Therapeutic efficacy of a respiratory syncytial virus fusion inhibitor. *Nat. Commun.* **2017**, *8* (1).

(8) Mackman, R. L.; Sangi, M.; Sperandio, D.; Parrish, J. P.; Eisenberg, E.; Perron, M.; Hui, H.; Zhang, L.; Siegel, D.; Yang, H.; Saunders, O.; Boojamra, C.; Lee, G.; Samuel, D.; Babaoglu, K.; Carey, A.; Gilbert, B. E.; Piedra, P. A.; Strickley, R.; Iwata, Q.; Hayes, J.; Stray, K.; Kinkade, A.; Theodore, D.; Jordan, R.; Desai, M.; Cihlar, T. Discovery of an oral respiratory syncytial virus (RSV) fusion inhibitor (GS-5806) and clinical proof of concept in a human RSV challenge study. *J. Med. Chem.* **2015**, *58* (4), 1630–1643.

(9) Cockerill, G. S.; Angell, R. M.; Bedernjak, A.; Chuckowree, I.; Fraser, I.; Gascon-Simorte, J.; Gilman, M. S. A.; Good, J. A. D.; Harland, R.; Johnson, S. M.; Ludes-Meyers, J. H.; Littler, E.; Lumley, J.; Lunn, G.; Mathews, N.; McLellan, J. S.; Paradowski, M.; Peeples, M. E.; Scott, C.; Tait, D.; Taylor, G.; Thom, M.; Thomas, E.; Villalonga Barber, C.; Ward, S. E.; Watterson, D.; Williams, G.; Young, P.; Powell, K. Discovery of sisunatovir (RV521), an inhibitor of respiratory syncytial virus fusion. *J. Med. Chem.* **2021**, *64* (7), 3658–3676.

(10) Cianci, C.; Yu, K.-L.; Combrink, K.; Sin, N.; Pearce, B.; Wang, A.; Civiello, R.; Voss, S.; Luo, G.; Kadow, K.; Genovesi, E. V.; Venables, B.; Gulgeze, H.; Trehan, A.; James, J.; Lamb, L.; Medina, I.; Roach, J.; Yang, Z.; Zadjura, L.; Colonno, R.; Clark, J.; Meanwell, N.; Krystal, M. Orally active fusion inhibitor of respiratory syncytial virus. *Antimicrob. Agents Chemother.* **2004**, *48* (2), 413–422.

(11) PubChem. *Rilematovir*. https://pubchem.ncbi.nlm.nih.gov/compound/Rilematovir (accessed 2023-07-01).

(12) PubChem. *Sisunatovir*. https://pubchem.ncbi.nlm.nih.gov/compound/Sisunatovir (accessed 2023-07-01).

(13) Marty, F. M.; Chemaly, R. F.; Mullane, K. M.; Lee, D.-G.; Hirsch, H. H.; Small, C. B.; Bergeron, A.; Shoham, S.; Ljungman, P.; Waghmare, A.; Blanchard, E.; Kim, Y.-J.; McKevitt, M.; Porter, D. P.; Jordan, R.; Guo, Y.; German, P.; Boeckh, M.; Watkins, T. R.; Chien, J. W.; Dadwal, S. S. A phase 2b, randomized, double-blind, placebo-controlled multicenter study evaluating antiviral effects, pharmacokinetics, safety, and tolerability of presatovir in hematopoietic cell transplant recipients with respiratory syncytial virus infection of the lower respiratory tract. *Clin. Infect. Dis.: an official publication of the Infectious Diseases Society of America* **2020**, *71* (11), 2787–2795.

(14) Stray, K.; Perron, M.; Porter, D. P.; Anderson, F.; Lewis, S. A.; Perry, J.; Miller, M.; Cihlar, T.; DeVincenzo, J.; Chien, J. W.;

Jordan, R. Drug resistance assessment following administration of respiratory syncytial virus (RSV) fusion inhibitor presatovir to participants experimentally infected with RSV. *J. Infect. Dis.* **2020**, *222* (9), 1468–1477.

(15) Gesellschaft für medizinische Prävention und Kommunikation mbH. *Sanofi informiert: Beyfortus® – neue RSV-Prävention für Neugeborene und Säuglinge - GPK mbH.* https://gpk.de/sanofi-informiert-beyfortus-neue-praevention-fuer-neugeborene-und-saeuglinge/ (accessed 2024-02-03).

(16) FDA approves new drug to prevent RSV in babies and toddlers. *FDA,* Tue, Jul 18, 2023. https://www.fda.gov/news-events/press-announcements/fda-approves-new-drug-prevent-rsv-babies-and-toddlers (accessed 2024-02-03).

(17) Resch, B. Product review on the monoclonal antibody palivizumab for prevention of respiratory syncytial virus infection. *Hum. Vaccines Immunother.* **2017**, *13* (9), 2138–2149.

(18) Zhang, W.; Zheng, Q.; Yan, M.; Chen, X.; Yang, H.; Zhou, W.; Rao, Z. *Structural characterization of the HCoV-229E fusion core*, 2018. DOI: 10.2210/pdb5zhy/pdb.

(19) Simon, A.; Völz, S.; Höfling, K.; Kehl, A.; Tillman, R.; Müller, A.; Kupfer, B.; Eis-Hübinger, A.-M.; Lentze, M. J.; Bode, U.; Schildgen, O. Acute life threatening event (ALTE) in an infant with human coronavirus HCoV-229E infection. *Pediatric pulmonology* **2007**, *42* (4), 393–396.

(20) Vassilara, F.; Spyridaki, A.; Pothitos, G.; Deliveliotou, A.; Papadopoulos, A. A rare case of human coronavirus 229E associated with acute respiratory distress syndrome in a healthy adult. *Case reports in infectious diseases* **2018**, 1–4.

(21) Williamson, E. J.; Walker, A. J.; Bhaskaran, K.; Bacon, S.; Bates, C.; Morton, C. E.; Curtis, H. J.; Mehrkar, A.; Evans, D.; Inglesby, P.; Cockburn, J.; McDonald, H. I.; MacKenna, B.; Tomlinson, L.; Douglas, I. J.; Rentsch, C. T.; Mathur, R.; Wong, A. Y. S.; Grieve, R.; Harrison, D.; Forbes, H.; Schultze, A.; Croker, R.; Parry, J.; Hester, F.; Harper, S.; Perera, R.; Evans, S. J. W.; Smeeth, L.; Goldacre, B. Factors associated with COVID-19-related death using OpenSAFELY. *Nature* **2020**, *584* (7821), 430–436.

(22) O'Driscoll, M.; Ribeiro Dos Santos, G.; Wang, L.; Cummings, D. A. T.; Azman, A. S.; Paireau, J.; Fontanet, A.; Cauchemez, S.; Salje, H. Age-specific mortality and immunity patterns of SARS-CoV-2. *Nature* **2021**, *590* (7844), 140–145.

(23) Hasöksüz, M.; Kiliç, S.; Saraç, F. Coronaviruses and SARS-COV-2. *Turk. J. Med. Sci.* **2020**, *50* (SI-1), 549–556.

(24) Li, Z.; Tomlinson, A. C.; Wong, A. H.; Zhou, D.; Desforges, M.; Talbot, P. J.; Benlekbir, S.; Rubinstein, J. L.; Rini, J. M. The human coronavirus HCoV-229E S-protein structure and receptor binding. *eLife* **2019**, *8*.

(25) Pasquereau, S.; Nehme, Z.; Haidar Ahmad, S.; Daouad, F.; van Assche, J.; Wallet, C.; Schwartz, C.; Rohr, O.; Morot-Bizot, S.; Herbein, G. Resveratrol inhibits HCoV-229E and SARS-CoV-2 coronavirus replication in vitro. *Viruses* **2021**, *13* (2).

(26) Frediansyah, A.; Nainu, F.; Dhama, K.; Mudatsir, M.; Harapan, H. Remdesivir and its antiviral activity against COVID-19: A systematic review. *Clin. Epidemiol. Global Health* **2021**, *9*, 123–127.

(27) Parang, K.; El-Sayed, N. S.; Kazeminy, A. J.; Tiwari, R. K. Comparative antiviral activity of remdesivir and anti-HIV nucleoside analogs against human coronavirus 229E (HCoV-229E). *Molecules* **2020**, *25* (10).

(28) Kono, M.; Tatsumi, K.; Imai, A. M.; Saito, K.; Kuriyama, T.; Shirasawa, H. Inhibition of human coronavirus 229E infection in human epithelial lung cells (L132) by chloroquine: involvement of p38 MAPK and ERK. *Antiviral Res.* **2008**, *77* (2), 150–152.

(29) Anjani; Kumar, S.; Rathi, B.; Poonam. Recent updates on the biological efficacy of approved drugs and potent synthetic compounds against SARS-CoV-2. *RSC Adv.* **2023**, *13* (6), 3677–3687.

(30) Hoffmann, M.; Mösbauer, K.; Hofmann-Winkler, H.; Kaul, A.; Kleine-Weber, H.; Krüger, N.; Gassen, N. C.; Müller, M. A.; Drosten, C.; Pöhlmann, S. Chloroquine does not inhibit infection of human lung cells with SARS-CoV-2. *Nature* **2020**, *585* (7826), 588–590.

(31) Amstutz, A.; Speich, B.; Mentré, F.; Rueegg, C. S.; Belhadi, D.; Assoumou, L.; Burdet, C.; Murthy, S.; Dodd, L. E.; Wang, Y.; Tikkinen, K. A. O.; Ader, F.; Hites, M.; Bouscambert, M.; Trabaud, M. A.; Fralick, M.; Lee, T. C.; Pinto, R.; Barratt-Due, A.; Lund-Johansen, F.; Müller, F.; Nevalainen, O. P. O.; Cao, B.; Bonnett, T.; Griessbach, A.; Taji Heravi, A.; Schönenberger, C.; Janiaud, P.; Werlen, L.; Aghlmandi, S.; Schandelmaier, S.; Yazdanpanah, Y.; Costagliola, D.; Olsen, I. C.; Briel, M. Effects of remdesivir in patients hospitalised with COVID-19: a systematic review and individual patient data meta-analysis of randomised controlled trials. *Lancet Respir. Med.* **2023**.

(32) Grundeis, F.; Ansems, K.; Dahms, K.; Thieme, V.; Metzendorf, M.-I.; Skoetz, N.; Benstoem, C.; Mikolajewska, A.; Griesel, M.; Fichtner, F.; Stegemann, M. Remdesivir for the treatment of COVID-19. *The Cochrane database of systematic reviews* **2023**, *1* (1), CD014962.

(33) Yang, M.; Wei, J.; Huang, T.; Lei, L.; Shen, C.; Lai, J.; Yang, M.; Liu, L.; Yang, Y.; Liu, G.; Liu, Y. Resveratrol inhibits the replication of severe acute respiratory syndrome coronavirus 2 (SARS-CoV-2) in cultured Vero cells. *Phytother. Res.* **2021**, *35* (3), 1127–1129.

(34) van Brummelen, R.; van Brummelen, A. C. The potential role of resveratrol as supportive antiviral in treating conditions such as COVID-19 – A formulator's perspective. *Biomed. Pharmacother.* **2022**, 1–5.

(35) Sake, S. M.; Kosch, C.; Blockus, S.; Haid, S.; Gunesch, A. P.; Zhang, X.; Friesland, M.; Trummer, S. B.; Grethe, C.; Kühnel, A.; Rückert, J.; Duprex, W. P.; Huang, J.; Rameix-Welti, M.-A.; Empting, M.; Fischer, N.; Hirsch, A. K. H.; Schulz, T. F.; Pietschmann, T. Respiratory syncytial virus two-step infection screen reveals inhibitors of early and late life cycle stages. *Antimicrob. Agents Chemother.* **2022**, *66* (12), e01032-22.

(36) Ishikawa, M.; Hashimoto, Y. Improvement in aqueous solubility in small molecule drug discovery programs by disruption of molecular planarity and symmetry. *J. Med. Chem.* **2011**, *54* (6), 1539–1554.

(37) Morimoto, J.; Miyamoto, K.; Ichikawa, Y.; Uchiyama, M.; Makishima, M.; Hashimoto, Y.; Ishikawa, M. Improvement in aqueous solubility of achiral symmetric cyclofenil by modification to a chiral asymmetric analog. *Sci. Rep.* **2021**, *11* (1), 12697.

(38) Usmani, K. A.; Karoly, E. D.; Hodgson, E.; Rose, R. L. In vitro sulfoxidation of thioether compounds by human cytochrome P450 and flavin-containing monooxygenase isoforms with particular reference to the CYP2C subfamily. *Drug Metab. Dispos.* **2004**, *32* (3), 333–339.

(39) Gillis, E. P.; Eastman, K. J.; Hill, M. D.; Donnelly, D. J.; Meanwell, N. A. Applications of Fluorine in Medicinal Chemistry. *J. Med. Chem.* **2015**, *58* (21), 8315–8359.

(40) Cohen, D. T.; Buchwald, S. L. Mild palladium-catalyzed cyanation of (hetero)aryl halides and triflates in aqueous media. *Org. Lett.* **2015**, *17* (2), 202–205.

(41) Yuan, G.; Zheng, J.; Gao, X.; Li, X.; Huang, L.; Chen, H.; Jiang, H. Copper-catalyzed aerobic oxidation and cleavage/formation of C-S bond: a novel synthesis of aryl methyl sulfones from aryl halides and DMSO. *Chem. Commun.* **2012**, *48* (60), 7513–7515.

(42) Heppell, J. T.; Islam, M. A.; McAlpine, S. R.; Al-Rawi, J. M. A. Functionalization of quinazolin-4-ones part 3: synthesis,

structures elucidation, DNA-PK, PI3K, and cytotoxicity of novel 8-aryl-2-morpholino-quinazolin-4-ones. *J. Heterocycl. Chem.* **2019**, *56* (1), 124–141.

(43) Jang, K.; Kim, Y.; Kim, B.; Lee, B.; Lui, J.; Yu, E. S. Compound for organic optpelectronic diode, organic optoelectronic diode comprising same, and display device. U. S. Patent 2018/0006242 A1, Jan. 4, 2018 OR2023.

(44) Alexandre, F.-R.; Berecibar, A.; Wrigglesworth, R.; Besson, T. Novel series of 8H-quinazolino[4,3-b]quinazolin-8-ones via two Niementowski condensations. *Tetrahedron* **2003**, *59* (9), 1413–1419.

(45) Gueiffier, A.; Viols, H.; Chapat, J. P.; Chavignon, O.; Teulade, J. C.; Dauphin, G. Heterocyclic compounds with a bridgehead nitrogen atom. Synthesis in the imidazo[1,2-c]quinazoline series. *J. Heterocycl. Chem.* **1990**, *27* (2), 421–425.

(46) Fillion, E.; Trépanier, V. É.; Heikkinen, J. J.; Remorova, A. A.; Carson, R. J.; Goll, J. M.; Seed, A. Palladium-catalyzed intramolecular reactions of (E)-2,2-disubstituted 1-alkenyldimethylalanes with aryl triflates. *Organometallics* **2009**, *28* (12), 3518–3531.

(47) Nate, H.; Sekine, Y.; Honma, Y.; Nakai, H.; Wada, H.; Takeda, M.; Yabana, H.; Nagao, T. Synthesis of 2-phenylthiazolidine derivatives as cardiotonic agents. I. 2-Phenylthiazolidine-3-thiocarboxamides. *Chem. Pharm. Bull.* **1987**, *35* (5), 1953–1968.

(48) Doni, E.; Mondal, B.; O'Sullivan, S.; Tuttle, T.; Murphy, J. A. Overturning established chemoselectivities: selective reduction of arenes over malonates and cyanoacetates by photoactivated organic electron donors – supplementary information. *J. Am. Chem. Soc.* **2013**, *135* (30), 10934–10937.

(49) Liu, R.; Valiyaveettil, S.; Mok, K.-F.; Vittal, J. J.; Hoong, A. K. M. Solid-state self-assembly of 1,4-bis(2-carboxybenzyloxy)benzene in the presence and absence of aromatic amines. *CrystEngComm* **2002**, *4* (95), 574.

(50) Shen, C.; Wang, L.; Wen, M.; Shen, H.; Jin, J.; Zhang, P. Synthesis of benzimidazo[1,2-c]quinazolines via metal-free intramolecular C–H amination reaction. *Ind. Eng. Chem. Res.* **2016**, *55* (11), 3177–3181.

(51) Qian, Y.; Schürmann, M.; Janning, P.; Hedberg, C.; Waldmann, H. Activity-based proteome profiling probes based on Woodward's reagent K with distinct target selectivity – supporting information. *Angew. Chem., Int. Ed. Engl.* **2016**, *55* (27), 7766–7771, S14.

(52) Wang, R.; Li, Y.; Jin, R.-X.; Wang, X.-S. Copper-catalyzed oxidative C(sp3)-H/C(sp2)-H cross-coupling en route to carbocyclic rings – supplementary materials. *Chem. Sci.* **2017**, *8* (5), 3838–3842 (15).

(53) Zhang, Z.; Wang, X.; Huang, S.; Yan, B.; Liu, L.; Wang, H.; Han, J.; Huang, Z.; Cao, W. Preparation of substituted purinediones as MLKL inhibitors. U. S. Patent 2019/0381052, Dec. 19, 2019 OR2023.

(54) Orfi, L.; Waczek, F.; Pato, J.; Varga, I.; Hegymegi-Barakonyi, B.; Houghten, R.; Ker, G. Improved, high yield synthesis of 3H-quinazolin-4-ones, the key intermediates of recently developed drugs. *Curr. Med. Chem.* **2004**, *11* (19), 2549–2553.

(55) Elsocht, M.; Giron, P.; Maes, L.; Versées, W.; Gutierrez, G. J.; Grève, J. de; Ballet, S. Structure-activity relationship (SAR) study of spautin-1 to entail the discovery of novel NEK4 inhibitors. *Int. J. Mol. Sci.* **2021**, *22* (2).

(56) Gao, Z.; Guo, H.; Guo, Y.; Zhu, X. General and efficient synthesis of quinazolinones under CF3COOH catalysis and solvent-free conditions. *ChemistrySelect* **2021**, *6* (42), 11599–11602.

(57) Shirude, P. S.; Nair, S. K.; Sistla, R. K.; Ganguly, A. K.; Sarabu, R. Synthesis of Febrifugine derivatives and pharmaceutically acceptable salts treating an array of diseases. U. S. Patent 2021/0163443, Jun. 3, 2021 OR2023.

(58) Kulkarni, S. S.; Singh, S.; Shah, J. S.; Low, W.-K.; Talele, T. T. Synthesis and SAR optimization of quinazolin-4(3H)-ones as poly(ADP-ribose)polymerase-1 inhibitors. *Eur. J. Med. Chem.* **2012**, *50*, 264–273.

(59) Singh, R.; Zhou, H. Mass tags for quantitative analysis. International Patent WO 02/42427 A2, May 30, 2002 OR2023.

(60) Gevorgyan, A.; Hopmann, K. H.; Bayer, A. Formal C-H carboxylation of unactivated arenes. *Chem. - Eur. J.* **2020**, *26* (27), 6064–6069.

(61) Dean, M. A.; Hitchcock, S. R. Synthesis and application of oxadiazines as chiral ligands for the enantioselective addition of diethylzinc to aldehydes. *Tetrahedron: Asymmetry* **2010**, *21* (20), 2471–2478.

(62) Xu, C.; Du, W.; Zeng, Y.; Dai, B.; Guo, H. Reactivity switch enabled by counterion: highly chemoselective dimerization and hydration of terminal alkynes – supporting information. *Org. Lett.* **2014**, *16* (3), 948–951.

(63) Dotsenko, I.; Dragoli, D.; Lewis, J. Inhibitors of NHE-mediated antiport. International Patent WO 2018/129557 A1, July 12, 2018, OR2023.

(64) Montiel, L. E.; Zepeda, L. G.; Tamariz, J. Efficient total synthesis of racemic bisabolane sesquiterpenes curcuphenol and xanthorrhizol starting from substituted acetophenones. *Helv. Chim. Acta* **2010**, *93* (7), 1261–1273.

(65) Lafleur, K.; Huang, D.; Zhou, T.; Caflisch, A.; Nevado, C. Structure-based optimization of potent and selective inhibitors of the tyrosine kinase erythropoietin producing human hepatocellular carcinoma receptor B4 (EphB4). *J. Med. Chem.* **2009**, *52* (20), 6433–6446.

(66) Srikrishna, A.; Ravikumar, P. The first total synthesis of (±)-γ-herbertenol, a herbertene isolated from a non-herbertus source. *Synthesis* **2007**, *2007* (1), 65–74.

(67) Denton, R. M.; Scragg, J. T.; Saska, J. A concise synthesis of 4′-O-methyl honokiol – supporting information. *Tetrahedron Lett.* **2011**, *52* (20), 2554–2556.

(68) Rameix-Welti, M.-A.; Le Goffic, R.; Hervé, P.-L.; Sourimant, J.; Rémot, A.; Riffault, S.; Yu, Q.; Galloux, M.; Gault, E.; Eléouët, J.-F. Visualizing the replication of respiratory syncytial virus in cells and in living mice. *Nat. Commun.* **2014**, *5* (1), 1–10.

(69) Pfefferle, S.; Schöpf, J.; Kögl, M.; Friedel, C. C.; Müller, M. A.; Carbajo-Lozoya, J.; Stellberger, T.; Dall'Armi, E. von; Herzog, P.; Kallies, S.; Niemeyer, D.; Ditt, V.; Kuri, T.; Züst, R.; Pumpor, K.; Hilgenfeld, R.; Schwarz, F.; Zimmer, R.; Steffen, I.; Weber, F.; Thiel, V.; Herrler, G.; Thiel, H.-J.; Schwegmann-Wessels, C.; Pöhlmann, S.; Haas, J.; Drosten, C.; Brunn, A. von. The SARS-coronavirus-host interactome: identification of cyclophilins as target for pan-coronavirus inhibitors. *PLoS Pathog.* **2011**, *7* (10), 1-15.

(70) Blight, K. J.; McKeating, J. A.; Rice, C. M. Highly permissive cell lines for subgenomic and genomic hepatitis C virus RNA replication. *J. Virol.* **2002**, *76* (24), 13001–13014.